

# Modifying the proteostasis status: the role of cross-organelle communication

---

**Kanunnikau, Matea**

**Doctoral thesis / Disertacija**

**2020**

*Degree Grantor / Ustanova koja je dodijelila akademski / stručni stupanj:* **University of Split, Faculty of Science / Sveučilište u Splitu, Prirodoslovno-matematički fakultet**

*Permanent link / Trajna poveznica:* <https://urn.nsk.hr/urn:nbn:hr:166:030651>

*Rights / Prava:* [Attribution-NonCommercial-NoDerivatives 4.0 International/Imenovanje-Nekomercijalno-Bez prerada 4.0 međunarodna](#)

*Download date / Datum preuzimanja:* **2024-04-23**

*Repository / Repozitorij:*

[Repository of Faculty of Science](#)



UNIVERSITY OF SPLIT





FACULTY OF SCIENCE

Postgraduate University Study of Biophysics

**DOCTORAL THESIS**

MODIFYING THE PROTEOSTASIS STATUS: THE  
ROLE OF CROSS-ORGANELLE COMMUNICATION

Matea Kanunnikau

Split, October 2020

University of Split, Faculty of Science  
Department of Physics, Postgraduate University Study of Biophysics

**“Modifying the proteostasis status: the role of cross-organelle communication”**

Matea Kanunnikau completed her doctoral thesis under supervision of Anita Kriško, Ph.D. as a necessary part of obligations to attain a Ph.D. title.

Achieved academic title: Doctor of Philosophy (Ph.D.) in Natural Sciences, Biology

A composition of the Expert Board for Assessment and Defending of the Doctoral Thesis:

1. Prof. Katarina Vukojević, M.D.-Ph.D. \_\_\_\_\_

2. Prof. Irena Drmić Hofman, Ph.D. \_\_\_\_\_

3. Prof. Biljana Balen, Ph.D. \_\_\_\_\_

We confirm that the PhD thesis has been defended on \_\_\_\_\_ November 06 2020

Coordinator of the Study: Prof. Mile Dželalija, Ph.D. \_\_\_\_\_

DEAN:

\_\_\_\_\_  
Prof. Nikola Koceić-Bilan, Ph.D.

## ACKNOWLEDGMENTS

---

*Since this seems to really be happening, I would like to give my special thanks to all the people who believed in me, especially when I had trouble to do the same.*

*I am endlessly grateful to my mentor Anita Kriško for trusting me and granting me the opportunity to join her group. I am thankful for her patience and guidance throughout the years, and I am particularly grateful for being my friend.*

*To my dearest colleagues and lab-mates: "The 4MAT" - thank you! Thank you for all the support, advice and laughter you have given me, because you made this journey far better than I have hoped for.*

*Special round of applause for the best laboratory technician Tea Copic, who I would have been lost without.*

*A greatest hug and thank you for my very special friend and colleague, Musa. Thank you for giving me strength, advice, love and "višnja" when I needed it the most.*

*Big thank you to the entire administration in MedILS, and Irena Bitunjac, you have saved me countless times.*

*To my friends and professors at Methodist University, particularly Alexis Lanza and the Advanced Biochemistry class, as well as Dr. Britton who introduced me to research in the first place.*

*To my husband and daughter, for making this journey almost too challenging to finalize, thankfully to no avail.*

*To my beloved cat and dog, for teaching me an important skill of patience every time both of them demanded my undivided attention the moment I started writing my thesis.*

*To my family and friends outside the lab, thank you for giving me strength to endure and love to persevere. To my mom Bilja and dad Kreša, my brother Viktor and sister Marija: you made this happen. Thank you Belarus for your guidance and support, and thank you E for all the nights you slept and let me write.*

*Lastly and most importantly, I would like to thank my sister Andrea, without who this journey would not have been completed and the thesis unwritten. Thank you, thank you, thank you!*

*I dedicate this work to you Priljepuše.*

*„Tko rani rani, sam u nju upada" V.P.*

**Modifying the proteostasis status: the role of cross-organelle communication**

Matea Kanunnikau

Thesis performed at Mediterranean Institute for Life Sciences

## Abstract

Perpetual exposure to fluctuating intrinsic and environmental conditions constitute a challenge for maintaining a stable proteome, and this predicament is surmounted by an intricate system of precisely controlled mechanisms that constitute proteostasis. Proteostasis, or protein homeostasis, is orchestrated by an elaborate interlock of signaling pathways collectively known as the proteostasis network, with molecular chaperones constituting its most prominent component. The compartmentalized eukaryotic cell has ascertained organelle-specific chaperones to surmount challenges to proteostasis, and this idiosyncrasy was resolved to be used to study cell-wide effect upon proteostasis modifications in distinct cellular compartments. This study revealed an elaborate cross-organelle communication networking system upon compartmentalized improvement of proteostasis, induced by chaperone enrichment, as well as mild deterioration of proteostasis, induced by chaperone deletions. Comprehensive and detailed experiments confirmed that the improvement of proteostasis, as well as its mild deterioration initiates a cell-wide response which, ultimately, entails replicative lifespan extension, irrespective of the origin of alteration. This research postulates that this cell-wide response is orchestrated by sensing and mediating the protein folding quality status of the proteome in distinct cellular compartments, a response termed here cross-organelle stress response (CORE).

(149 pages, 68 figures, 19 tables, 192 references, original in English)

Thesis deposited in:

- National and University Library in Zagreb
- University Library in Split
- Library of the Faculty of Science, University of Split

Keywords: CORE, molecular chaperones, proteostasis deterioration, proteostasis improvement, Snf1, TOR

Supervisor: Anita Kriško, Ph.D.

Reviewers: 1. Prof. Katarina Vukojević, M.D.-Ph.D.

2. Prof. Irena Drmić Hofman, Ph.D.

3. Prof. Biljana Balen, Ph.D.

Thesis accepted: 21<sup>st</sup> October 2020

## **Modifikacija statusa proteostaze: uloga komunikacije između staničnih organela**

Matea Kanunnikau

Rad je izrađen na Mediteranskom institutu za životne znanosti

### Sažetak

Kontinuirana izloženost oscilirajućim uvjetima, unutarnjim i vanjskim, predstavljaju izazov za očuvanjem uravnoteženog proteoma što regulirano proteostatskom mrežom. Najistaknutiji segment navedene mreže su molekularni šaperoni koji uslijed svoje dinamičnosti i raznolikosti omogućavaju stabilizaciju proteina. Separacijom stanice u zasebne odjeljke stečeni su pripadajući šaperoni karakteristični za svaki organel. Kompartmentalizacijom eukariotske stanice je omogućeno uspostavljanje te očuvanje proteostaze u izdvojenim odjeljcima. Ova činjenica je bila poticaj za proučavanje utjecaja poboljšanja i pogoršanja proteostaze u izdvojenim staničnim odjeljcima na stanicu. Obuhvatnim i detaljnim eksperimentima je pokazano da modifikacija proteostaze, bilo delecijom ili overekspresijom pojedinih šaperona, kulminira produljenjem replikativnog životnog vijeka, neovisno o ishodištu same modifikacije. Pretpostavka ovog istraživanja je da je ovaj cijelo-stanični odaziv proveden kroz raspoznavanje i korespondenciju konformacijske vrsnoće proteoma u zasebnim staničnim odjeljcima, odaziv formuliran u ovoj studiji kao odaziv na stres kroz organele (CORE).

(149 stranica, 68 slika, 19 tablica, 192 literaturnih navoda, izvornik napisan na engleskom jeziku)

Rad je pohranjen u:

- Nacionalnoj sveučilišnoj knjižnici u Zagrebu
- Sveučilišnoj knjižnici u Splitu
- Knjižnici Prirodoslovno-matematičkog fakulteta Sveučilišta u Splitu

Ključne riječi: molekularni šaperoni, poboljšanje proteostaze, pogoršanje proteostaze, Snf1, TOR

Mentor: dr.sc. Anita Kriško

Ocjenjivači: 1. prof. dr. sc. Katarina Vukojević, dr. med.

2. prof. dr. sc. Irena Drmić Hofman

3. prof. dr. sc. Biljana Balen

Rad prihvaćen: 21. listopada 2020.

# Table of Contents

1. INTRODUCTION.....	1
1. Cellular proteostasis system.....	1
1.1 The proteostasis network.....	1
1.2 Protein biogenesis.....	2
1.3 Protein folding.....	3
1.4 Assisted protein folding.....	4
1.5 Chaperones.....	5
1.5.1 HSP70 system.....	7
1.5.2 HSP90.....	7
1.5.3 HSP100.....	8
1.5.4 Noteworthy compartmentalized molecular chaperones.....	9
1.5.5 sHSPs.....	9
1.6 Degradation.....	10
1.7 Sequestration of damaged proteins.....	11
1.8 Preservation of cellular proteostasis.....	12
1.8.1 Heat shock response.....	13
1.8.2 Unfolded protein response.....	13
1.9 Failure to preserve cellular proteostasis.....	14
1.10 Aging.....	15
1.10.1 Free-radical theory of aging.....	15
1.10.2 Conformational diseases.....	16
1.11 Yeast as an eukaryotic model organism.....	17
1.12 <i>Saccharomyces cerevisiae</i> – the budding yeast.....	18
1.12.1 General overview.....	18
1.12.2 Growth phases.....	19
1.12.2.1 Lag phase.....	20
1.12.2.2 Exponential phase.....	20
1.12.2.3 Diauxic shift.....	21
1.12.2.4 Post-diauxic phase.....	21
1.12.2.5 Stationary phase.....	21
1.12.3 Nutritional physiology.....	21
1.12.3.1 Glucose sensing pathways.....	22
1.12.3.2 Sensing and import of glucose.....	22
1.12.3.4 Glucose induction and repression.....	23
1.12.3.5 cAMP/PKA pathway.....	25
1.12.3.6 Target of Rapamycin (TOR) pathway.....	25
1.12.3.6.1 TORC1.....	26
1.12.3.6.2 TORC2.....	27
1.12.3.7 Convergence of nutrient sensing mechanisms.....	28
1.12.4 <i>S. cerevisiae</i> as a model organism for aging.....	28
1.12.5 Replicative lifespan measurement.....	30
1.12.6 Chronological lifespan measurements.....	30
1.12.7 Hallmarks of aging in yeast.....	30

1.12.8 Longevity regulation in yeast.....	32
2. MATERIALS AND METHODS.....	34
2.1 Materials.....	34
2.1.1. Reagents.....	34
2.1.2. Buffers.....	36
2.1.3. Kits.....	39
2.1.4. Antibodies.....	39
2.1.6. Oligonucleotides.....	40
2.1.7. Media.....	42
2.1.8. Plasmids and fluorophores.....	43
2.1.10. Consumables and laboratory equipment.....	44
2.1.11. Software and databases.....	44
2.1.12. Strains.....	45
2.2. METHODS.....	46
2.2.1 Yeast culture.....	46
2.2.1.1 Cultivation and growth conditions.....	46
2.2.1.2 Growth rate analysis.....	46
2.2.1.3 Replicative lifespan measurements.....	47
2.2.1.4 Chronological lifespan measurements.....	48
2.2.1.5 Yeast cell fixation.....	48
2.2.2 Molecular biology.....	49
2.2.2.1 DNA extraction.....	49
2.2.2.2 Plasmid extraction from <i>S. cerevisiae</i> .....	49
2.2.2.3 Plasmid extraction from <i>E. coli</i> .....	49
2.2.2.4 Chaperone inactivation procedure.....	50
2.2.2.4 PCR: polymerase chain reaction.....	51
2.2.2.5 Enzymatic manipulation of DNA.....	52
2.2.2.6 Yeast transformation experiments.....	54
2.2.2.7 Metabolic labeling of nascent proteins with L-AHA.....	54
2.2.3 RNA methods.....	55
2.2.3.1 Preparation of yeast RNA extract.....	55
2.2.3.2 Quantitative real-time PCR.....	55
2.2.3.3 RNA Sequencing and analysis.....	55
2.2.3.4 Feature counting.....	56
2.2.3.5 Differential expression analysis.....	56
2.2.4 Protein extraction and analysis.....	57
2.2.4.1 Preparation of yeast protein extracts.....	57
2.2.4.2 Protein concentration measurement.....	57
2.2.4.3 Protein carbonylation measurement.....	58
2.2.4.4 SDS - PAGE and Western Blotting.....	58
2.2.5 Mitochondrial methods.....	59
2.2.5.1 Isolation of mitochondria.....	59
2.2.5.2 Blue Native-PAGE.....	59
2.2.5.3 Analysis of the mitochondrial morphology and protein import apparatus.....	60
2.2.6 Biochemical procedures.....	60
2.2.6.1 Respiration measurement.....	60



2.2.6.2 Geldanamycin treatments.....	60
2.2.6.3 Torin treatments.....	61
2.2.5 Fluorescence microscopy.....	61
2.2.5.1. Flow cytometry.....	61
2.2.5.2 ROS measurement.....	61
2.2.5.3 Measurement of Mitochondrial Mass.....	61
2.2.5.4 Assessment of mitochondrial membrane potential.....	62
2.2.5.5 Overexpression level measurement.....	62
2.2.6 Imaging.....	63
2.2.6.1 Microscope slide preparation.....	63
2.2.6.2 Live cell imaging and analysis.....	63
2.2.7 Statistical analysis.....	63
3. RESULTS.....	65
3.1 Part I: Mild proteotoxicity ensuing chaperone deletions leads to cross-organelle stress response (CORE) resulting in lifespan extension.....	65
3.1.1 Chaperone deletion in any cellular compartment induces cell-wide protein stress.....	65
3.1.2 Compartmentalized failure of proteostasis results in respiration decline.....	66
3.1.3 Compartmentalized proteotoxicity mediates a cell-wide response.....	70
3.1.4 CORE pathway induces a variable change in the components of the RC complexes.....	74
3.1.5 Chaperone deletion results in mitochondrial fragmentation.....	75
3.1.6 Hsf1 incompletely involved in regulation of the CORE pathway.....	80
3.1.7 Chaperone deficient strains evince extended lifespan.....	82
4.1 DISCUSSION PART I.....	85
4.1.1 CORE pathway elicits upregulation of cellular maintenance genes.....	85
4.1.2 CORE pathway alters the expression of metabolic genes.....	87
4.1.3 CORE pathway activation results in impaired mitochondria.....	89
4.1.4 CORE pathway activation is an improbable response to faulty protein import.....	90
4.1.5 CORE pathway activation results in lifespan extension.....	91
4.1.6 CORE pathway activation does not result in retrograde response nor the HSR activation.....	92
3.2 Part II: Mild proteotoxicity ensuing chaperone overexpressions leads to glucose starvation-like response resulting in lifespan extension.....	95
3.2.1 Chaperone enrichment leads to the alleviation of protein misfolding.....	96
3.2.2 Chaperone enrichment induces a glucose starvation-like response.....	99
3.2.3 ChES display enhanced oxygen consumption resulting from increased mitochondrial mass.....	101
3.2.4 Snf1 activation is required for observed glucose starvation-like response in the ChES.....	104
3.2.5 ChES response leads to the deactivation of TORC1.....	106
3.2.6 Snf1 activation in ChES is dependent on Tor1 deactivation.....	108
3.2.7 Pivotal features of ChES response are evoked by Tor1 deactivation.....	112
3.2.8 TORC1 is activated upon Hsp82 chaperone overexpression.....	115
3.2.8 Hsp82 chaperone downregulation is the initiating event preceding chaperone enrichment.....	118
3.2.9 Chaperone enrichment leads to the extension of RLS.....	120
3.2.10 Snf1/AMPK activation is required for chaperone-mediated RLS extension.....	121

4.2 DISCUSSION PART II.....	124
4.2.1 Enrichment of studied chaperones elicits mitigation of protein misfolding.....	124
4.2.2 ChES display metabolic paradigm suggestive of glucose-starvation response.....	125
4.2.3 Snf1 kinase is negatively regulated by Tor1.....	126
4.2.4 ChES response relies on Tor1 deactivation.....	127
4.2.5 Hsp82 chaperone mediates the proteome quality to TORC1.....	127
4.2.6 Replicative lifespan extension in ChES is contingent on increased respiration.....	128
5. CONCLUSION.....	130
6. BIBLIOGRAPHY.....	133
CURRICULUM VITAE.....	148
LIST OF PUBLICATIONS.....	150

## List of figures

Figure 1	Representation of proteostasis network in the cell .....	2
Figure 2	The energy landscape of protein folding .....	4
Figure 3	Progression of polypeptide chains .....	5
Figure 4	Representation of 50 chaperone families .....	6
Figure 5	Proposed mechanism of action for Hsp26 and Hsp42 .....	10
Figure 6	Illustration of cycle of progressive augmentation .....	14
Figure 7	Depiction of protein carbonylation .....	16
Figure 8	Depiction of <i>Saccharomyces cerevisiae</i> .....	18
Figure 9	Graphical representation of <i>S. cerevisiae</i> 's growth phases .....	20
Figure 10	Illustration of glucose induction and repression mechanism .....	23
Figure 11	Regulation of Snf1 in response to glucose availability .....	24
Figure 12	Depiction of Mig1 mode of action in response to glucose availability .....	25
Figure 13	Structure of TORC1 .....	27
Figure 14	Structure of TORC2 .....	27
Figure 15	Convergence of nutrient-sensing pathways .....	28
Figure 16	Illustration of replicative and chronological lifespan in yeast .....	29
Figure 17	Depiction of comparison of symmetric division in old vs young yeast cells .....	31
Figure 18	Representative growth curve .....	47
Figure 19	Representation of RLS measurement .....	48
Figure 20	Schematic presentation of Ssc1 chaperone inactivation .....	50
Figure 21	Schematic presentation of Lh1 chaperone inactivation .....	50
Figure 22	Schematic presentation of Egd2 chaperone inactivation .....	50
Figure 23	Schematic presentation of Tcpl chaperone inactivation .....	51
Figure 24	Representation of homologous recombination .....	54
Figure 25	Principle component analysis-based filtering of RNASeq replicates .....	57
Figure 26	Deletion of chaperones induces protein stress characterized by increased HSP90 levels .....	66
Figure 27	Induced protein stress leads to a decline in respiration .....	67
Figure 28	Decline in respiration is not a result of defective RC complexes .....	68

Figure 29	Chaperone deficient strains exhibit a decline in MPP .....	69
Figure 30	Chaperone deletion induces a decrease in ATP levels without affecting the production of ROS .....	70
Figure 31	Expression levels of indicated genes .....	72
Figure 32	Compartmentalized proteotoxicity mediates a cell-wide response .....	74
Figure 33	CORE pathway induces a variable change in the components of the RC complexes .....	76
Figure 34	Chaperone deficient strains exhibit mitochondrial fragmentation .....	77
Figure 35	Chaperone deficient strains' mitochondrial protein import is not defected .....	78
Figure 36	Transcript levels of COA3-null mutant and WT treated with CCCP show a partial overlap with the chaperone deficient strains .....	80
Figure 37	Hsf1 incompletely involved in regulation of the CORE pathway .....	82
Figure 38	CORE pathway activation elicits replicative lifespan extension .....	84
Figure 39	Core pathway activation leads to chronological lifespan extension .....	85
Figure 40	Diagram illustrating the changes in gene expression that results in the modification of the citrate production .....	89
Figure 41	Fundamentals of mitohormesis .....	93
Figure 42	Illustration depicting sequence of events following chaperone deletions in yeast <i>Saccharomyces cerevisiae</i> .....	95
Figure 43	Overexpression levels of chaperones verified by flow cytometry.....	96
Figure 44	ChES exhibit alleviation of protein misfolding .....	98
Figure 45	ChES exhibit decreased tendency for protein aggregation .....	99
Figure 46	iChES exhibit increased tendency for protein aggregation .....	100
Figure 47	Chaperone enrichment induces a glucose starvation-like response .....	101
Figure 48	Chaperone enrichment induces increased oxygen consumption in ChES .....	102
Figure 49	Oxygen consumption eventuated from increased mitochondrial mass.....	104
Figure 50	Respiratory chain complexes remain unchanged in ChES .....	105
Figure 51	ChES display a significant increase in Snf1 levels .....	106
Figure 52	Snf1 deficiency abolishes oxygen consumption increase characteristic of ChES .....	107
Figure 53	Amount of newly synthesized proteins is decreased in ChES .....	108

Figure 54 Overexpression of studied chaperones leads to a reduction of phosphorylated Sch9 levels .....	109
Figure 55 Constitutive activity of Tor1 results in increased translation activity .....	110
Figure 56 Tor1 serves as a negative regulator of Snf1 .....	111
Figure 57 Tor1 deactivation is required for a response characteristic of ChES .....	112
Figure 58 Inhibition of TOR pathway results in significantly increased oxygen consumption .....	113
Figure 59 Tor1 deactivation necessary for ChES response .....	114
Figure 60 Torin treated $\Delta$ Snf1 mutant show decreased respiration and a downregulation of most metabolic activities .....	115
Figure 61 Overexpression of Hsp82 chaperone in ChES eliminates the increase in Snf1 activity observed previously .....	116
Figure 62 Overexpression of Hsp82 does not lead to an increase in protein translation observed in ChES .....	118
Figure 63 Inhibition of Hsp82 chaperone leads to differential gene expression shifts comparable to ChES .....	119
Figure 64 Inhibition of Hsp82 chaperone leads to increased respiration .....	120
Figure 65 Chaperone enrichment leads to replicative lifespan extension .....	122
Figure 66 RLS extension is contingent on Snf1 activation and TOR deactivation, and is attributable to respiration increase in ChES .....	123
Figure 67 Schematic representation of sequence of events following chaperone enrichment .....	130
Figure 68 Schematic representation of compendium from both studies .....	133

## List of tables

Table 1 Reagents .....	35
Table 2 Buffers and solutions .....	37
Table 3 Kits .....	40
Table 4 Primary antibodies .....	40
Table 5 Secondary antibodies .....	41

Table 6 Oligonucleotides used for qPCR .....	41
Table 7 Oligonucleotides used for cloning .....	43
Table 8 Media composition .....	43
Table 9 Plasmids .....	44
Table 10 Fluorophores .....	44
Table 11 Laboratory materials and equipment .....	45
Table 12 Software .....	45
Table 13 Databases .....	46
Table 14 Yeast strains .....	46
Table 15 Bacterial strains .....	47
Table 16 PCR conditions and compositions .....	52
Table 17 PCR program used .....	52
Table 18 Restriction digestion reaction .....	53
Table 19 Ligation reaction .....	54

## List of abbreviations

AMPK	AMP-activated protein kinase
ALS	Amyotrophic lateral sclerosis
ATP	Adenosine triphosphate
AUC	Area under the curve
cAMP	cyclic AMP
caTor1	constitutively active Tor1
CCCP	Carbonyl cyanide m-chlorophenylhydrazone
ChESs	Chaperone enriched strains
CIC	Mitochondrial citrate transporter
CLS	Chronological lifespan
CORE	Cross-organelle stress response

CR	Calorie restriction
CS	Citrate synthase
DNA	Deoxyribonucleic acid
ER	Endoplasmic reticulum
ERAD	ER - associated degradation
ERAD-L	ERAD luminal
ERQC	ER quality control
GSH	Glutathione
HSF	Heat shock factor 1
Hsp	Heat shock protein
HSR	Heat shock response
iChESs	Strains enriched with inactivated chaperones
IRE-1	Inositol requiring enzyme-1
Lhs1	Lumen Hsp seventy
MMP	Mitochondrial membrane potential
NAC	Nascent polypeptide-associated complex
NBD	Nucleotide binding domain
OXPHOS	Oxidative phosphorylation
PC	Protein carbonylation
PN	Proteostasis network
PKA	Protein kinase A
PP1	Protein phosphatase 1
PQC	Protein quality control
RC	Respiratory chain
RLS	Replicative lifespan
RNA	Ribonucleic acid
ROS	Reactive oxygen species
SBD	Substrate binding domain
sHsps	small heat shock proteins

Snf1	Sucrose non-fermenting 1
Ssc1	Stress-seventy subfamily C 1
Sod1	Mitochondrial manganese superoxide dismutase
Sod2	Cytosolic copper-zinc superoxide dismutase
TCA	Tricarboxylic acid
Tcp1	Tailless complex polypeptide 1
TOR	Target of rapamycin
TORC1	TOR complex 1
TORC2	TOR complex 1
UPR	Unfolded protein response
UPS	Ubiquitin proteasome system
WT	Wild-type



# 1. INTRODUCTION

## 1. Cellular proteostasis system

Proteins, versatile and complex macromolecules involved in nearly every biological process, are considered to be a crucial factotum of every cell. Their engagement in cellular functions ranges from transport, signaling, movement to regulation, and catalysis of chemical reactions. In order for the cell to function properly, it relies on the constant precise quality control mechanisms to effectively regulate and maintain the stability of all cellular proteins, referred to as the proteome. The maintenance of the proteome stability is commonly known as protein homeostasis or proteostasis, and it is considered to be inseparably linked to lifelong health and survival of the cell. However, numerous intrinsic and environmental conditions pose a threat to the integrity of the proteome. Harsh intracellular conditions, such as macromolecular crowding, formation of reactive oxygen species (ROS), and constant emergence of partially folded nascent polypeptide chains that have the propensity to aggregate, continuously expose proteins to damage and, consequently, challenge the maintenance of proteostasis (Milardi & Rizzarelli, 2011). These challenges, under optimal conditions, are surmounted by an elaborate system of fine-tuned mechanisms comprised of intertwined cellular machinery networks, some of which include: biosynthesis, folding, assembly/disassembly, trafficking and clearance (Morimoto, 2008).

### 1.1 The proteostasis network

Eukaryotic cells of higher mammals, such as humans, express more than 10,000 different proteins at any moment (Klaips, Jayaraj, & Hartl, 2018). Given that cellular proteome is not permanently established, as it adjusts to adapt to various intrinsic and extrinsic conditions, it puts a strain on sustaining its functional integrity. This proteome cohesion, the proteostasis, is achieved by continuously maintaining the balance between folding, misfolding and, ultimately, degradation or aggregation of the cellular proteins. The system accountable for maintaining the balance is collectively known as the proteostasis network (PN) (Sala et al., 2017).

Whilst proteostasis is ultimately governed by a number of modulating mechanisms, the PN can be partitioned into four prominent assemblies (Figure 1), intricately reciprocated by the network of molecular chaperones:

- protein biogenesis

## INTRODUCTION

- protein folding and conformational maintenance
- degradation of damaged proteins
- sequestration of damaged proteins (Klaips et al., 2018; Sampaio-Marques, Ludovico, & Ludovico, 2018)

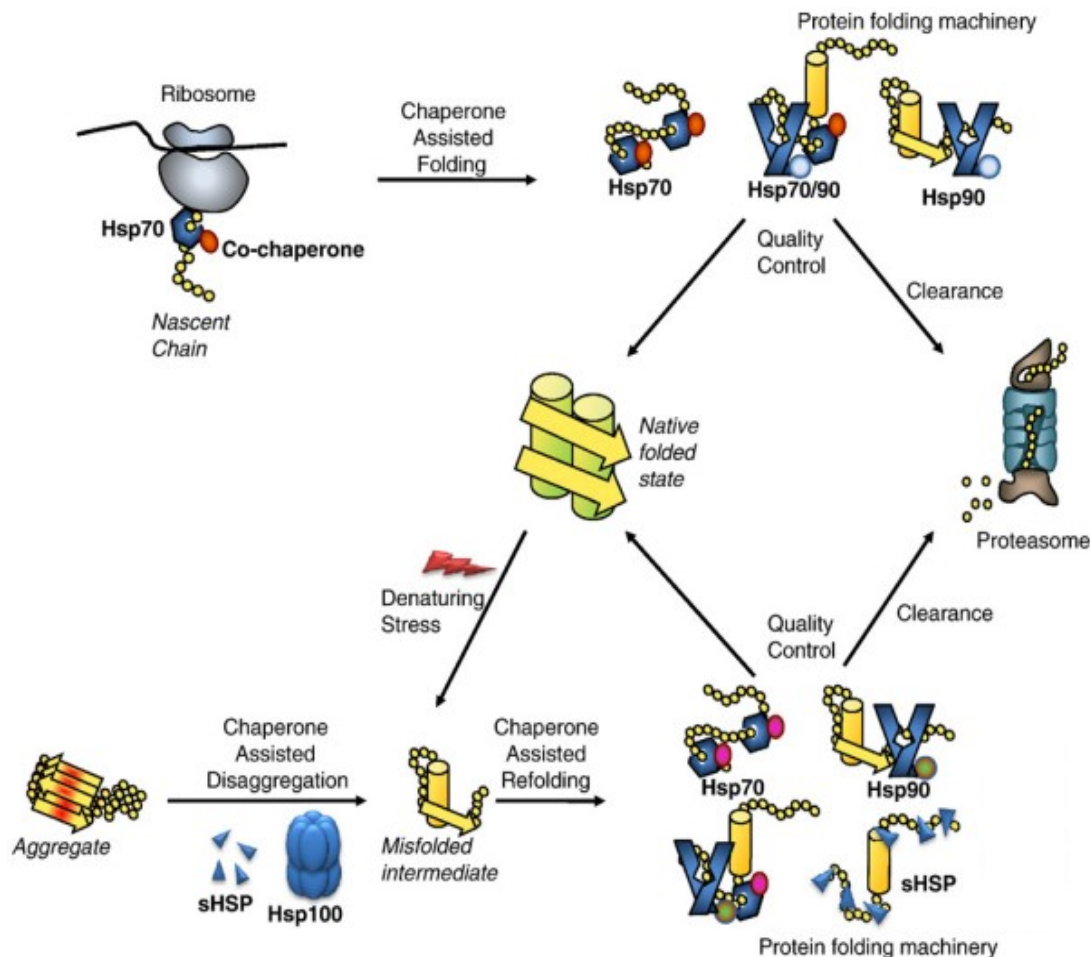


Figure 1| **Representation of proteostasis network in the cell** (adapted from Voisine, Søndergaard Pedersen, & Morimoto, 2010).

### 1.2 Protein biogenesis

In the cell, mRNA-directed protein synthesis takes place on organelles known as ribosomes from the genetic information encoded within the nucleic acid. Eukaryotic ribosome is an 80S macromolecular assembly consisting of 2 subunits; the 40S small and 60S large subunit. Both subunits are built from 80 ribosomal proteins and 4 RNA chains (Yusupova & Yusupov, 2017). The protein synthesis starts at the peptidyl transferase center (PTC) located on the large

ribosomal subunit. It is a site of peptide bond formation, where the PTC catalyzes the covalent bond formation between the amino acids (Polacek, Norbert & Mankin, 2005). As the polypeptide chain is being elongated, it extends through a nascent peptide exit tunnel (NPET) which originates at PTC and traverses the large subunit (Klepacki et al., 2011; Lu & Deutsch, 2005). This tunnel is 100Å long, with a diameter between 10 and 20Å which allows for the formation of  $\alpha$ -helical structure within the ribosome (Zhang & Rospert, 2013). Since proteins are unable to attain their native structure within the ribosome, the efficient folding ensues after the polypeptide synthesis.

### 1.3 Protein folding

The proper function for most proteins relies upon a correct fold into a native three-dimensional structure that is unique for each protein. Even though some parts of proteins can, in principle, be folded co-translationally while the nascent polypeptide chain is still attached to the ribosome, the majority of proteins attain their most thermodynamically-stable native conformation in the cytosol, endoplasmic reticulum (ER) or the mitochondria (Dobson, 2004).

It has been thought previously that the folding process involves obligatory steps in the intermediate folded states, however it is now clear that it is a stochastic search of the conformations attainable by the proteins (Dobson, 2003). The energy surface, or ‘landscape’ of protein folding can be represented by a funnel, which the newly synthesized polypeptide backbone enters (Dobson, 2003). In the descending trajectory of the funnel, the proteins fold into energetically favorable conformation, resulting in the overall lessening in energy and increase in entropy (Figure 2) (Dobson, 2004).

Although small polypeptide chains can obtain correct conformation within few milliseconds, the unaided biosynthesis of large complex proteins can take up to several hours, leaving their hydrophobic side chain exposed to interact with the crowded cellular environment, making them prone to aggregation (Hartl et al., 2011; Milardi & Rizzarelli, 2011; Svetlov, 2005). In order to avoid that, protective assistance that results in expedited protein folding is adopted. This assistance partly consists of molecular chaperones.

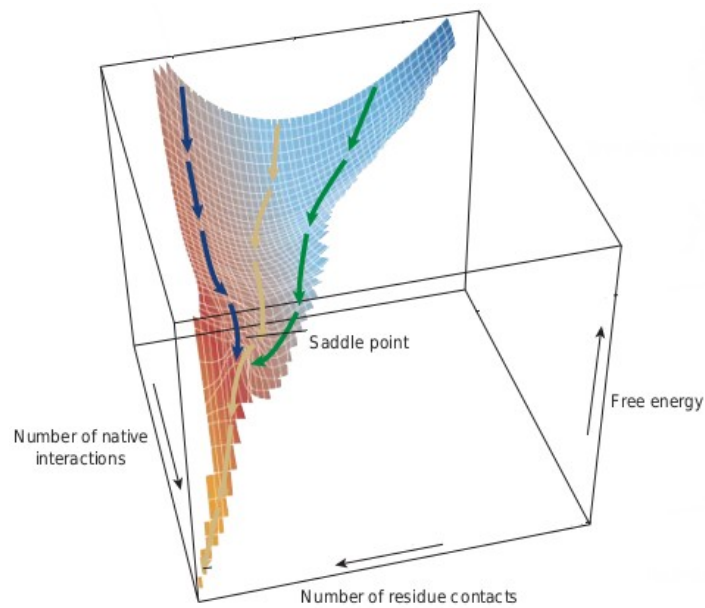


Figure 2| **The energy landscape of protein folding.** Funnel-view depicting the protein folding process as the proteins fold into their native structure, reaching the most favorable state of low energy. Given that the native conformation is more stable than the denatured one, this stochastic search mechanism effectively attains the lowest energy structure (adapted from Dobson, 2004; Dobson, Šali, & Karplus, 1998).

#### 1.4 Assisted protein folding

Thousands of different proteins are synthesized in a cell each minute, and they all require to attain a correct native conformation in order to function properly. Since protein folding is typically not a spontaneous process, most proteins call for a robust molecular chaperone network to safeguard efficient fold (Hartl & Hayer-Hartl, 2002). The modus operandi of molecular chaperones is to bind to the exposed hydrophobic area of the unfolded protein, thereby preventing the non-productive folding step, without remaining a constituent in the final protein configuration (Deuerling & Bukau, 2004). The binding of the chaperone physically prevents the intramolecular misfolding, as well as the intermolecular aggregation (Hartl & Hayer-Hartl, 2002). Figure 3 depicts the folding progression of the polypeptide chains, and all possible conformations they can attain during the, commonly named, folding funnel process. The roughness of the energy landscape indicates transient kinetically trapped conformations in local energy minimum, with energy barriers between conformational states (Onuchic et al., 1996).

These low-energy traps need to be overcome to resume the favorable folding path, and it generally requires chaperone activity (adapted from Hartl et al., 2011).

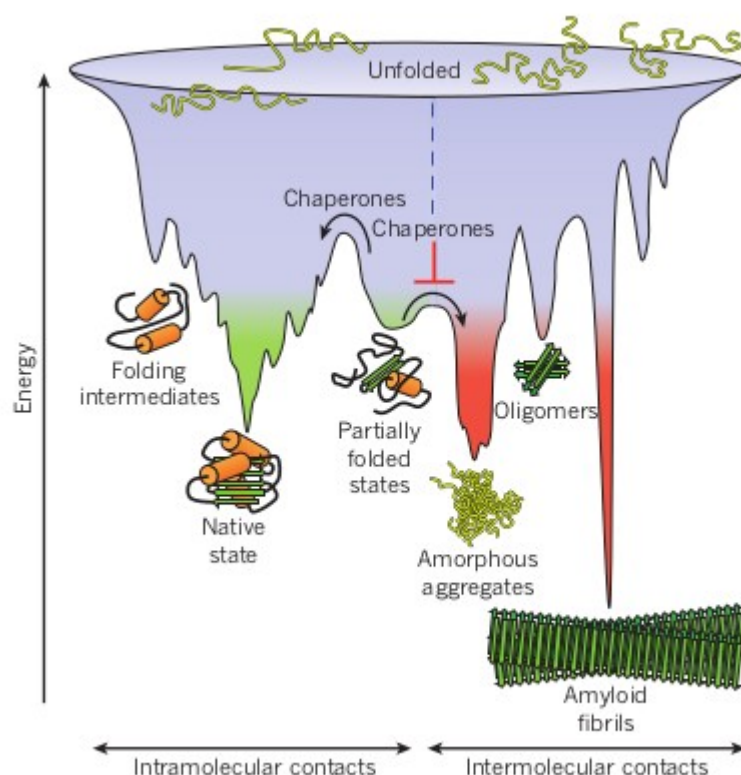


Figure 3| **Progression of polypeptide chains.** Folding funnel diagram that illustrates all attainable conformations in the energy landscape. These include unfolded, transient intermediates, partially folded, and aggregated states. It also shows the energy barriers which can be overcome by the assistance of molecular chaperones (Hartl et al., 2011).

### 1.5 Chaperones

The elaborate system of molecular chaperones consists of highly conserved specialized proteins that regulate folding and assembly of other proteins. They stabilize the protein by forming a non-covalent bond with hydrophobic residues and facilitate the folding process without altering the biologically active conformation. Chaperones were originally named “Heat shock proteins (HSP)” based on their abundant expression ensuing heat shock conditions, and were classified according to the molecular weight of their monomers; HSP100, HSP90, HSP70, HSP60, and small HSP (sHSPs). Aside from their involvement in the protein folding process, molecular chaperones have a pivotal role in miscellaneous aspects of proteome maintenance comprising of

## INTRODUCTION

assembly and disassembly, translocation, as well as aggregate degradation and refolding (Alderson, Kim, & Markley, 2016). In accordance with that, chaperones can be further categorized based on their interactions with the client proteins as ‘holdase’, ‘foldase’ or ‘disaggregase’ (Tiroli-Cepeda & Ramos, 2011). Holdases (HSP40, sHSPs) are a collection of chaperones that bind and ‘hold’ the unfolded or partially folded proteins, stabilizing it and preventing aggregation. They are ATP-independent, and their substrates are typically delivered to foldases. Foldases (HSP90, HSP70 and HSP60) are ATP-driven and they actively refold unfolded proteins. Disaggregases (HSP100) also rely on ATP hydrolysis to rescue aggregated proteins by breaking them up into smaller polypeptides which can then be transferred to holdase and/or foldase ensuing refolding (Kumar et al., 2015). There is a total of 63 different chaperone families identified in *Saccharomyces cerevisiae*, 50 of which are charted in the Figure 4 below, due to clustering of functionally identical ones.

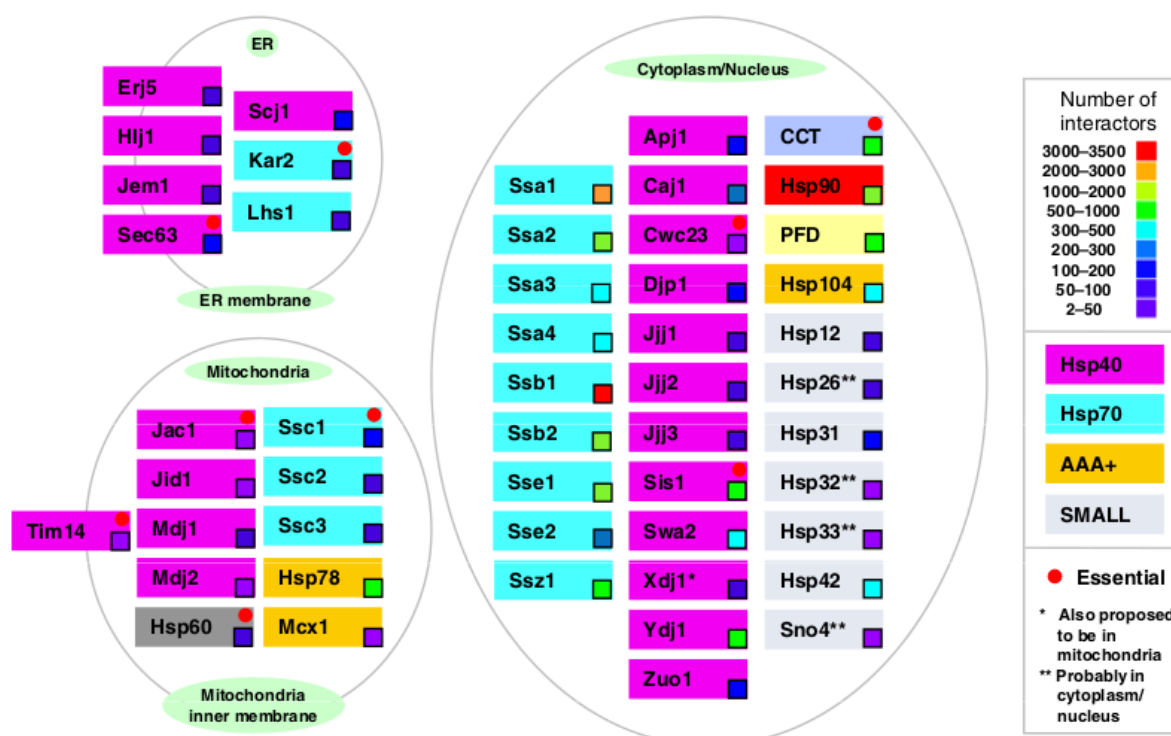


Figure 4| **Representation of 50 chaperone families recognized in *Saccharomyces cerevisiae*.** This chart illustrates subcellular formulation of chaperones, their molecular weight, types and names (adapted from Gong et al., 2009).

### 1.5.1 HSP70 system

Highly conserved family of chaperones, HSP70, are key organizers of folding and protein homeostasis control in the cell. They are abundant, comprising 1-2% of the cellular proteome, and are situated in various subcellular compartments (Figure 3.) (Tiroli-Cepeda & Ramos, 2011). The expression of genes in general can be constitutive, meaning that they are transcribed at a constant level, or induced in response to environmental conditions, such as heat shock. Constitutive forms of HSP70 (HSC70) are localized to cytoplasm and nucleus, while stress-inducible forms are found in mitochondria, ER, lysosomes, as well as cytosol and nucleus (Hartl et al., 2011). The family of HSP70 chaperones is involved in numerous cellular processes besides folding, some of which include refolding, translocation, assembly and disassembly.

HSP70 chaperone contains 2 domains: nucleotide binding domain (NBD) located at the N-terminus, and the substrate binding domain (SBD) located at the C-terminus (Tiroli-Cepeda & Ramos, 2011). The NBD is a 45 kDa ATPase consisting of two subdomains that encompass the ATP-binding site. The SBD is a 25 kDa domain, involved in recognition of the partially folded/unfolded client proteins. These client proteins are identified by the 5-residue motif found in the exposed hydrophobic regions that would be otherwise enclosed within the native protein fold (Fernández-Fernández & Valpuesta, 2018). This peptide binding domain is composed of two subdomains that have two distinct activity conformations – open and closed. The open conformation is activated with the binding of ATP, and it is induced in low affinity for client proteins, while the ATP hydrolysis closes the conformation, enabling entrapment of the substrate with high affinity (Fernández-Fernández & Valpuesta, 2018). These conformational changes, and the overall activity of the HSP70 chaperone is achieved by the allosteric coupling of the two domains.

The generally low basal process of the ATP hydrolysis is strongly amplified by the action of HSP40 (DnaJ) co-chaperone, the most important co-chaperone of HSP70. It is also involved in client protein targeting, and substantial change domain configuration (Alderson et al., 2016).

### 1.5.2 HSP90

HSP90 is an essential ATP-dependent molecular chaperone involved in various signaling pathways, such as signal transduction, telomere maintenance, apoptosis, cell cycle controls, as well as the conformational maintenance. Numerous signal-transduction molecules, such as



## INTRODUCTION

---

kinases, are transferred from HSP70 to HSP90 for finalization of protein folding, and they, together with the contribution of co-chaperones, such as tetratricopeptide repeat (TPR), form a dynamic multichaperone machine. This highly conserved chaperone is a pivotal regulator of proteostasis, maintaining the homeostasis in both physiological and stress conditions (Schopf et al., 2017).

HSP90 chaperone is encoded for by two distinct genes: HSP82 and HSC82 in budding yeast, and Hsp $\alpha$  and Hsp $\beta$  (also named Hsp90AA1 and Hsp90AB1) in humans (Schopf et al., 2017; Synoradzki & Bieganowski, 2015). This cytosolic chaperone operates as a dimer, consisting of a highly conserved ATP-binding N-terminal (30 kDa), substrate interactive C-terminal (20 kDa), and a flexible middle domain (35 kDa) that is involved in substrate binding (Hartl et al., 2011; Tirolì-Cepeda & Ramos, 2011). The structural rearrangement of the HSP90 domains functions much like the described HSP70 conformational change upon ATP binding/hydrolysis. Binding of ATP leads to compaction of monomers, while its hydrolysis causes the HSP90 domain disjunction (Hartl et al., 2011).

### 1.5.3 HSP100

Cells subjected to overwhelming amounts of stress are prone to protein aggregate formation, as the chaperone network becomes overloaded. These cytotoxic agglomerations can be rescued by HSP100 chaperone family, most notably HSP104 acting as a disaggregase.

It is a member of the AAA<sup>+</sup> (ATPase associated) superfamily, as it contains structurally conserved ~230 amino acid ATP-binding domain. Its functional form is a hexameric ring that forms a central tunnel through which aggregated protein substrates are translocated for disentanglement. Energy from ATP hydrolysis is used to extract entangled single polypeptide chain that will be further subjected to refolding or degradation. HSP104 chaperone strictly requires interaction with the HSP70 family, and their cooperation is essential for survival under stress conditions (Doyle et al., 2013; Mogk et al., 2018).



### 1.5.4 Noteworthy compartmentalized molecular chaperones

- Cytosolic Tcp1

Tailless complex polypeptide 1 (Tcp1), also referred to as T-complex 1, is an essential cytosolic chaperone belonging to the group II chaperonin family. It is involved in protein assembly, particularly of cytoskeletal proteins tubulin and actin (Ursic et al., 1994).

- Ribosome bound NAC

Nascent polypeptide-associated complex (NAC) is a heterodimeric protein that interacts with short nascent chain emerging from the ribosome exit tunnel. Located in the cytosol, it is the initial chaperone that associates with the polypeptide, protecting ~300 of its amino acid residues against damaging proteolytic processes. By doing so, polypeptide chain is prevented to (mis)fold prematurely. It consists of three subunits: alpha, beta1 and beta3, which are encoded by genes *EDG2*, *EDG1* and *BTT1* respectively (Bukau et al., 2000; Klaips et al., 2018; Preissler & Deuerling, 2012).

- Mitochondrial Ssc1

Belonging to the HSP70 family, stress-seventy subfamily C 1 (Ssc1) chaperone is involved in mitochondrial protein dynamics. Its primary roles include translocation of protein into the mitochondria and their subsequent folding (Verghese et al., 2012).

- Endoplasmic reticulum Lhs1

Lumen HSP seventy 1 (Lhs1) is an atypical member of the HSP70 family of molecular chaperones, as it functions as a ‘holdase’ chaperone. It is located in the lumen of ER, and it is involved in protein translocation into ER, as well as a critical contributor for reduction of thermal aggregation (Verghese et al., 2012).

### 1.5.5 sHSPs

Small heat shock proteins, or sHSPs, belong to the family of copious ubiquitous proteins that act as one of primary defense mechanism against proteotoxicity in stressful conditions (Tiroli-Cepeda & Ramos, 2011; Ungelenk et al., 2016). sHSPs family contains chaperones with masses varying from 12 to 43 kDa, with two most studied chaperones Hsp26 and Hsp42 (Verghese et al.,

## INTRODUCTION

2012). Both of these sHSPs help preventing the aggregation by binding to misfolded proteins to form soluble complexes, or help promote aggregation by binding to small aggregates and forming visible protein aggregates termed Q-bodies. It has been suggested that Hsp26 and Hsp42 prevent the formation of tight insoluble aggregates by sequestering partially unfolded proteins or emerging protein aggregates. Based on this mechanism of action, sHSPs are thought to act as both ‘holdases’ and ‘aggregases’ as they suppress aggregation and sequester protein aggregates assisting in their solubilization (Figure 5) (Ungelenk et al., 2016).

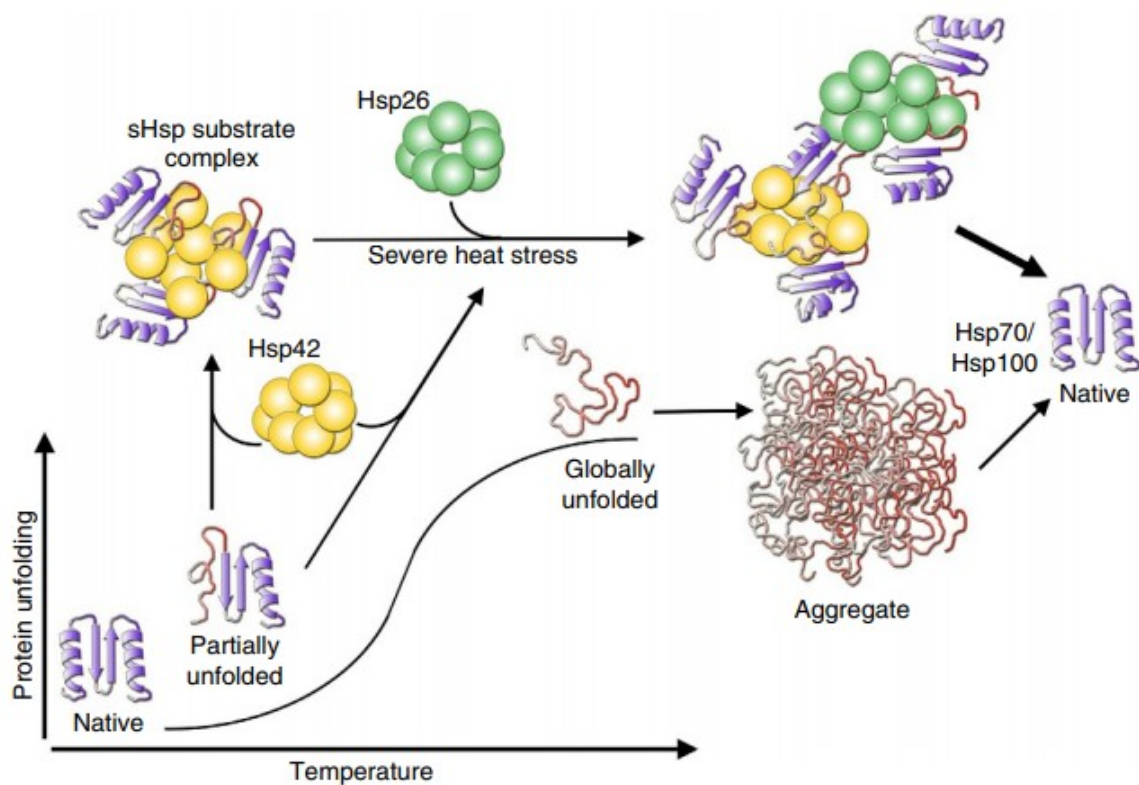


Figure 5| **Proposed mechanism of action for Hsp26 and Hsp42** (adapted from Ungelenk et al., 2016).

## 1.6 Degradation

Terminally misfolded proteins, either ones that failed to attain native state in due time or damaged proteins unable to refold, are eliminated by the processes of proteolytic degradation (Klaips et al., 2018). Two prominent proteolytic degradation systems that contribute to cellular homeostasis are ubiquitin proteasome system and autophagic/lysosomal system.

---

- The ubiquitin proteasome system (UPS)

One of the main degradation pathways involved in the regulation of protein quality control (PQC), UPS, consists of two main elements: the targeting and marking by the ubiquitination process and the degradation process at the proteasome.

Ubiquitination is the process of marking substrates destined for destruction by the proteasome. It involves the covalent bonding of a small heat-stable protein, ubiquitin, to misfolded substrate. Ubiquitin proteins have a propensity to self-conjugate, which results in the formation of polyubiquitin chains (B. Chen et al., 2011; Koga et al., 2011). These chains are recognized by the 19S regulatory cap of the proteasome, where the substrates are deubiquitinated and partially unfolded into nascent polypeptide chains. These nascent polypeptides can then be passed to the 20S proteolytic subunit of the proteasome for degradation (Ciechanover & Kwon, 2017; Sampaio-Marques et al., 2018).

The UPS process is also pivotal to the PQC in the ER, as it is involved in the degradation of misfolded proteins in the ER lumen (Sala et al., 2017). If the ER-associated degradation (ERAD) process fails, the autophagic/lysosomal system is activated (B. Chen et al., 2011; Ciechanover & Kwon, 2017).

- Autophagic/lysosomal system

In contrast to the UPS, which mediates degradation of small short-lived proteins, autophagy is a major degradation system for insoluble long-lived proteins and protein aggregates. This degradation process involves the formation of autophagosome, a double membrane vesicle that encapsulates the targeted clients, followed by its fusion to the vacuole (or lysosome in higher eukaryotes). The misfolded proteins transported by the autophagosome are released into the lumen of the vacuole for degradation by resident vacuolar hydrolases (Reggiori & Klionsky, 2013).

## 1.7 Sequestration of damaged proteins

When all aforementioned protective measures fail, spatial PQC provides the last line of defense for protein homeostasis regulation in the form of protein sequestration into aggregates. This facet of diverse processes of proteostasis was recently recognized due to the unexpected systematic distribution of damaged and aggregated proteins within the cell. Irreparable protein aggregates

## INTRODUCTION

---

tend to fuse into larger complexes referred to as inclusions (Hill et al., 2017). These inclusions frequently accumulate in two distinct PQC compartments:

- Juxta nuclear quality control site (JUNQ)
  - dynamic region exhibiting a rapid turnover of damaged proteins
  - abundant in 26S proteasomes and disaggregating molecular chaperones
  - proximal to perinuclear ER zone implicated in ERAD
  - targeted by ubiquitinated proteins
  - preferred spatial control site for damaged proteins (Hill et al., 2017; Kaganovich, Kopito, & Frydman, 2008)
- Peripheral, vacuole-associated insoluble protein deposit (IPOD)
  - substantially less dynamics
  - proximal to pre-autophagosomal structure
  - targeted by non-ubiquitinated proteins
  - spatial control site utilized in stress conditions or when JUNQ is overwhelmed (Hill et al., 2017; Rothe et al., 2018).

Recognition and clearance of inclusions from either of the spatial protective site requires the assistance of molecular chaperones, particularly HSP70s, HSP42, HSP90, and HSP104.

It was shown that the spatial sequestration of aggregated proteins not only limits their toxicity, but also ensures the retention of damaged proteins within the mother yeast cell, thus granting the succeeding generations to be damage-free.

### 1.8 Preservation of cellular proteostasis

Protein homeostasis relies on balance maintenance between folded and misfolded proteins. Life at optimal physiological conditions generates the continuous supply of misfolded and damaged proteins to the PN via inefficient translation, improper folding and translocation, or others, scantily perturbing the balance (Chen et al., 2011). It is, however, the suboptimal settings that are severely endangering the protein homeostasis. Those include, but are not limited to:

- environmental stressors – temperature fluctuation, nutrient deprivation
- metabolic stressors – oxidative stress, mitochondrial dysregulation, increase in protein biogenesis
- genetic diseases
- cancer

- 
- aging (Voisine, Søndergaard Pedersen, & Morimoto, 2010; Chen et al., 2011; Wang & Kaufman, 2016).

In order to ameliorate the impact of stress conditions and restore the homeostasis, cells retaliate by activating prompt and potent stress responses pathways which elevate the expression of proteostasis network constituents. Two well characterized response mechanisms are the heat shock response (HSR) and the unfolded protein response (UPR).

### 1.8.1 Heat shock response

HSR, a highly conserved defense mechanism, is activated seconds after stress exposure that resulted in disruption of proteostasis. It is the main pathway responsible for regulation of protein damage in cytosol and nucleus. The HSR is indirectly activated by the mechanism of stress detection in form of misfolded proteins. Its major regulator, the transcription factor heat shock factor 1 (HSF-1), is retained inactive under nonstress conditions by being bound to the HSP90 molecular chaperone. Upon detection of unbalanced levels of misfolded proteins, HSP90 is dissociated from HSF-1 and is recruited to assist in unfolding and refolding of denatured polypeptides. As it is no longer repressed, HSF-1 transcription factor is activated by trimerization, and translocated to the nucleus, where it activates the expression of HSR genes (Buchberger et al., 2010; Jovaisaite et al., 2014; Kyriakakis et al., 2015).

### 1.8.2 Unfolded protein response

UPR is responsible for detection of accumulated damaged proteins in the ER – referred to as  $UPR^{ER}$ , and the mitochondria – referred to as  $UPR^{mt}$ .  $UPR^{ER}$  is activated by the induction of signal transduction cascade commenced by the oligomerization of the transmembrane protein inositol requiring enzyme-1 (IRE-1). The oligomerization of IRE-1 ultimately leads to activation of gene expression involved in export and degradation of denatured proteins (Jovaisaite et al., 2014).  $UPR^{mt}$  has been observed in mammalian cells and nematodes as a protective mechanism of protein homeostasis in the organelle (Haynes & Ron, 2010).

### 1.9 Failure to preserve cellular proteostasis

Despite the elaborate machinery of proteostasis network and the potent nature of cellular stress responses, the perpetual accumulation of aberrant proteins inevitably overwhelms the constituents of the PN, ultimately leading to the collapse of proteostasis. The proteostasis decline in turn leads to proteotoxicity and cellular dysfunction incurred by agglomeration of protein aggregates. As depicted in Figure 6, accumulation of aberrant proteins in the cells caused by intrinsic or extrinsic stressors, mutation or aging, disrupts the proteostasis network machinery as the misfolded proteins compete for available chaperones. The decline in proteostasis consequently leads to a further increase in misfolded proteins, propelling a malicious cycle that progressively aggravates cellular health resulting in absolute collapse of proteostasis (Hipp et al., 2014; Radwan et al., 2017).

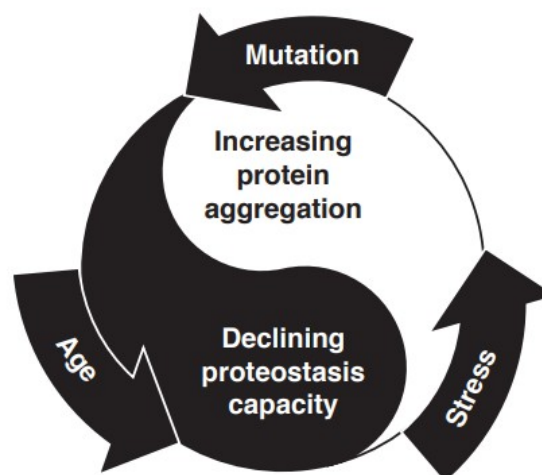


Figure 6| **Illustration of cycle of progressive augmentation.** A malicious cycle that leads to collapse of proteostasis and, ultimately, cellular dysfunction and death (adapted from Hipp et al., 2014).

Inability to reestablish proteostasis has been shown to be the hallmark of aging and the cause of many protein conformational diseases associated with deposition of misfolded proteins.

### 1.10 Aging

Aging could be defined as a progressive functional deterioration brought on by the accumulation of cellular damage that culminates in death. Due to the complex and multifaceted nature of aging, it has been difficult to develop a singular adequately unified theory to explain this process, which led to formulation of several theories describing particular concepts pertaining to aging. These theories can be categorized into two groups:

- programmed aging
  - assumes that aging process follows biological timetable which is genetically controlled, and it regulates systems accountable for homeostasis and defense response maintenance
- damage or error aging
  - assumes that accumulation of damage induced by different stressors as the cause of aging includes oxidative stress aging theory, somatic DNA damage theory, and telomere shortening (Oliveira et al., 2016).

The functional decline occurs on cellular as well as molecular level, not precluding proteins. The fact that proteins are no exception to this is of great importance, given that agglomeration of toxic aggregates and the loss of proteostasis are, almost universally, considered to be the distinguishing features of aging. In addition to proteostasis collapse and accumulation of aberrant proteins, mitochondrial dysfunction is also commonly associated with aging, and all of these age-related features are thought to be, in part, instigated by the increased generation of ROS. This gave rise to two aging theories most relevant to our research, and the following review will be focused on them.

#### 1.10.1 Free-radical theory of aging

Generation of ROS is an inevitable fundamental by-product of metabolism and aerobic respiration, therefore, life itself. Primary source is the mitochondrial electron transport chain that may leak electron to the surrounding oxygen, reducing it to form the primary free radical in mammalian cells - superoxide anion ( $O_2^-$ ). Increased production of ROS, in stress conditions or aging, may cause extensive damage to cellular macromolecules, such as DNA, lipids, and most importantly, proteins. The oxidative modification of proteins, most abundant macromolecules in the cells, alters their secondary and tertiary structures, rendering them dysfunctional or

## INTRODUCTION

nonfunctional, and can be reversible and irreversible. Reversible oxidation mainly impacts methionine and cysteine, which are the sulfur-containing amino acids. These modifications can be recovered by cellular antioxidant defense systems, such as glutathione (GSH), vitamins, and other small molecules (Korovila et al., 2017). The irreversible protein oxidation is accountable for majority of free radical-mediated damage, which may result in formation of toxic protein aggregates if not promptly degraded. The most prevalent type of irreversible protein oxidation is protein carbonylation (Figure 7). Direct oxidation of amino acid side chains of lysine, threonine, proline and arginine results in carbonyl derivatives which may be used as a marker for protein oxidation. It is this accumulation of proteins damaged by irreversible protein oxidation behind the conjecture of the free-radical theory of aging. Proposed by Harman, the theory suggests that progressive oxidative damage to the macromolecules overwhelms the proteolytic systems, and such extensive build-up leads to cellular dysfunction, aging and age-related neurodegenerative diseases (Harman, 1956).

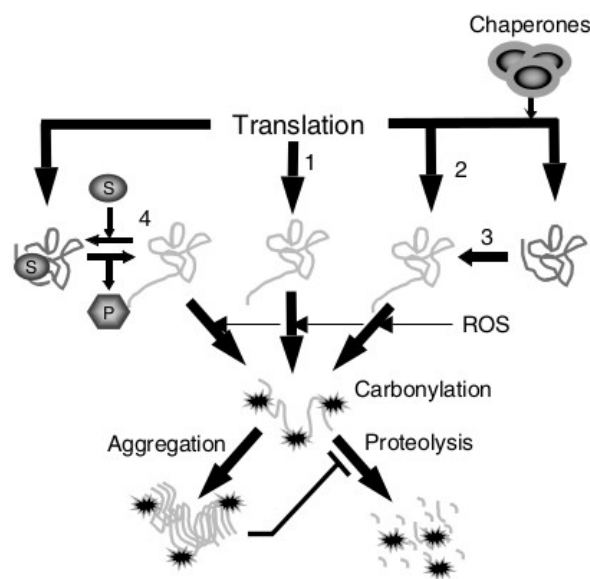


Figure 7| **Depiction of protein carbonylation.** Although irreversibly damaged proteins are marked for degradation by proteolytic systems, heavily carbonylated proteins form aggregates of high molecular weights inaccessible to proteases. This leads to a decline in cellular function, which in turn results in senescence and conformational diseases. (adapted from Nystrom, 2005).

### 1.10.2 Conformational diseases

As mentioned previously, the loss of proteostasis and accumulation of aberrant protein aggregates is a universal indicator of aging that is exacerbated with progression of time. This is



also recognized as a basis of many diseases referred to as protein conformational diseases that encompass more than 40 disorders (Gidalevitz et al., 2011; Surguchev & Surguchov, 2010). Although apparently completely unrelated, many diseases, such as Alzheimer's disease, cystic fibrosis, diabetes and cancer, can all be classified under the same category of conformational maladies. At the origin of these diseases is a common feature that proteins either fail to fold correctly or fail to remain correctly folded leading to formation of distinct intra- or extracellular proteinaceous inclusions devoid of  $\alpha$ -helices that contain high ratio of post-translational modifications (Surguchev & Surguchov, 2010; Vendruscolo et al., 2011; Yerbury et al., 2016). These diseases can be divided into two categories:

- neurodegenerative diseases
  - Alzheimer's disease, Parkinson's disease, Huntington's disease, amyotrophic lateral sclerosis (ALS), supranuclear palsy, and others
- non-neurodegenerative diseases
  - cystic fibrosis, type II diabetes, cancer, and even schizophrenia (Bader et al., 2012; Chiti & Dobson, 2006; Leliveld et al., 2008).

Understanding the underlying processes of proteostatic mechanism and its improvement could aid in prevention or alleviation of aforementioned diseases and even aging, and many of these could be studied using a simple single-celled organism – baker's yeast.

### 1.11 Yeast as an eukaryotic model organism

Almost 33 years ago, Botstein and Fink postulated whether yeast, eukaryotic single-celled microorganism, could be the ideal model organism for various research sectors (Botstein, Chervitz, & Cherry, 1997). Today, due to myriad advantages of yeast, that speculation has been transformed into a verifiable truth, as it came to be the most studied eukaryotic organism. Some of these advantages include the ease of culturing, highly versatile DNA transformation system, and the facility of genetic manipulation (Sherman, 1998).

On the premise that many basic components of the cell cycle mechanism have been conserved, it has been a paradigm to successfully study rudimentary processes in yeast and, consequently, understand complex processes in higher organisms (Gershon & Gershon, 2000). Out of two

## INTRODUCTION

species that have been widely used in research, *Schizosaccharomyces pombe* and *Saccharomyces cerevisiae*, the latter, used for this study, will be reviewed in greater detail.

### 1.12 *Saccharomyces cerevisiae* – the budding yeast

Yeast species that has been utilized since ancient times to convert sugar rich substrates into diverse palatable alcoholic beverages was given a fairly descriptive name – “*Saccharo-mycēs*” meaning “the sugar mold” and “*cerevisiae*” translating to “of beer” (Salari & Salari, 2017). It has also acquired colloquial names for the application of byproducts of fermentation process: “baker’s yeast” as carbon dioxide is used in baking for bread leavening, and “brewer’s yeast” for the ethanol used in brewing. In the scientific community, however, *Saccharomyces cerevisiae* is commonly referred to as the “budding yeast”, derived from the process of cellular division where the daughter cell resembles a bud (Figure 8).

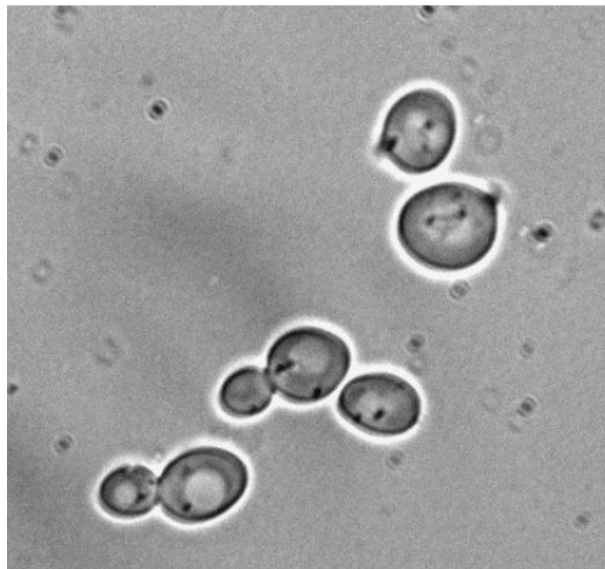


Figure 8| **Depiction of *Saccharomyces cerevisiae*** (adapted from Mauricio Valerio-Santiago, 2011).

#### 1.12.1 General overview

*S. cerevisiae* is a round to ovaloid eukaryotic unicellular organism belonging to the Kingdom Fungi, phylum *Ascomyota*, commonly located on the exterior of plants. Substantial risk of severe environmental changes precipitated by such habitat consequently led to an adaptation strategy in

form of a robust cell wall. It consists of two layers: the protective lattice of mannoproteins located on the outside, and the elastic and resilient layer of glucan polymers alongside chitin located on the inside (Levin, 2005). The cell wall accounts for 30% of dry weight of the cell, and it conserves the cell shape essential for the budding process (Lesage & Bussey, 2006).

It naturally occurs in 2 ploidities - haploids which mate to produce diploids, and diploids which undergo meiosis to produce haploids (Salari & Salari, 2017). Haploid cells display gender differentiation, as they exist in 2 mating types – type **a** and type  $\alpha$ . Difference between the two types is the form of pheromone produced, pheromone **a** or  $\alpha$ , to attract the opposite mating type. Both haploid and diploid yeast cells are also able to reproduce by asymmetrical budding during which a ‘mother’ cell produces a considerably smaller ‘daughter’ cell.

### 1.12.2 Growth phases

Cellular growth is a highly regulated process which can generally be split into quite distinct phases, and yeast cells are no different. When inoculated in nutrient rich medium, yeast cells exhibit disparate phases of growth (Figure 9)

- *lag phase* – initial adaptive phase in which cells are biochemically active, but not dividing, and are attuning to the new environment;
- *exponential phase* – the phase of rapid proliferation in which cells undergo fermentative growth consuming glucose or galactose and producing ethanol;
- *post-diauxic phase* – occurs after depletion of glucose carbon source and, if no other nutrient is limited, the cells switch from fermentative to respiratory-based growth on ethanol. This switch is referred to as the ‘diauxic shift’;
- *stationary phase* - phase entered upon complete nutrient exhaustion, cells are arrested in quiescent non-proliferating state (Busti et al., 2010; Stahl et al., 2004).

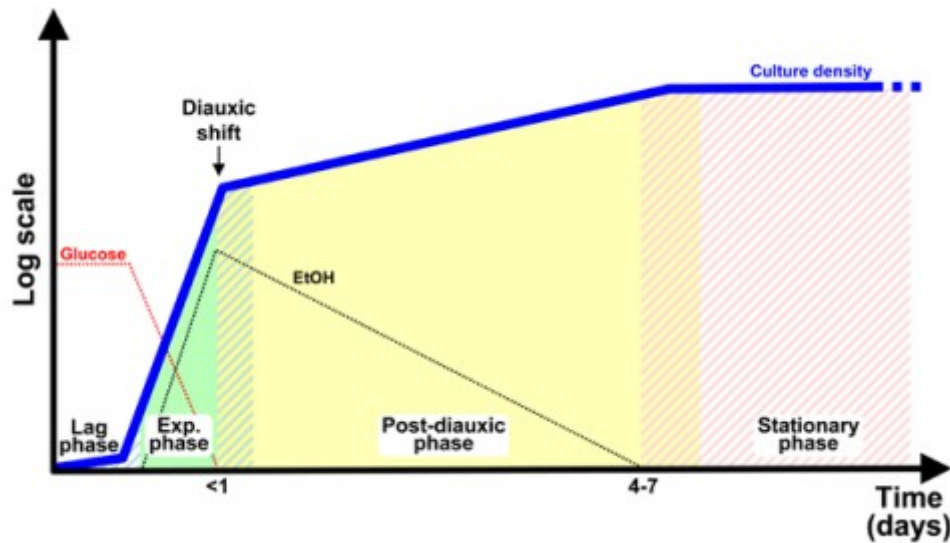


Figure 9| **Graphical representation of *S. cerevisiae*'s growth phases** (adapted from Busti et al., 2010).

#### 1.12.2.1 Lag phase

This growth phase is considered to be crucial for optimal utilization of consecutive fermentative growth. After the transfer to sugar rich media, yeast cells remain dormant as they adjust to their new environment by eliciting metabolic changes. These metabolic changes are induced by substantial modifications of gene expression, most notably those of translational machinery, RNA and protein synthesis and processing, as well as DNA synthesis and repair (Brejning et al., 2003).

#### 1.12.2.2 Exponential phase

Rapid proliferation phase is, almost unequivocally, considered the true uniform interval of growth with exceptionally steady pattern of gene expression. *S. cerevisiae* is, somewhat surprisingly, said to be a negative Pasteur effect yeast, meaning that it favors fermentative glucose metabolism over respiration in abundance of oxygen (Lloyd et al., 1983). This is also known as the Crabtree effect, or Warburg effect in mammalian cells, in which occurrence of energy-inefficient fermentation at high oxygen and glucose levels takes place (Alteriis & Carten, 2018).

#### 1.12.2.3 Diauxic shift

As the availability of the glucose in the medium decreases, yeast cells undergo fundamental reorganization of the cellular machinery, placing a transient halt on proliferation. This brief growth arrest, at which cells switch from fermentative to a fully respiratory metabolism, is referred to as the diauxic shift. It allows for aerobic catabolism of evolved ethanol that was accumulated during the exponential growth phase. This switch is achieved by a substantial change in all levels of cellular processes, most notably induction of respiration metabolism genes, and an almost complete destruction of translational machinery (Brauer et al., 2005; Derisi et al., 1997; Fuge et al., 1994; Stahl et al., 2004).

#### 1.12.2.4 Post-diauxic phase

The cell division resumption, following the diauxic shift lag period, is the onset of post-diauxic growth phase. This slow growth rate can last for several days, until the complete expenditure of ethanol, when the cells enter stationary growth phase.

#### 1.12.2.5 Stationary phase

With the depletion of a critical nutrient, yeast cells enter a quiescent state where cellular division truly ceases. This is followed by numerous biochemical, physiological and morphological changes, such as accumulation of glycogen and trehalose, thickened cell wall, accumulation of carbohydrates, chromosome condensation, and increased resilience to stress. This stage is the ultimate survival phase in starvation conditions.

### 1.12.3 Nutritional physiology

Harsh environmental conditions and fluctuating nutrient availability call for rapid intracellular responses that will allow organisms to adapt in order to thrive and survive. To conform to the ever-changing content of nutrients, the yeast *Saccharomyces cerevisiae* has evolved several nutrient-sensing and nutrient-controlling pathways. These coordinated mechanisms enable yeast cells to either arrest growth and enter quiescent stationary phase upon sensing nutrient depletion, or to transition quickly to the proliferating state taking advantage of accessible nutrients. The presence of nutrients dictates the growth rate of yeast cells and impacts their transcription, translation, metabolism and cellular development (Broach, 2012).

### 1.12.3.1 Glucose sensing pathways

Yeast are able to utilize a wide variety of nutrients and obtain energy either by fermentation of sugars, such as glucose, galactose, maltose and sucrose, or by oxidation of fermentation by-products, such as ethanol, lactate or glycerol (Zaman, Lippman, Zhao, & Broach, 2008). Glucose is, however, their preferred source of carbon and energy, and is consumed first due to the regulation of nutrient metabolism (Smets et al., 2010). Not only is glucose used for energy, it is also a key molecule in many signaling pathways involved in regulation of gene expression (Zaman et al., 2008). Those signaling pathways consist of glucose sensing, import and transport of glucose, and repression or induction of genes involved in metabolism.

### 1.12.3.2 Sensing and import of glucose

Extracellular levels of glucose are sensed by the glucose sensors Snf3 and Rgt2 located in the cell membrane. Seemingly no longer able to import glucose, these receptors produce an intracellular signal brought on by conformational changes upon glucose binding. It is thought that Snf3 is a high-affinity glucose sensor, meaning that it is induced by low levels of extracellular glucose, and its transcription is repressed in high glucose concentrations. On contrary, Rgt2 is a low-affinity sensor, expressed in conditions of high levels of extracellular glucose (Johnston, 1999). The regulation of transcriptional activity by these receptors enables yeast to attune glucose import in response to its extracellular concentrations (Kayikci & Nielsen, 2015).

Glucose import in the yeast cells is performed by facilitated diffusion through transmembrane proteins known as the hexose transporters. *S. cerevisiae* has at least 20 hexose transporters, encoded by the HXT genes, with varying affinity for glucose (Busti et al., 2010; Ozcan & Johnston, 1999). Low-affinity transporters, such as Hxt1, Hxt3 and Hxt4, permit growth in high glucose concentrations, and their transcription is induced by the intracellular signal generated by the Rgt2 sensor. On the other hand, high-affinity transporters, such as Hxt2, Hxt6 and Hxt7, are expressed when glucose is scarce, with concentrations below 0.1% (Figure 10). The signal for induction of high-affinity transporter genes is generated by the Snf3 sensor (Ozcan & Johnston, 1999).

### 1.12.3.4 Glucose induction and repression

Glucose can act as a positive or negative regulator of transcriptional activity as its presence determines expression or repression of particular genes. As mentioned previously, in the presence of glucose, availability signal is mediated by transmembrane sensors Snf3 and Rgt2, and glucose is imported via hexose transporters (Figure 10). This glucose induction leads to activation of SCF<sup>Grr1</sup> protein complex, which in turn inhibits the Rgt1 transcriptional repressor. Inhibition of Rgt1 induces the expression of *HXT* genes allowing greater glucose transport and utilization (Johnston, 1999). Presence of glucose also leads to inactivation of Snf1 kinase, whose inactivation leads to repression of genes involved in metabolism of alternative carbon sources, a process known as glucose repression (Smets et al., 2010).

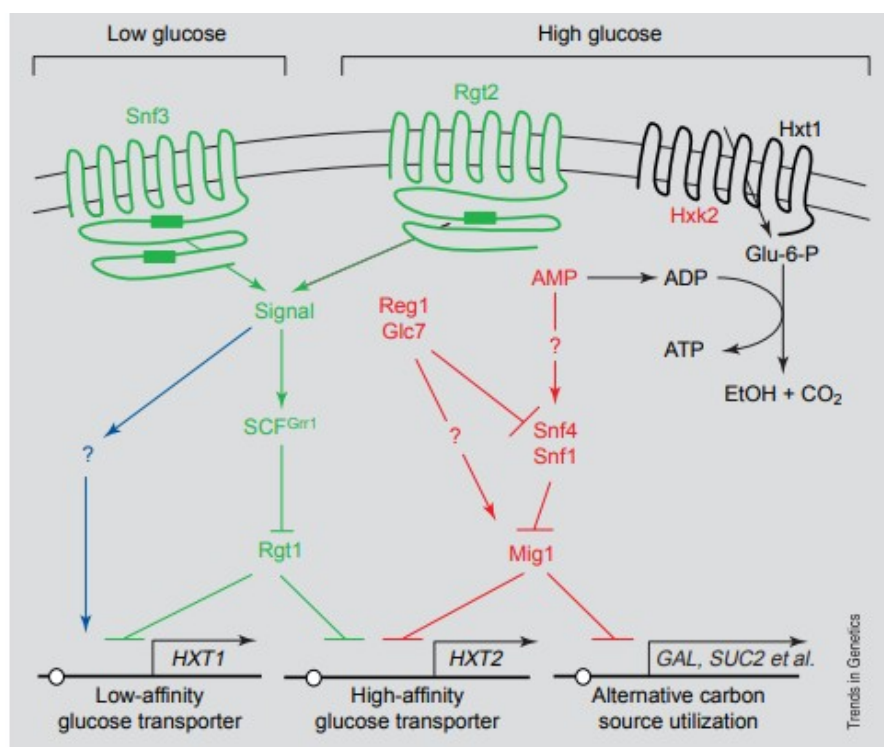


Figure 10| **Illustration of glucose induction and repression mechanism** (adapted from Johnston, 1999).

Central component of the glucose repression pathway is a serine/threonine protein kinase Sucrose non-fermenting 1 (Snf1), a highly conserved homologue of mammalian AMP-activated protein kinase (AMPK). Snf1 is a heterotrimer complex containing the Snf1 catalytic  $\alpha$ -subunit, one of Sip1, Sip2, Gal83  $\beta$ -subunits and the Snf4  $\gamma$ -subunit (Busti et al., 2010; Nayak et al.,



## INTRODUCTION

2006). The catalytic  $\alpha$ -subunit is composed out of catalytic domain (KD) and the regulatory domain (RD) (Gancedo, 1998).

In the high glucose conditions, when glucose repression is in effect, Snf1 kinase is kept inactive by the auto-inhibited conformational change brought on by binding of the KD and RD domains of the Snf1  $\alpha$ -subunit (Figure 11) (Busti et al., 2010).

The activated state of Snf1 kinase, in response to glucose depletion, is attained under two conditions:

- KD activation loop of Snf1  $\alpha$ -subunit is phosphorylated at a conserved threonine residue (T210)
- Snf4, with support of Sip1, Sip2 or Gal83, interacts with the RD of Snf1  $\alpha$ -subunit (Figure 11).

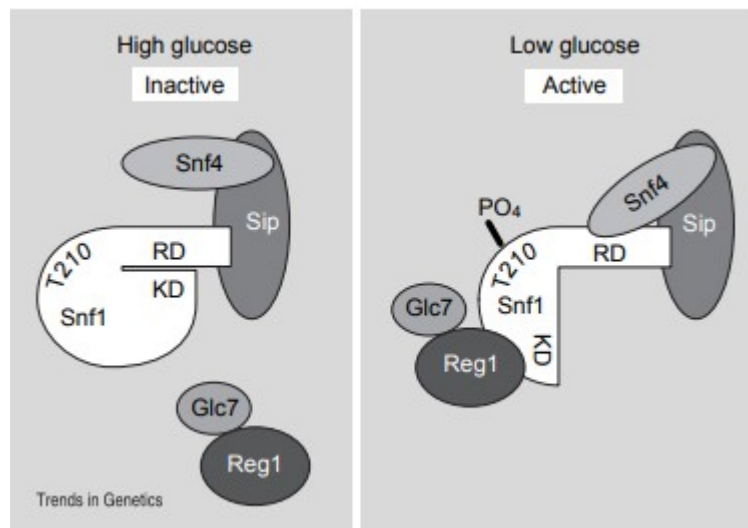


Figure 11| **Regulation of Snf1 in response to glucose availability** (adapted from Johnston, 1999).

Snf1 alters the transcriptional activity of genes primarily by modulating its downstream target – the transcriptional repressor Mig1 (Busti et al., 2010; Johnston, 1999). When glucose is available, Mig1 is localized in the nucleus, where it binds to the promoter of glucose-repressed genes inhibiting their expression (Figure 12). Upon glucose depletion, activated Snf1 phosphorylates Mig1 inhibiting its repressor function. Mig1, consequently, translocates into the cytoplasm causing the removal of glucose repression from several genes (Johnston, 1999; Smets et al., 2010).



Once glucose becomes available, Snf1 protein kinase is inactivated via rapid dephosphorylation by protein phosphatase 1 (PP1) complex comprised of Glc7 catalytic subunit and Reg1 regulatory subunit (Figure 12). As a result, Snf4 interaction with the regulatory domain of Snf1  $\alpha$ -subunit is inhibited, preventing its activation.

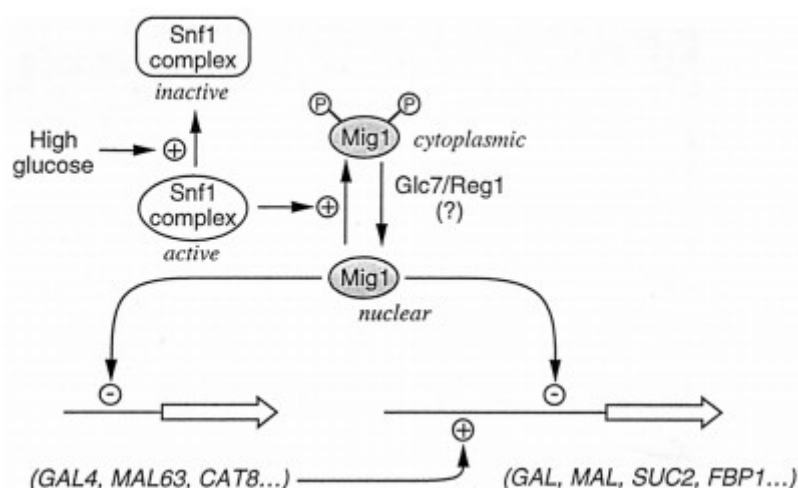


Figure 12| **Depiction of Mig1 mode of action in response to glucose availability** (adapted from Gancedo, 1998).

#### 1.12.3.5 cAMP/PKA pathway

cAMP/PKA pathway is a major signaling pathway positively activated by the extracellular glucose detection. It is involved in large number of cellular physiology scenarios, coordinating stress response, cell growth, proliferation and development (Busti et al., 2010). Protein kinase A (PKA) is heterotetramer essential for yeast viability (Smets et al., 2010). It is a conserved serine/threonine kinase composed out of 2 catalytic and 2 regulatory domains (Busti et al., 2010). It is activated upon import and phosphorylation of glucose due to the rapid increase in cyclic AMP (cAMP). cAMP binds to the regulatory subunit of PKA leading to the dissociation and activation of the catalytic subunit of PKA. Activation of the PKA pathway has been associated with decreased stress response and increased mRNA stability (Rolland et al., 2002).

#### 1.12.3.6 Target of Rapamycin (TOR) pathway

Target of Rapamycin (TOR) was identified while pursuing targets of the macrolide antifungal drug rapamycin, hence its name. It is a Ser/Thr protein kinase, highly conserved in eukaryotes from yeast to humans (Inoue & Nomura, 2018). It is also a central component of a nutritionally

## INTRODUCTION

---

controlled pathway that regulates transcriptional activity, lipid and protein synthesis, ribosome biogenesis, autophagy, aging, metabolism, stress response, cell cycle and cellular growth in response to availability and quality of nutrients in the environment. Unlike most eukaryotes that contain a single protein, yeast cells have 2 closely related ones – Tor1 and Tor2 (Smets et al., 2010). Both kinases are 282 kDa in size, and share 64% similarity to each other. They are also founding members of the phosphatidylinositol kinase-related protein kinase (PIKK) family as they contain a conserved lipid kinase motif (Ikai et al., 2011; Loewith & Hall, 2011). Tor1 and Tor2 kinases form two functionally and structurally distinct dimeric complexes referred to as TOR complex 1 (TORC1) and TOR complex 2 (TORC2).

### 1.12.3.6.1 TORC1

TORC1 regulates transient aspects of cellular growth primarily in response to the abundance and quality of nitrogen source in the environment. It is associated with mediation of essential functions of TOR mentioned previously. The dimeric complex is composed out of Kog1, Tco89 and Lst8 subunits and either Tor1 or Tor2 (Figure 13). It is thought to be localized on the vacuolar membrane, a main storage organelle of diverse metabolic compounds (Loewith & Hall, 2011).

While TORC1 is active, in response to abundance of amino acids, catabolic cellular processes, such as autophagy are inhibited, while anabolic processes, such as protein and lipid synthesis, are induced (Inoue & Nomura, 2018). Activated TORC1 regulates aforementioned cellular processes mainly via Sch9 protein kinase. Sch9 is one of the most distinguished downstream targets and the major component of TORC1 pathway, and it requires TORC1-mediated phosphorylation for activation (Loewith & Hall, 2011).

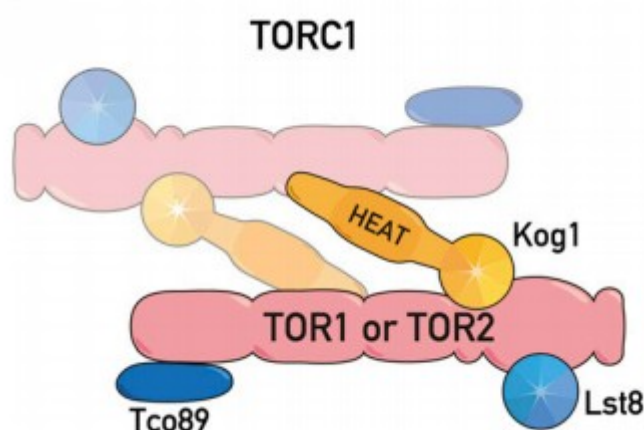


Figure 13| **Structure of TORC1** (adapted from Loewith & Hall, 2011).

#### 1.12.3.6.2 TORC2

Unlike TORC1, TORC2 is not inhibited by rapamycin, and is thus considerably less characterized. So far, it is understood that TORC2 is involved in mediation of spatial cellular elements, such as cell wall integrity regulation and control of actin cytoskeleton polarization (Ikai et al., 2011; Smets et al., 2010). TORC2 dimer contains only TOR2 together with Avo1, Avo2, Avo3, Tsc11, Lst8, Bit61 and Slm2 subunits (Figure 14). Its localization has so far been confirmed to the plasma membrane, and its major downstream target has been identified to be Ypk protein kinase (Loewith & Hall, 2011).

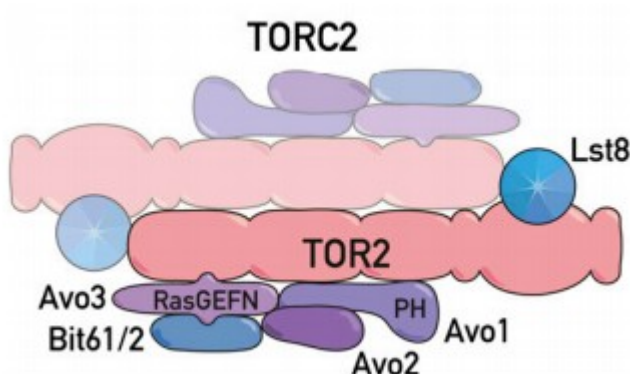


Figure 14| **Structure of TORC2** (adapted from Loewith & Hall, 2011).

One of the most intriguing function of TOR, or more precisely TORC1, is its implication in the regulation of lifespan, and the plausible potential for the extension of human life expectancy.

## INTRODUCTION

### 1.12.3.7 Convergence of nutrient sensing mechanisms

It was shown that all of these nutrient sensing pathways intersect and even regulate each other in order to survive or thrive according to nutrient availability (Figure 15) (De Virgilio, 2012). Although the cross-communication between signaling pathways remains yet to be fully elucidated, there are some recorded findings illuminating the entire concept. PKA and TORC1 were shown to antagonize each other, TORC1 activation prevents the activation of Snf1 and nuclear accumulation of PKA (Figure 15) (Orlova et al., 2006; Ramachandran & Herman, 2011; Soulard et al., 2010).

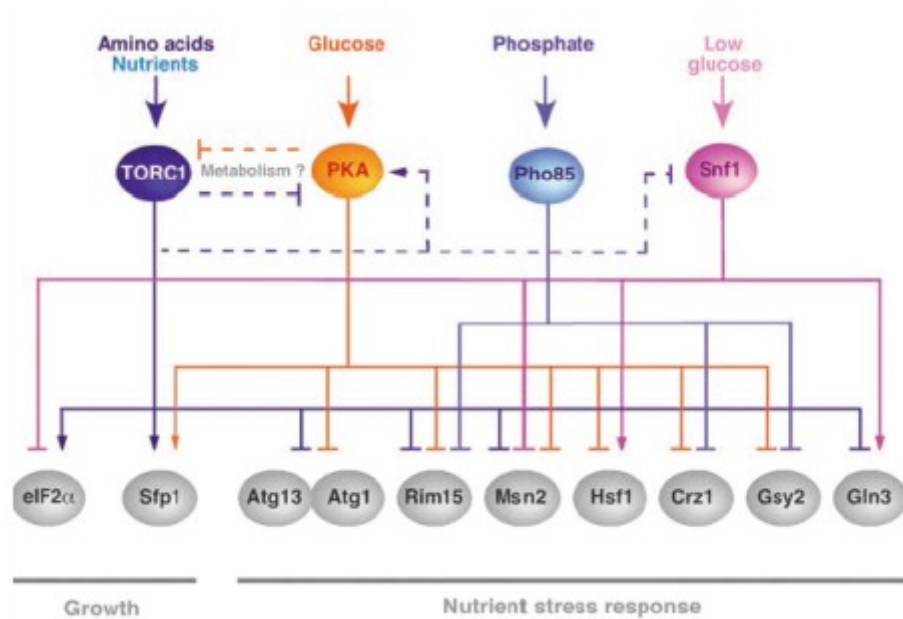


Figure 15| **Convergence of nutrient-sensing pathways** (adapted from De Virgilio, 2012).

### 1.12.4 *S. cerevisiae* as a model organism for aging

That *S. cerevisiae* is not spared of the aging process was demonstrated by Barton in 1950, as it became evident that yeast cells have a finite replicative potential (Barton, 1950). Process of aging is chaperoned by the characteristic age-associated morphological changes that include the thickening of the cell wall and the enlargement of the cell, as well as phenotypical changes, such as: ROS accumulation, DNA fragmentation, aggregation of damaged and carbonylated proteins. Additionally, many of these processes are greatly relevant in human aging. The extent of genes evolutionary conserved from yeast to humans, particularly of molecular mechanism underlying the aging processes, were shown to be invaluable. Ever since the first aging study over 60 years

ago, research on this simple unicellular eukaryote has been unprecedented for understanding the fundamental aspects of aging. One of the most riveting prospects of using *S. cerevisiae* is the existence of two distinct paradigms: mitotic and post-mitotic aging. This provides an exceptional opportunity to juxtapose aging processes of both dividing and non-dividing cells. The two models of aging in yeast are commonly referred to as the replicative (budding) lifespan and the chronological (stationary) lifespan (Figure 16). Although the two models were considered to be completely distinct at first, it is now evident that they do partially overlap, particularly in underlying aging processes such as TOR pathway, calorie restriction, etc. Furthermore, aging processes common for both lifespan assays are highly conserved in higher eukaryotes, and it is anticipated that pathways shared by both chronological and replicative lifespan will elucidate aging process in humans (Janssens & Veenhoff, 2016, 2016; Kaeberlein et al., 2007; Longo et al., 2012; Oliveira et al., 2016; Zimmermann et al., 2018).

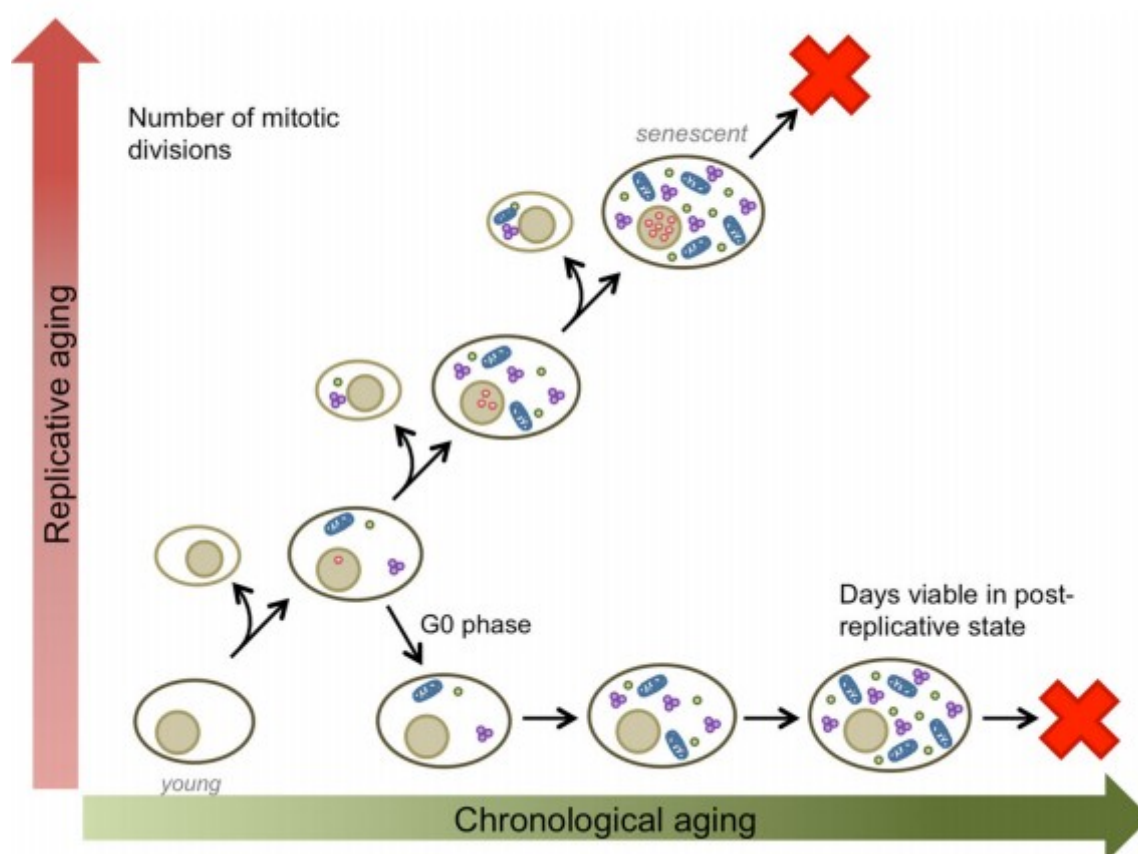


Figure 16| **Illustration of replicative and chronological lifespan in yeast.** (adapted from Oliveira et al., 2016)

### 1.12.5 Replicative lifespan measurement

This particular assessment of aging, replicative lifespan (RLS), is defined by the number of daughter cells produced by a mother cell prior to senescence. Due to the asymmetric division, daughter cells can be easily distinguished from the mother cell, predominantly by difference in size and thickness of their cell wall. Earliest aging research performed on yeast, published over 60 years ago, was analyzed using the replicative lifespan assay and it, to this day, remains by far the most frequently used lifespan measuring assay (Barton, 1950; Minois et al., 2004; Mortimer & Johnston, 1959).

The fundamental methodology for RLS analysis is conducted using a microscope with an integrated micromanipulator device. This device contains a fiber glass needle that is controlled by a joystick that translates fine hand movements into precise and fine-tuned motions. The needle is used to carefully remove daughter cells from the mothers, thus enabling an accurate interpretation of the replicative lifespan.

### 1.12.6 Chronological lifespan measurements

Chronological lifespan (CLS) is defined by the length of time a non-dividing mother cell can survive in a nutrient deficient medium. CLS was developed as a contrasting method that complements RLS by granting insights into post-mitotic aging. This assay is conducted either during the stationary phase, or more commonly, during the post-diauxic phase of growth (Longo & Fabrizio, 2002; Longo et al., 2012).

The fundamental methodology for CLS analysis is conducted by assessing colony-forming units (CFU) of yeast over time as a measure of viability. Cells are grown to reach stationary or post-diauxic phase, and samples are continually plated on rich media, until 99.9% of population becomes nonviable (Fabrizio & Longo, 2003; Postnikoff & Harkness, 2014).

### 1.12.7 Hallmarks of aging in yeast

To accurately study longevity in yeast *S. cerevisiae*, the ability to assess and recognize aging is paramount. Although the onset of aging is not as apparent as in humans, yeast cells do exhibit particular characteristics that facilitate the identification of aging. These characteristics can be partitioned into conspicuous morphological and the inconspicuous cellular and molecular alterations upon aging.

### Morphological and physiological changes

Most striking and apparent developments of aging are the changes of cellular appearance and these characteristics will, together with other not as discernible ones, be discussed further on.

- Enlargement of the cell and the thickening of the cell wall

It was shown that the cell size reflects lifespan potential in *S. cerevisiae*, and the size of mother cells increases with each bud, from the initial slight size discrepancy between mother and daughter cells, to remarkably large mother cells as they age. Cell wall thickening is also observed with aging mother cells.

- Loss of asymmetry

Asymmetric division is a process which warrants the production of healthy and damage-free daughter cells by mother cell retaining the, so called, aging determinants. These determinants include, in part, damaged and aggregated proteins, dysfunctional mitochondria, extrachromosomal ribosomal DNA circles (ERC) (Higuchi-Sanabria et al., 2015). It was shown, however, that the control of damage inheritance fails with age as mother cells are unable to keep aging determinants contained (Figure 17).

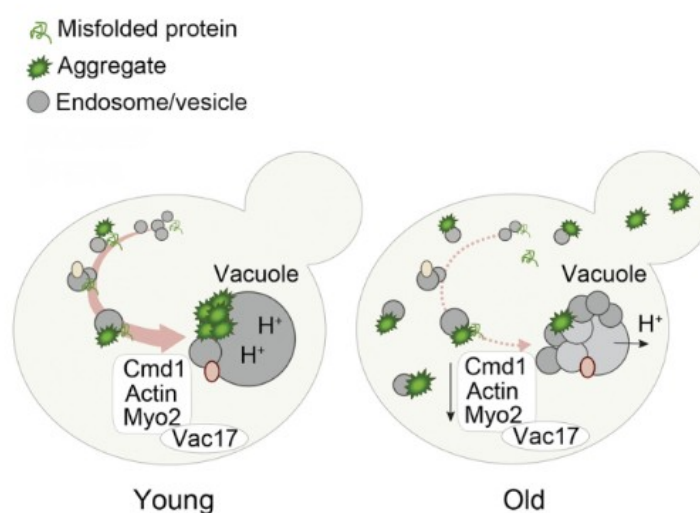


Figure 17| **Depiction of comparison of symmetric division in old vs young yeast cells** (adapted from Hill et al., 2017)



## INTRODUCTION

Loss of asymmetry leads to premature aging of the daughter cells which are often very large and unable to separate from the mother (Bitterman et al., 2003).

- Accumulation of bud scars

Each daughter cell, or bud, that separates from the mother cell leaves a permanent ring-shaped structure referred to as the bud scar. Their accumulation can be used as a marker to determine the number of daughters produced by the mother cell, and hence the replicative lifespan.

- Nucleolar fragmentation

Yeast cells manifest aging related genomic instability in form of ERCs, which are tandem repeat circles of DNA from the ribosomal DNA region formed by homologous recombination. These circles were found to accumulate with replicative age and are thought to reduce lifespan of yeast cells by overloading the replication machinery (Janssens & Veenhoff, 2016).

### Cellular and molecular changes

There have been nine distinct features of aging identified, all of which constitute commonalities in molecular and cellular aging across different organisms (López-Otín et al., 2013). These hallmarks of aging include genomic instability, telomere attrition, epigenetic alterations, loss of proteostasis, deregulated nutrient sensing, mitochondrial dysfunction, cellular senescence, stem cell exhaustion, and altered intercellular communication (López-Otín et al., 2013).

### 1.12.8 Longevity regulation in yeast

Research on yeast aging and the regulation of longevity has implicated several key factors which contributed to the extension of lifespan, some of which will be briefly discussed further on.

- Lifespan extension by calorie restriction (CR)

The mechanism of lifespan extension by CR is considered to be evolutionary conserved in multiple model organisms ranging from yeast to mammals. In yeast, CR is accomplished by decreasing the available glucose in the media from 2% to 0.5% or lower (Mei & Brenner, 2015). The resulting increase in lifespan has been, in part, attributed to respiration being favored over fermentation in limiting glucose environment, and the increase in Sir2, which is a histone deacetylase showed to reduce the formation of ERCs (Bitterman et al., 2003; Kaeblerlein et al., 2007). The exact mechanism underlying the lifespan extension remains to be fully elucidated.

- Lifespan extension by decrease of TOR activity



It was shown that decreased activity of TOR, or more precisely TORC1, increases both RLS and CLS in yeast. Interestingly, the same mechanism was implicated in lifespan extension of other organisms, such as flies, worms and mice, suggesting an evolutionary conserved function of TOR (Kaeberlein et al., 2007). Also, deletion of a gene encoding for Sch9 protein kinase was shown to extend lifespan in yeast, worms and mice (Kaeberlein, 2010). It has been proposed that inhibition of TOR and Sch9 is involved in underlying CLS extension of calorie restriction mechanism.

## 2. MATERIALS AND METHODS

### 2.1 Materials

#### 2.1.1. Reagents

Reagents used for this study are listed in the table below together with their respective suppliers.

Table 1. Reagents

Name	Source
Acetic acid	Kemika (Zagreb, Croatia)
Acrylamide solution 40%	Sigma Aldrich (St. Louis, USA)
Agar	Becton, Dickinson and Company (BD) (New Jersey, USA)
Agarose	Invitrogen (CA, USA)
Albumin Fraction V, protease-free BSA	Roth (Karlsruhe, Germany)
Antimycin	Sigma Aldrich (St. Louis, USA)
ATP	Sigma Aldrich (St. Louis, USA)
Bacto™ Peptone	Becton, Dickinson and Company (BD) (New Jersey, USA)
Bacto™ Tryptone	BD (New Jersey, USA)
Bacto™ Yeast Extract	BD (New Jersey, USA)
Bradford reagent	Sigma Aldrich (St. Louis, USA)
Bovine Serum Albumin (BSA)	Roth (Karlsruhe, Germany)
Bromophenol Blue	Sigma Aldrich (St. Louis, USA)
CCCP	Fluka (St. Louis, USA)
Coomassie Brilliant-Blue	Sigma Aldrich (St. Louis, USA)
D-(+)-Glucose, anhydrous p.a.	Kemika (Zagreb, Croatia)
D-Sorbitol	Sigma Aldrich (St. Louis, USA)
Dextrose	Sigma Aldrich (St. Louis, USA)
Digitonin	Merck (New Jersey, USA)
Dimethylsulfoxide (DMSO)	Roth (Karlsruhe, Germany)
dNTP mix	NEB (MA, USA)
Ethylenediaminetetraacetic acid (EDTA)	Fluka (Munich, Germany)
Ethanol	Kemika (Zagreb, Croatia)

Ethidium bromide	Sigma Aldrich (St. Louis, USA)
FCCP	Sigma Aldrich (St. Louis, USA)
Film UltraCruz, Autoradiography, Blue, 5x7	SantaCruz (Texas, USA)
Formaldehyde	Kemika (Zagreb, Croatia)
Geldanamycin	Roth (Karlsruhe, Germany)
Glucose	Kemika (Zagreb, Croatia)
Glycerol	Kemika (Zagreb, Croatia)
Glycine	Roth (Karlsruhe, Germany)
Hygromycine B	Life Technologies (CA, USA)
H <sub>2</sub> O Nuclease-free	Thermo Fisher Scientific Inc (MA, USA)
H <sub>2</sub> SO <sub>4</sub>	Sigma Aldrich (St. Louis, USA)
Isopropanol	Sigma Aldrich (St. Louis, USA)
Lithium acetate (LiAc)	Sigma Aldrich (St. Louis, USA)
Luminol reagent A and B	Santa Cruz Biotechnology (Texas, USA)
Milk powder	Roth (Karlsruhe, Germany)
Minimal SD agar base	Clontech (Mountainview, USA)
Minimal SD base	Clontech (Mountainview, USA)
Methanol	Sigma Aldrich (St. Louis, USA)
Nitrocellulose membrane	Thermo Fisher Scientific Inc (MA, United States)
PEG	Kemika (Zagreb, Croatia)
PMSF (phenylmethanesulfonyluoride)	Sigma Aldrich (St. Louis, USA)
Ponceau S	Sigma Aldrich (St. Louis, USA)
Potassium acetate	Kemika (Zagreb, Croatia)
Precision Plus Kaleidoscope, 5pk	Bio-Rad (Hercules, USA)
Protease inhibitor cocktail	Thermo Fisher Scientific Inc (MA, United States)
Sodium dodecyl sulfate (SDS)	Thermo Fisher Scientific Inc (MA, United States)
SYBR green	Bio-Rad (Hercules, USA)
N,N,N',N'-Tetramethylethylenediamine (TEMED)	Acros Organic/Fischer scientific ( New Hampshire, USA)
Torin	Invitrogen (Carlsbad, USA)
Tris	Sigma Aldrich (St. Louis, USA)
Triton X-100	Sigma Aldrich (St. Louis, USA)

## MATERIALS AND METHODS

Tween-20	Sigma Aldrich (St. Louis, USA)
Polyoxyethylen-Sorbitan-monolaurat (Tween)	Roth (Karlsruhe, Germany)
Uracil DO supplement	Clontech (Mountainview, USA)
YPD Medium	Clontech (Mountainview, USA)
Zymolyase (2000U)	Zymo Research (Freiburg, Germany)
$\beta$ -mercaptoethanol	Sigma Aldrich (St. Louis, USA)
2,4-Dinitrophenylhydrazine	Sigma Aldrich (St. Louis, USA)
3-Fluoracetic acid	Sigma Aldrich (St. Louis, USA)
3, 3', 5, 5'-Tetramethylbenzidine (TMB)	Sigma Aldrich (St. Louis, USA)

### 2.1.2. Buffers

All buffers and solutions used in this study are listed in the table below.

Table 2. Buffers and solutions

Name	Component	Concentration
Agarose gel solution	Agarose	1%
	TAE buffer	-
Blocking buffer	Milk powder (or BSA)	5% (1%)
	PBST	-
BN-PAGE loading dye	Brilliant blue G-250	5%
	6-aminohexanoic acid	500 mM
	Bis-Tris methane	100 mM, pH 7.0
Coomassie destaining solution	Methanol	30%
	Acetic acid	10%
Coomassie staining solution	Coomassie Brilliant Blue	0.25%
	Methanol	40%
	Acetic acid	10%
Complex IV staining solution	KPi	50 mM, pH 7.4
	Diaminobenzidine	0.5 mg/mL
	Reduced cytochrome c	1 mg/mL
Complex V staining solution	Tris/HCl	5 mM, pH 8.3
	Glycine	220 mM

## MATERIALS AND METHODS

	ATP	8 mM
	MgSO <sub>4</sub>	14 mM
	Pb(NO <sub>3</sub> ) <sub>2</sub>	0.2%
Digitonin buffer	Digitonin	
	Tris/HCl	20 mM, pH 7.4
	EDTA	5 mM
	NaCl	100 mM
	Glycerol	10%
	PMSF	1 mg/mL
DNP derivatization solution (concentrated)	DNPH	0.02 g
	3-Fluoroacetic acid	1 mL
DNP derivatization solution (diluted)	DNP derivatization solution (concentrated)	6 µL
	PBS (1×)	10 mL, pH 6.0-6.5
Fixation buffer	Sorbitol	1.2 M
	Potassium phosphate diatomic	0.1 M, pH 7.5
Laemmli sample buffer	SDS	10%
	Glycerol	20%
	β-mercaptoethanol	10 mM
	Bromophenol blue	0.05%
Phosphate buffer saline (PBS)	NaCl	137 mM
	KCl	2.7 mM
	Na <sub>2</sub> HPO <sub>4</sub>	10 mM
	KH <sub>2</sub> PO <sub>4</sub> /HCl	1.8 mM, pH 7.4
PBS Tween (PBST)	PBS	1X
	Tween-20	0.1%
RNA loading buffer	Sucrose	10%
	Deionized formamide	90%
	Bromophenol blue	0.05%
	Xylene cyanol	0.05%
SDS-PAGE resolving gel	Acrylamide	7.5%
	SDS	0.1%

## MATERIALS AND METHODS

	APS	0.1%
	TEMED	0.05%
	Tris.HCl	386 mM, pH 8.8
SDS-PAGE stacking gel	Acrylamide	4%
	SDS	0.1%
	APS	0.1%
	TEMED	0.05%
	Tris.HCl	80 mM, pH 6.8
SDS running buffer	Tris/HCl	25 mM, pH 6.8
	Glycine	200 mM
	SDS	0.1%
Spheroplast lysis buffer	Sorbitol	0.6 M
	Tris-Hcl	10 mM, pH 7.4
	PMSF	1 mM
TAE buffer	EDTA	2 mM
	Tris/acetic acid	40 mM, pH 8.0
TE buffer (50x)	EDTA	50 mM
	Tris/HCl	500 mM, pH 8.0
TE-SDS buffer	TE buffer (50×)	200 mL
	SDS	10%
Tris-Buffered Saline (TBS)	NaCl	150 mM
	Tris/HCl	50 mM, pH 7.5
TBST (TBS and Tween-20)	NaCl	150 mM
	Tween-20	0.05%
	Tris/HCl	50 mM, pH 7.5
Zymolyase buffer	Zymolyase	50-60 U
	Protease inhibitor	1:100
Wash buffer I	PBS (1×)	
Wash buffer II	PBS (1×)	50:50
	96% ethanol	
Wash buffer III	PBS (1×)	
	Tween	0.1%

### 2.1.3. Kits

Kits used in this study are listed in the table below together with their respective suppliers

Table 3. Kits

Name	Source
Click-iT® L-azidohomoalaine (AHA) Kit	Invitrogen (Carlsbad, USA)
iScript™ cDNA Synthesis Kit	BioRad (Hercules, USA)
iTaq™ Universal SYBR Green Supermix	BioRad (Hercules, USA)
NADP/NADPH Quantification Kit	Sigma (St. Louis, USA)
NucleoSpin RNA Extraction kit	Machery-Nagel (Duren, Germany)
Quick Ligation™ Kit	New England Biolabs (Ipswich, USA)
RNeasy Mini Kit	Qiagen (Venlo, Netherlands)
Wizard® SV Gel and PCR Clean-Up System	Promega (Fitchburg, USA)
Wizard® SV Minipreps DNA Purification System	Promega (Fitchburg, USA)

### 2.1.4. Antibodies

All primary and secondary antibodies used in this study are listed in the tables 4 and 5 below.

Table 4. Primary antibodies

Antibody	Source	Dilution
Anti-DNP	Sigma-Aldrich (Taufkirchen, Germany)	1:5000
Anti-6X His tag	Abcam (Cambridge, UK)	1:10000
Anti-phosphoSch9 Rabbit	Courtesy of Robbie Loewith	1:2500
Anti-Sch9 Rabbit pAb	Abcam (Cambridge, UK)	1:2500
Anti-Ssc1 Rabbit mAb	Courtesy of Sven Dennerlein	1:5000
Anti-Tcp1 Rabbit pAb	Abcam, (Cambridge, UK)	1:1000

## MATERIALS AND METHODS

Table 5. Secondary antibodies

Antibody	Source	Dilution
Goat anti-Rabbit IgG (H+L) Alexa Fluor 488	Thermo Fisher Scientific (Darmstadt, Germany)	1:2000
Goat anti-Rabbit HRP	Jackson ImmunoResearch (Pennsylvania, USA)	1:5000

### 2.1.6. Oligonucleotides

Primers used for qPCR analysis and cloning are listed in the tables 6 and 7 respectively.

Table 6. Oligonucleotides used for qPCR

Primer	Sequence (5' → 3')- Forward	Sequence (5' → 3')-Reverse
ACO1	GCTAATAACTGGCCATTGGATGTCA	AAGGTTTCTAATTGGCCATCACGT T
ATP1	ATGTTGGCTCGTACTGCTGCTATTC	GCAATACCATCACCGACTGCAAG
ATP20	ATGCTAAGCAGGATCCAAAATTATAC CA	TCTGTAGGCTTTAGAGCAAAGTT TAGG
ATP6	ATGTTTAATTTATTAATAACATATATT ACATCACCATTA	TAAATAGCTTCTTGTGAAATTAAT CATCTTGAAC
CIT1 F	ATGTCAGCGATATTATCAACAACCTAG CAA	GGTTTACCCTGTTCTTTCTTGAA TTTTTTA
COB	ATGGCATTTAGAAAATCAAATGTGTA TTTAAGTT	TATGCACATCTCTTATAATATGTTC AACAGA
COX1	ATGGTACAAAGATGATTATATTCAAC AAATGC	ATTAAAGCAGGCATTACTAAGAA GAAAATCA
COX2	ATGTTAGATTTATTAAGATTACAATTA ACAACATTTCAT	GTCCATGTTTAAATATATTTATATGC AATAGGATT
COX3	ATGACACATTTAGAAAGAAGTAGAC ATCAAC	TATGTAGCTTCAGCTACAATATCT CTAAATC
COX4	ATGCTTTCACTACGTCAATCTATAAG ATTTTT	TCTAACCTAGCTAAACCAGTTTCT TGAT
CYC1	ACTGAATTCAAGGCCGGTTCTG	TGTTATTTTCGTCCCACAACACGT TTT T
DER1	ATGGATGCTGTAATACTGAATCTC	ATGCTGGATAAATTTATCTGGTAT
ENO2	ATGGCTGTCTCTAAAGTTTACGCTAG	TTGGTCCCTAACATCTAGGTTGGC C



FUM1	ATGTTGAGATTACCAATTGTAGTTG CAAG	AGGCAATGGCATTCTTTCACGAG C
IDH1	GCTTAACAGAACAATTGCTAAGAG	GTTGATGATTTCATTTCGTGAAGTC
IDH2	TGTAAAGCAACCTTCAATCGGAAGA	GAATGGTCGTTAATCCGTTGACA AA
HRD1	ATGGTGCCAGAAAATAGAAGGA	ATGCTGGATAAATTTATCTGGTAT
HSP26	ATGTCATTTAACAGTCCATTTTTTG	TTAGTTACCCACGATTCTTGA
HSP42	ATGAGT2TTTTATCAACCATCCCTAT	TCAATTTTCTACCGTAGGGTTGA
HSP60	ATGTTGAGATCATCCGTTGTTC	TTACATCATACCTGGCATTCTT
HSP15	TGTCTCTCAAATTGGTGATGGTCAA	TCTTTGGGGCTAAAGTAGTGGTG GT
KAR2	GTTTTTCAACAGACTAAGCGCT	CTACAATTCGTCGTGTTCGAAA
MCX1	ATGTTGAAATCTGCAAGCCAAAA	TTATGTTAACGTTCTCTTGGGAA
MDH1	ATGTTGTCAAGAGTAGCTAAACGTG C	CTCTTCTGGAGTAAACCCCTTGA C
PDA1	CTTTCAACATGGCCAAATTATGGAA	CACCAGTCCTTAGCAAACCTTGGA TG
PD11	ATGAAGTTTTCTGCTGGTGCCG	TTACAATTCATCGTGAATGGCATC
PGI1	ATGTCTGAACCAGCTCAAAAGAAAC AAAA	ATGTCTGAACCAGCTCAAAAGAA ACAAAA
PIM1	ATGCTAAGAACAAGAACCACAAAG ACC	TTCAATTGATGCTGGAACTCTTGC CA
POT1	GGTAAGGGTGAATCGAAGAGGAAG A	AGTTCAAATCAGCCCTCAAAGGT TC
POX1	GTTGGGTGATTATACTGAAATTTGG	CCTTTGTAATTCATCGGAAATAT G
PYK1	ATGTCTAGATTAGAAAGATTGACCT CATTAAA	TACAATTCTTCGGACTTTCTGGCG TT
SEC62	ATGTCAGCCGTAGGTCCAG	GGCTTTTTTCATTGATGGCTTTC
SOD1	ATGGTTCAAGCAGTCGCAGTGTTAA A	TTGAAAGGATTGAAGTGAGGACC AG
SOD2	ATGTTGCGGAAAACAGCAGCTGC	ATTGGTCAACAGCAGTGTTGAAT CC
SSA1	ATGTCAAAAGCTGTTCGGTATTG	TTAATCAACTTCTTCAACGGTTG
TDH1	ATGATCAGAATTGCTATTAACGGTTT CG	AGGTAGCGATCTTGACACCATCA AT
UBC6	ATGTCTAGGGCTAAGAGAATTAT	TCACTTCAACAATTCCTCGATG

## MATERIALS AND METHODS

Table 7. Oligonucleotides used for cloning

Primer	Sequence (5' → 3')- Forward	Sequence (5' → 3')-Reverse
Snf1 upstream flanking region	GCGGCGTGGATGCAAAAG GAT	TATGTCGACCTGTGTTTGTGTTGT TG
Snf1 downstream flanking region	TATGAGCTCTGGTGGAAAC GTAAAAGAA	TTCTGGCAGCATGATTTGATATCG G

### 2.1.7. Media

Media formulation used in this study is listed in the table below.

Table 8. Media composition

Medium	Composition
LB medium	0.5% yeast extract, 1% tryptone, 1% NaCl
LB cryo storage medium	0.5% yeast extract, 1% tryptone, 1% NaCl, 15% glycerol
YPEG medium	1% yeast extract, 2% peptone, 3% ethanol, 3% glycerol
YPEG medium	1% yeast extract, 2% peptone, 3% ethanol, 3% glycerol, 2.5% agar
YPD medium	1% yeast extract, 2% peptone, 2% glucose
YPD agar medium	1% yeast extract, 2% peptone, 2% glucose, 2.5% agar
YPD cryo storage medium	1% yeast extract, 2% peptone, 2% glucose, 30% glycerol

### 2.1.8. Plasmids and fluorophores

All plasmids and fluorophores used in this study are listed in the table 9 and 10, respectively.

Table 9. Plasmids

Vector	Accession	Purpose	Source
pBG1805	YDR 212W	Overexpression of Tcp1 cytoplasmic molecular chaperone	Dharmacon, Thermo Scientific (Darmstadt, Germany)
pBG1805	YHR 193C	Overexpression of Egd2 cytoplasmic molecular chaperone	Dharmacon, Thermo Scientific (Darmstadt, Germany)
pBG1805	YJR045C	Overexpression of Ssc1 mitochondrial molecular chaperone	Dharmacon, Thermo Scientific (Darmstadt, Germany)
pBG1805	YKL073W	Overexpression of Lhs1 ER molecular chaperone	Dharmacon, Thermo Scientific (Darmstadt, Germany)
pUG35	MitoLoc	Imaging the mitochondrial network morphology and membrane potential	(Vowinckel et al., 2015)
pYES2		Empty vector control	Dharmacon, Thermo Scientific (Darmstadt, Germany)

Table 10. Fluorophores

Fluorophore	Excitation wavelength	Emission wavelength	Source
Green Fluorescent Protein (GFP)	458 nm	505-530 nm	Thermo Fisher Scientific Inc (MA, USA)
2',7'-dichlorofluorescein diacetate (H2DCFDA)	492-495 nm	517-527 nm	Sigma (St. Louis, USA)
3, 3'-dihexyloxacarbocyanine iodide (DiOC6(3))	482 nm	504 nm	Sigma (St. Louis, USA)
10-N Nonyl acridine orange (NAO)	495 nm	519 nm	Sigma (St. Louis, USA)

### 2.1.10. Consumables and laboratory equipment

All consumables and the laboratory equipment used in this study is listed in the table below.

Table 11. Laboratory materials and equipment

Instrument	Manufacturer
Biophotometer	Eppendorf (Hamburg, Germany)
Centrifuge 5415R	Eppendorf (Hamburg, Germany)
Centrifuge 5810R	Eppendorf (Hamburg, Germany)
FACScalibur™	BD Biosciences (Hamburg, Germany)
Mini-protean™ Tetra Vertical Electrophoresis Gel	Bio-Rad (Hercules, USA)
Mini Trans-Blot®Cell	Bio-Rad (Hercules, USA)
Multichannel pipette	Eppendorf (Hamburg, Germany)
Nanodrop ND-1000	Thermo Fisher Scientific Inc (MA, USA)
Oxygraph	Hansatech (Norfolk, UK)
Pipette gun accu-jet pro	BrandTech Scientific Inc.
Pipetman pipette	Gilson (WI, USA)
Pipetman multichannel pipette	Gilson (WI, USA)
QuantStudio 6 Flex Real-Time PCR System	Thermo Fisher Scientific Inc (MA, USA)
Spinning disk confocal microscope	Perkin Elmer (MA, USA)
SporePlay Dissection microscope	Singer Instruments (Somerset, UK)
Sunrise™ Absorbance Microplate Reader	Tecan (Mannedorf, Switzerland)
SYNERGYM1 microplate reader	BioTek (VT, USA)
Vortex 2	IKA (Staufen, Germany)

### 2.1.11. Software and databases

Software and databases used for analysis of this study are listed in the table below.

Table 12. Software

Name	Company	Origin
DeSeq2 package within the Bioconductor software development project	(Huber et al., 2015; Love et al., 2014)	

EasyqpcR	(Le Pape, 2013)	
GraphPad Prism 6 & 7	GraphPad Software Inc.	California, USA
ImageJ	NIH	Maryland, USA
Mendeley	Mendeley Ltd	London, UK
Microsoft Office	Microsoft Corporation	Washington, USA
Python HTSeq 0.6.0.	EMBL Heidelberg	Heidelberg, Germany
R statistical package	R Core Team, 2012	
STAR 2.3.0e	TreeStar	Oregon, USA
Ubuntu	Canonical Ltd.	London, UK

Table 13. Databases

Database	Source
BLAST	<a href="http://blast.ncbi.nlm.nih.gov/Blast.cgi">http://blast.ncbi.nlm.nih.gov/Blast.cgi</a>
SacCer3 reference genome	<a href="https://www.ncbi.nlm.nih.gov/assembly/GCF_000146045.2/">https://www.ncbi.nlm.nih.gov/assembly/GCF_000146045.2/</a>
Saccharomyces gene database	<a href="http://www.yeastgenome.org">http://www.yeastgenome.org</a>

### 2.1.12. Strains

Strains and their respective genotypes are listed in the table below.

Table 14. Yeast Strains

Strain	Genotype	Source
BY4741	<i>MATa his3Δ1 leu2Δ0 met15Δ0 ura3Δ0</i>	Thermo Fisher Scientific Inc (MA, USA)
LHS1Δ	<i>MATa his3Δ1 leu2Δ0 met15Δ0 ura3Δ0 lhs1Δ::KanMX</i>	Thermo Fisher Scientific Inc (MA, USA)
SSC1Δ	<i>MATa his3Δ1 leu2Δ0 met15Δ0 ura3Δ0 ssc1Δ::KanMX</i>	Thermo Fisher Scientific Inc (MA, USA)
EGD2Δ	<i>MATa his3Δ1 leu2Δ0 met15Δ0 ura3Δ0 egd2Δ::KanMX</i>	Thermo Fisher Scientific Inc (MA, USA)
COA3Δ	<i>MATa pep4-3 his4-580 ura3-52 leu2-3,112; coa3Δ::HISMx6</i>	This study
LHS1ΔHSF1Δ	<i>MATa his3Δ1 leu2Δ0 met15Δ0 ura3Δ0 lhs1Δ::KanMX</i>	Thermo Fisher Scientific Inc (MA, USA)
SSC1ΔHSF1Δ	<i>MATa his3Δ1 leu2Δ0 met15Δ0 ura3Δ0</i>	Thermo Fisher Scientific

## MATERIALS AND METHODS

	<i>ssc1Δ::KanMX</i>	Inc (MA, USA)
EGD2ΔHSF1Δ	<i>MATa his3Δ1 leu2Δ0 met15Δ0 ura3Δ0 egd2Δ::KanMX</i>	Thermo Fisher Scientific Inc (MA, USA)
Petite yeast		(Goldring et al., 1971)

Table 15. Bacterial strains

*E. coli* strains used for cloning and plasmid expression listed in Table 15.

Strain	Genotype	Source
XL1-Blue	<i>recA1 endA1 gyrA96 thi-1 hsdR17 supE44 relA1 lac [F' proAB lacI q ZΔM15 Tn10 (Tet<sup>r</sup>)]</i>	Stratgene (CA, USA)
DH5α	<i>fhuA2 lac(del)U169 phoA glnV44 Φ80' lacZ(del)M15 gyrA96 recA1 relA1 endA1 thi-1 hsdR17</i>	Thermo Fisher Scientific Inc (MA, USA)

## 2.2. METHODS

### 2.2.1 Yeast culture

#### 2.2.1.1 Cultivation and growth conditions

Yeast cells were grown in liquid rich media or on synthetic minimal media supplemented with uracil dropout medium for selective growth of an auxotrophic yeast strain. Cells were incubated in liquid media or plates at 30°C.

All experiments were performed on yeast cells from mid-log phase, optical density at 600 nm (OD<sub>600</sub>) of 0.5-0.6, unless stated otherwise. Before every experiment, the yeast cultures were grown to stationary phase, were then diluted 100× and allowed to grow until mid-log phase.

#### 2.2.1.2 Growth rate analysis

Yeast strains were grown overnight at 30°C in their respective growth media, and were diluted to ~0.1 OD<sub>600</sub> units/mL. Their relative cell number was measured at 600 nm using a Biophotometer every 30 min until stationary phase was reached. Obtained results were charted in growth curve.

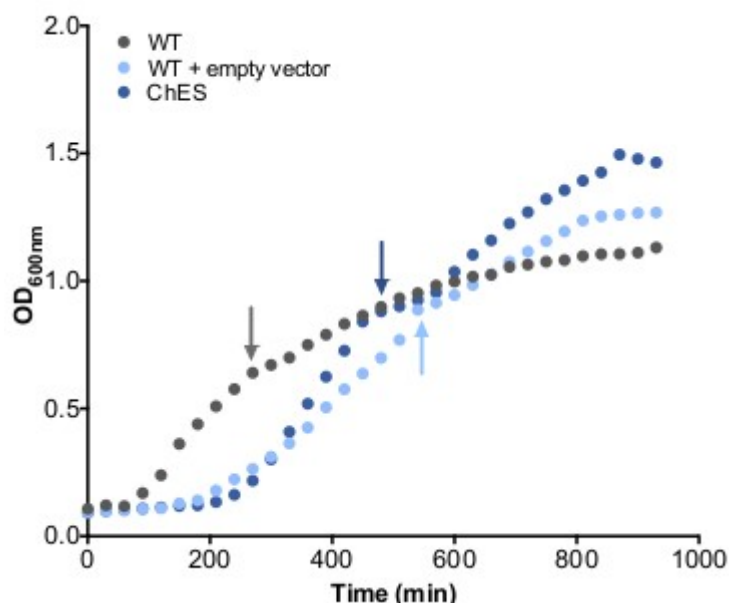


Figure 18 | **Representative growth curve.** Points at which the cells were harvested are noted by arrows (Perić et al., 2017).

### 2.2.1.3 Replicative lifespan measurements

Replicative lifespan (RLS) was performed by micromanipulation, using a micromanipulator device incorporated into a microscope (Singer Instruments). Experiments were performed at 30 °C, i.e., both the incubator and the room in which the micromanipulations were performed were kept at the mentioned temperatures. For this experiment, yeast cells were individually placed into a designated spot on an agar plate, approximately 90 cells total; 30 cells per plate. These cells were discarded once they have produced a bud, leaving their virgin daughter cells for the RLS assessment. The daughters produced by the mother cells were carefully separated from the mothers using the microdissection needle on the micromanipulator, and were then discarded on designated areas of the plate. Each separation was noted and counted towards the RLS measurement. These mother cells were monitored constantly over several days until senescence was reached, that is, until all those cells stopped budding.

Additionally, upon understanding that RLS measurement in most other laboratories in the world is evaluated during the day, with the plates being kept at +4 °C overnight, decision was made to test the effect it has on the lifespan of yeast. The results are depicted in the Figure 19 below. Consequently, our control measurements might not fully align with the literature-based ones, if

the measurements were without constant surveillance.

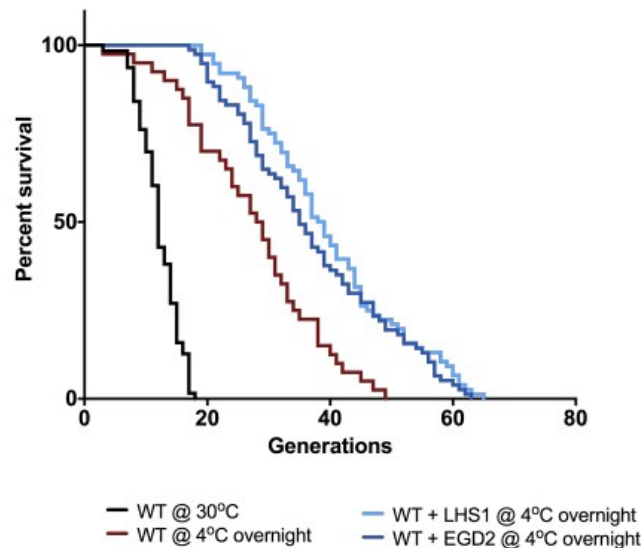


Figure 19| **Representation of RLS measurement** (Perić et al., 2017).

#### 2.2.1.4 Chronological lifespan measurements

Chronological lifespan (CLS) was performed on a stationary phase culture. After centrifugation at 4000×g for 5 min, the cells were resuspended in sterile deionized water and incubated at 30 °C with shaking. The survival of the non-dividing cells was evaluated by plating the serially diluted cells onto YPD plates every 3 days.

#### 2.2.1.5 Yeast cell fixation

Five mL of 37% formaldehyde was added to 45 mL of exponentially grown culture, and was incubated for 45 min at room temperature following thorough mixing. After the incubation period, the cells were pelleted by centrifugation at 1600 rpm for 4 min, and then washed twice with 1 mL ice-cold fixation buffer. The washed pellet was resuspended in 1mL fixation buffer that contained 2.5 µL zymolyase, and it was incubated for 1 h at 30 °C. After the spheroplasting process, samples were pelleted at 400 rpm for 5 min, and rinsed twice with ice-cold fixation buffer. For permeabilization, the cells were resuspended in 1 mL 70% ethanol, and stored at 4°C overnight.



## 2.2.2 Molecular biology

### 2.2.2.1 DNA extraction

The extraction of DNA was performed using a modified version of the method described by Powell & Diaceti (2007). A streak of cells was taken from an agar plate and transferred to an 1.5 mL plastic tube containing 660  $\mu$ L of 50TE-SDS buffer which contained 200 mL of 50TE buffer with 10% SDS solution, and was filtered through 0.45  $\mu$ M filter. Samples were then vortexed and incubated at 65 °C for 5 min, inverted and re-incubated for further 5 min. 340  $\mu$ L of 5 M potassium acetate was added and samples were placed at 4 °C until the proteins had coagulated. Once coagulated, the sample was centrifuged at 13,000 rpm for 10 min and 600  $\mu$ L of the supernatant was transferred to a new tube. 600  $\mu$ L of isopropanol was then added and the tube was mixed by inversion and incubated at room temperature for 10 min. After incubation the sample was centrifuged at 10,000 rpm for 10 min and the aqueous phase was discarded. The DNA pellet was then rinsed in 100  $\mu$ L of 95% ethanol at -20 °C and flush spun. The ethanol was then removed by pipette and the pellet was allowed to dry by placing the tube inverted onto absorbent paper. Once dry, the pellet was resuspended in 60  $\mu$ L TE 1 $\times$  by rubbing the tube across a rough surface, and incubated at 65 °C for 5 min. Once prepared, DNA was stored at -20 °C.

### 2.2.2.2 Plasmid extraction from *S. cerevisiae*

Plasmid extraction from yeast was performed following a previously described protocol (Singh & Weil, 2002) by using a kit for isolation of plasmid DNA (Wizard® SV miniprep – Promega).

### 2.2.2.3 Plasmid extraction from *E. coli*

10 mL of the overnight culture was used for the extraction, and it was performed following a standard procedure for miniprep kit as above.

### 2.2.2.4 Chaperone inactivation procedure

Inactivating mutations were introduced using the intact plasmid containing active chaperones (Gething & Sambrook, 1992). The domain architecture scheme was developed using BLAST

## MATERIALS AND METHODS

with default parameters (Boratyn et al., 2012). The inactivating mutations in each studied chaperone were as follows:

- Ssc1 chaperone was inactivated by deletion of C-terminal domain required for its translocation function (Blamowska et al., 2010)

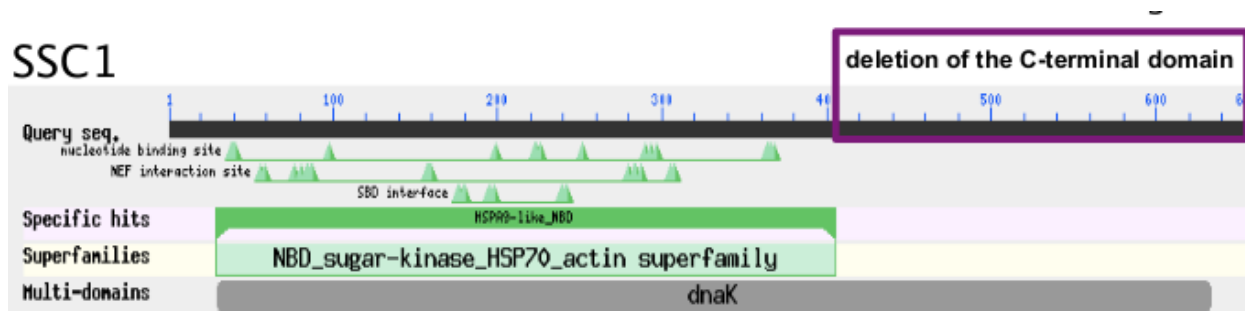


Figure 20| Schematic presentation of Ssc1 chaperone inactivation

- Lhs1 chaperone was inactivated by introduction of point mutation at aspartate 26 into alanine by site directed mutagenesis, which nulled its ATP-binding capacity (de Keyzer et al., 2009)

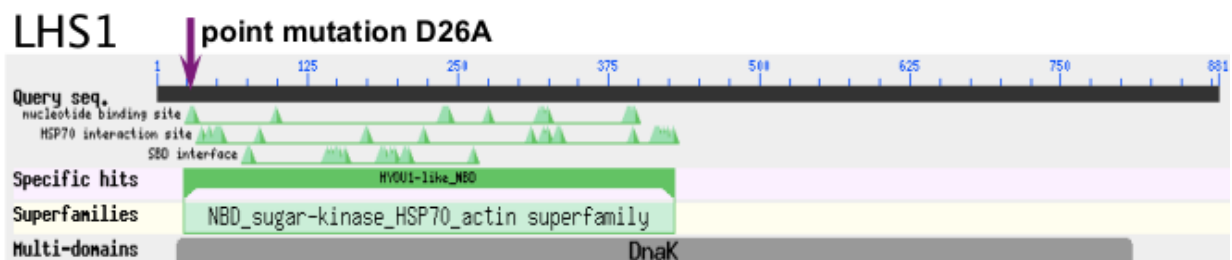


Figure 21| Schematic presentation of Lhs1 chaperone inactivation

- Egd2 chaperone was inactivated by deletion of its NAC domain (amino acids 17-72) (Ott et al., 2015)

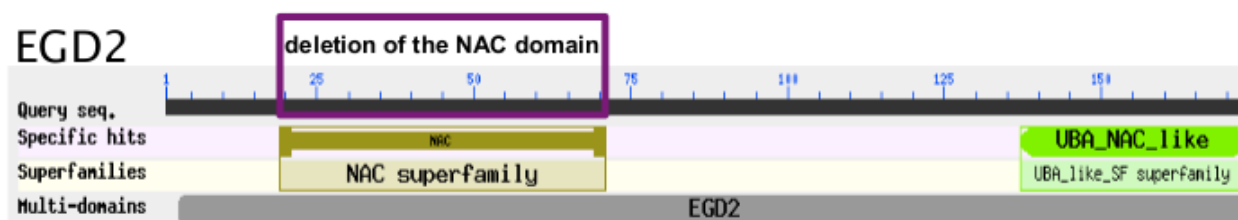


Figure 22| Schematic presentation of Egd2 chaperone inactivation

- Tcp1 chaperone was inactivated by deletion of a portion from its ATP-magnesium binding site (LGPV motif, amino acids 44-47), which nulled its ATP-binding capacity (Brackley & Grantham, 2009)

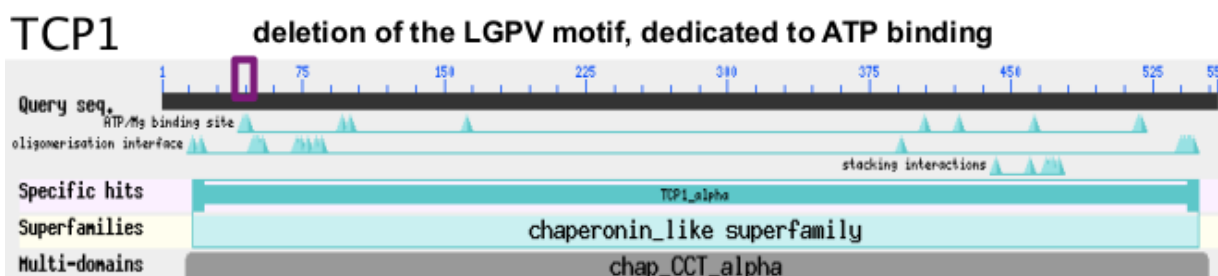


Figure 23| **Schematic presentation of Tcp1 chaperone inactivation**

Cloning was performed in *E. coli* XL1 Blue (Stratagene).

#### 2.2.2.4 PCR: polymerase chain reaction

PCR was performed for deletion and verification of deleted YDR477W (SNF1) gene. Gene was deleted and replaced with a Hygromycin B resistance cassette (pAG32 plasmid - Addgene). Primers used are in the Table 7.

Phusion Hot Start II High-Fidelity PCR master mix (Thermo Fisher Scientific) was used. The final volume of the PCR mixture was 50  $\mu$ L per reaction:

## MATERIALS AND METHODS

Table 16. PCR conditions and compositions

Components	Concentration	Volume used (μl)
Template DNA	100 ng/ μL	4
10X PCR buffer without MgCl <sub>2</sub>	1×	10
Forward primer	25 μM	2
Reverse primer	25 μM	2
Taq DNA polymerase	1.25 U	0.5
10 mM dNTP's	2.5 mM	4
MgCl <sub>2</sub>	2 mM	4
Nuclease free water		23.5

Table 17. PCR program used

Cycle	Temperature	Reaction Time
25 cycles	94 °C	4 min
	95 °C	30 sec
	52 °C	1 min
	72 °C	1 min
1 cycle	72 °C	1 min 30 sec
-	4 °C	Hold

PCR products were visualized in a 1% agarose gel. TAE (1×) buffer was used as running buffer at 100 V for 35 min, and the DNA was stained with 0.5 mg/mL ethidium bromide.

### 2.2.2.5 Enzymatic manipulation of DNA

Homologous recombination was used to construct a disruption in the YDR477W (SNF1) gene, following the general scheme described in the Figure 24. A complete list of primers used in this experiment can be found in the Table 7. HphMX4; hygromycin resistance marker, was PCR-amplified from pAG32 (Goldstein & Cusker, 1999) (PCR3 mixture), while approximately 500 bp upstream and downstream of the SNF1 gene were amplified separately (PCR1 and PCR2 mixtures). The primers used for the aforementioned amplifications had 5' and 3' ends overlapping the primers used for HphMX4 amplification, which was achieved by restriction digestion. The procedure was done following a protocol provided by the kit (New England BioLabs® Inc), and the reaction mixture can be seen in the Table 18. The purified digested samples (Wizard® SV Gel and PCR Clean-Up kit, Promega) were ligated following a protocol provided by the kit (New England BioLabs® Inc), and the reaction mixture can be seen in Table 19. Transformations (see method 2.2.2.6 for transformation procedure) were plated on YPD plus hygromycin 100 µg/mL. The integration of the deletion was confirmed via PCR.

Table 18. Restriction digestion reaction

Components	Concentration	Volume used (µL)
NEB CutSmart buffer	1×	2
BSA	100 µg/ µL	2
SacI/Sall	10,000 U	1
PCR product	1 µg	-
Nuclease free water	-	Up to 20 µL total volume

## MATERIALS AND METHODS

Table 19. Ligation reaction

Components	Concentration	Volume used (μL)
T4 DNA Ligase Buffer	10×	2
PCR1		
PCR2		1:1
PCR3	Equimolar to PCR1 and 2	
T4 DNA Ligase	1×	1
Nuclease free water	-	Up to 20 μL total volume

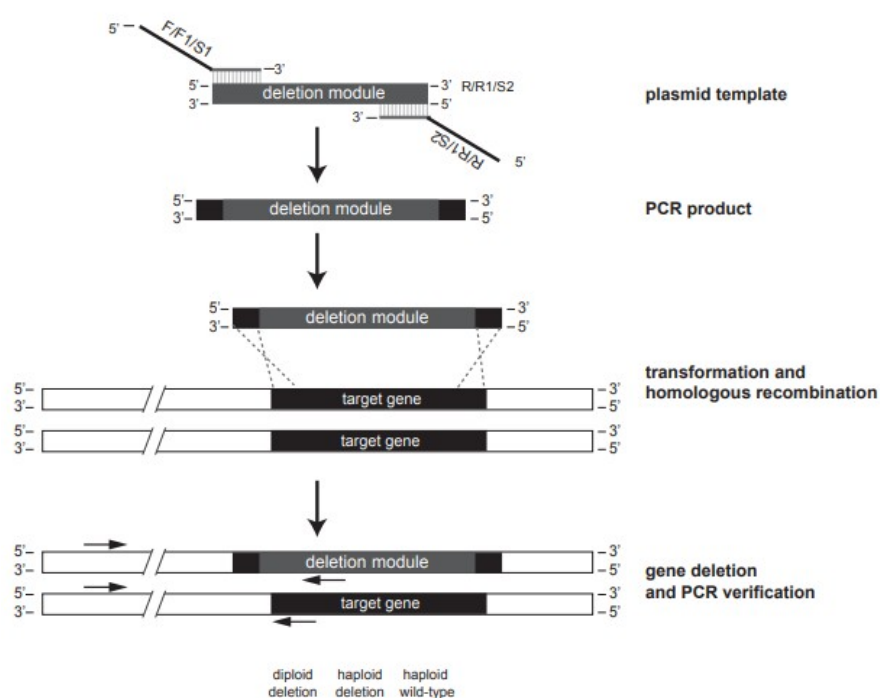


Figure 24| **Representation of homologous recombination** (Gardner & Jaspersen, 2014).

### 2.2.2.6 Yeast transformation experiments

Yeast transformation experiments were performed following a previously described protocol for high-efficiency transformation using the lithium acetate – PEG method (Gietz & Schiestl, 2008). Briefly, 50 mL log phase of culture was needed for 10 transformations. Cells were pelleted and thoroughly washed with sterile water. 360 µL of the transformation mix was added to each transformation microcentrifuge tube, and vortexed thoroughly. Negative control tube was always included. Transformation tubes were left overnight at the room temperature. The following day, 1 mL of YPD medium was added to each transformation reaction, incubated for 2-3 hr at 30 °C to ensure good expression. 2, 20 and 200 µL of the transformation mixture was plated onto the selective plates. Cells were plated less densely as plating density negatively affects transformation efficiency. Plates were incubated at 30 °C for 3-4 days.

### 2.2.2.7 Metabolic labeling of nascent proteins with L-AHA

The detection of newly synthesized proteins is done by using Click-iT® L-azidohomoalaine (AHA) kit (Invitrogen). AHA is a methionine amino acid analog that contains a modification, an azido moiety that can be incorporated into proteins during their synthesis, rendering it applicable for the nascent protein detection. The experiment was performed following the procedure provided by the kit.

## 2.2.3 RNA methods

### 2.2.3.1 Preparation of yeast RNA extract

RNA was extracted using the NucleoSpin RNA extraction kit (Machery&Nagel) and RNeasy Mini kit (Qiagen). When using the NucleoSpin RNA extraction kit, the protocol for up to  $3 \times 10^8$  yeast cells was followed. When using the RNeasy Mini kit, the protocol for enzymatic lysis was followed. Both protocols were provided with the extraction kits.

Extracted RNA was checked for purity and quality on 1% agarose gel. Samples were mixed in equal volumes with the sample loading buffer, and boiled at 65 °C for 5 min. Agarose gel was loaded with the denatured RNA samples, and run at 100 V for 1 hr. The gel was stained with 0.5 µg/mL ethidium bromide and observed for RNA integrity under UV light.

### 2.2.3.2 Quantitative real-time PCR

cDNA was reversely transcribed using iScript™ cDNA Synthesis Kit from 1000 ng of total RNA. The concentration of RNA was measured using NanoDrop. The resulting cDNA was diluted 100×, out of which 1 µL was mixed with 0.2 µL (25 µM) forward, 0.2 µL (25 µM) reverse primer, and 3.6 µL SYBRgreen in each well of 384 well plate. The reaction for the quantitative real-time PCR was run on a QuantFlexStudio 6 using 40 cycles, after which the melting curves for each well were determined. qPCR differential expression was estimated from three replicates using the EasyqpcR package by first removing the cycle threshold (Ct) values over 1 standard deviation from the mean Ct for each gene/strain combination (Le Pape, 2013). UBC6 gene was used as a reference gene for normalization, as its expression levels were found to be stable throughout the samples.

### 2.2.3.3 RNA Sequencing and analysis

RNA sequencing was performed using the Next Generation Sequencing (NGS) Illumina platform. 50bp single-end reads sequenced for differential expression analysis were mapped to the SacCer3 reference genome using the open source software package aligner STAR.

### 2.2.3.4 Feature counting

Feature (“raw read”) counts were obtained using the htseq-count tool version 0.6.0. of the Python HTSeq package (Anders et al., 2015), using the parameters: -a 10 -s no.

### 2.2.3.5 Differential expression analysis

Feature reads were analyzed for the detection of differentially expressed genes using the DeSeq2 package (Love et al., 2014) within the Bioconductor software development project (Huber et al., 2015) under R statistical package. The outliers were detected and filtered out with the principal component analysis (PCA) on regularized logarithm (rlog) transformed and normalized data (Figure 25).



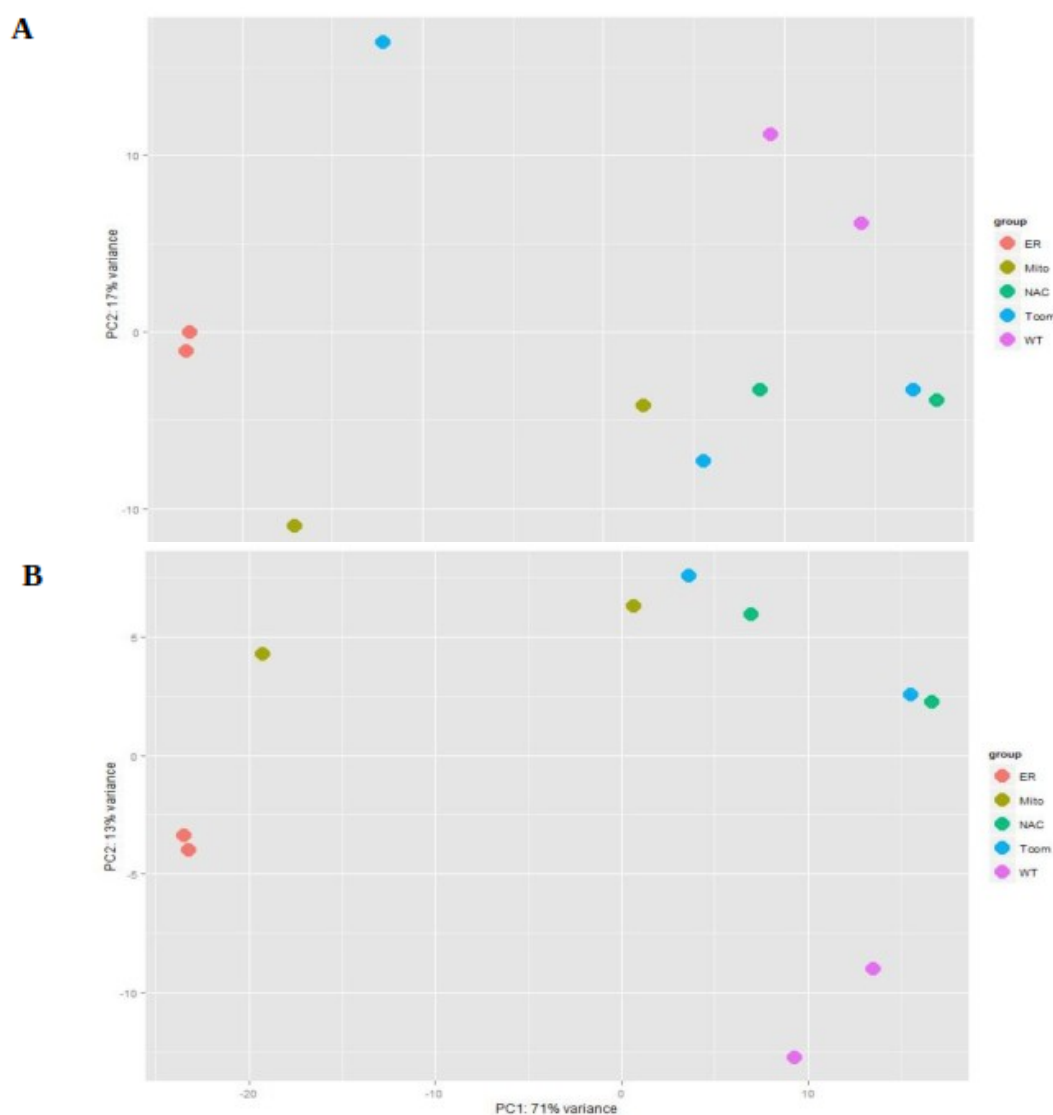


Figure 25| **Principle component analysis-based filtering of RNASeq replicates:** First two principal component coordinates were used to identify outlier replicates and gave (A) PCA plot before removal of outliers, and (B) PCA plot after removal of outliers (Perić et al., 2017).

## 2.2.4 Protein extraction and analysis

### 2.2.4.1 Preparation of yeast protein extracts

Cells were grown to mid-log phase, and were centrifuged for 5 min at 3000 rpm. The pellets were resuspended with 10 mL 1× phosphate buffer saline (PBS) and centrifuged for 5min at

## MATERIALS AND METHODS

---

3000 rpm. This step was repeated one more time in order to efficiently remove any growth media as it inactivates zymolyase. The pellets were then resuspended in zymolyase buffer and were shaken at 100 rpm on 37 °C for 1 hr. The volume of zymolyase directly depended on the size of the pellet, since it was of great importance that the volume was enough for the pellet to be completely resuspended, but it was usually between 500 µL and 1 mL. Very important to note that the resuspended pellets had to be shaken very gently but thoroughly, as the spheroplasts can be easily damaged, releasing the proteins. After 1 hr, the tubes were centrifuged at 3000 rpm. Supernatant was discarded. From here all work was done on ice. The cell pellets were resuspended in spheroplast lysis buffer at 1 mL of buffer per 0.5 g of cell pellet. The cells were vigorously vortexed for about 30 sec, and left on ice for 30 min, with occasional vortexing. After 30 min, cells were vortexed again for 2 min, and centrifuged at maximum speed until the supernatant was clear.

### 2.2.4.2 Protein concentration measurement

The concentration of the extracted yeast proteins was measured, following the protocol described by Bradford (Bradford, 1976). For these measurements, 96 well plate was used. The standard curve was constructed by measuring the absorbance of applying several Bovine Serum Albumine (BSA) solutions, with the concentrations ranging from 0 – 0.05 mg/mL. Water was used as a blank. 200 µL of Bradford reagent was added to 1 µL of sample (three replicates) and absorbance was measured at 570 nm using Tecan Sunrise Absorbance Microplate Reader after 1 hr incubation at room temperature with shaking.

### 2.2.4.3 Protein carbonylation measurement

Extracted proteins were diluted in PBS to a final concentration of 10 µg/mL. 100 µL of diluted proteins was added to each well. The plate was covered with an adhesive plastic and incubated either at 4 °C overnight or at 37 °C for 1 h. Plate was then washed three times with 200 µL wash buffer I per well. 200 µL of DNP derivation solution was added in each well, and the plate was incubated for 45 min in the dark. Plate was then washed three times with 200 µL of wash buffer II per well, and three times with 200 µL of wash buffer I per well. The remaining protein binding sites in the coated wells were blocked in 250 µL blocking buffer. The plate was incubated for 90min at room temperature with shaking. Plate was washed three times with 300 µL of wash buffer III per well. 100 µL of diluted anti-DNP primary antibody was added to each well. The

plate was incubated for 120 min at room temperature with shaking. Plate was then washed with 200  $\mu$ L of wash buffer III per well. 100  $\mu$ L of diluted Goat HRP secondary antibody was added to each well. The plate was incubated for 60 min at room temperature with shaking, and then washed with 200  $\mu$ L of wash buffer III per well. 100  $\mu$ L of TMB solution was added to each well, and was incubated until the color development stopped. Reaction was stopped by adding 100  $\mu$ L of Stop solution (0.3 M  $\text{H}_2\text{SO}_4$ ) to each well. The absorbance was read at 450 nm using the Tecan Sunrise plate reader.

#### 2.2.4.4 SDS - PAGE and Western Blotting

Proteins were extracted following the procedure previously described (2.2.4.1).

25  $\mu$ g of protein was mixed with Laemmli sample buffer, heated to 95  $^{\circ}\text{C}$  for 5 min, and allowed to cool before loading them onto two 7.5% SDS – polyacrylamide gels. The gels were run simultaneously at 50 mA in a vertical electrophoresis chamber with 1 $\times$  SDS Running buffer. One gel was stained with the Coomassie Brilliant Blue stain for 20 min with shaking, and destained using the destaining solution overnight. Second gel was transferred onto a nitrocellulose membrane at 200 mA for 1 h using a transfer chamber. The membrane was briefly stained with Ponceau stain, a reversible protein staining dye used to determine the transfer efficacy, and destained using ddH<sub>2</sub>O. Blocking of the membrane was performed for 1 h in 5% milk in PBS and Tween-20 (PBST), or in 5% BSA in Tris-Buffered Saline and tween-20 (TBST) when determining phosphorylated proteins. The membrane was then incubated with primary antibody diluted in the blocking buffer. The incubation was performed for 1 hr at room temperature, after which the membranes were meticulously washed with PBST, or TBST for detection of phosphorylated proteins. Secondary antibody was diluted in the blocking buffer, and the incubation of the membranes was carried out overnight at 4  $^{\circ}\text{C}$ . The detection of the proteins was achieved by incubating the membranes in Luminol reagent A and B according to the supplier's recommendation. The visualization was performed using FujiFilm developer. Protein amount in a band of interest was quantified by using ImageJ software: intensity of the band was normalized to the total protein amount, i.e. the intensity of the entire lane of the Coomassie-stained gel. Detailed use of antibodies for determination of each protein is listed in the Table 4.

## MATERIALS AND METHODS

---

### 2.2.5 Mitochondrial methods

#### 2.2.5.1 Isolation of mitochondria

Mitochondria were isolated using the following procedure.

500 mL of stationary culture was pelleted, and rinsed with 5 mL of 10 mM EDTA. The pellet was resuspended in 2 mL Ice-cold Sorbitol Buffer A supplemented with 0.3%  $\beta$ -mercaptoethanol. 50 U of zymolyase was added, and the samples were incubated at 37 °C for 1 h, after which the spheroplasts were harvested with centrifugation at 1,800 rpm for 15 min at 4 °C. The supernatant was discarded, and the pellet was resuspended gently in 5 mL ice-cold Sorbitol Buffer A and centrifuged at 2,500 rpm for 5 min at 4 °C. Supernatant was transferred to a new tube, and centrifuged 15,000 rpm for 15 min at 4 °C. Pellet was resuspended in 1.5 mL ice-cold Buffer B, and centrifuged again at 800 rpm for 5 min at 4 °C. Supernatant was transferred into a new tube, centrifuged once more at 15,000 rpm for 5 min at 4 °C, and the pellet was stored at -80 °C.

#### 2.2.5.2 Blue Native-PAGE

Blue Native Polyacrylamide Gel Electrophoresis (BN-PAGE) is a technique used to isolate and resolve protein complexes from biological membranes by molecular weight. It is all performed while enabling proteins to retain their native structures. Mitochondria extracted following previously described protocol (2.2.5.1) were resuspended in Digitonin buffer for 30 min at 4 °C. Lysates were cleared by centrifugation for 15 min at 20000 rpm, and 4 °C, after which 10 $\times$  loading dye was added. The samples were run on 4%–13% polyacrylamide gradient gels with 4% stacking gel. The in-gel activity of the mitochondrial respiration complexes was measured following a previously published procedure (Wittig et al., 2007) that states incubation in complex IV and complex V staining solution for 30 and 60 min, respectively.

#### 2.2.5.3 Analysis of the mitochondrial morphology and protein import apparatus

For the visualization of mitochondria and evaluation of its protein import processes in this research MitoLoc plasmid was used (Vowinckel et al., 2015). All of the studied yeast strains were firstly transformed with the plasmid following a transformation protocol described earlier (2.2.2.6). Microscope slides were prepared following a procedure from 2.2.6.1, and the live cell imaging performed using the same setup as depicted in 2.2.6.2. The exposure time was 100 ms

for GFP and 300 ms for mCherry with 5-10% laser intensity. The cells containing cytosolic mCherry agglomeration were counted manually. Upwards of 1000 cells per strain was surveyed in this experiment. All the images obtained were analyzed using ImageJ platform with the integrated MitoLoc software plugin named MitoMap. The ImageJ plugins used for analyses in this experiment can be freely obtained from the following site <https://www.gurdon.cam.ac.uk/institute-life/downloadspublic/imaging-plugins>

## 2.2.6 Biochemical procedures

### 2.2.6.1 Respiration measurement

An oxygraph equipped with a Clark-type electrode (Oxygraph, Hansatech, Norfolk, UK) was used to polarographically monitor oxygen uptake of the cells in exponential growth phase. 500  $\mu$ L of yeast culture at density of  $30 \times 10^6$  cells/mL was transferred to an airtight 1.5 mL oxygraph chamber in which the conditions were kept to 30 °C and stirring. Oxygen content was monitored for at least 4 min. Antimycin (final concentration 10  $\mu$ g/mL) was used as a control to ensure that the observed oxygen consumption was due to the mitochondrial activity.

### 2.2.6.2 Geldanamycin treatments

Wild type and the constitutively active Tor1 (caTor1) strains were treated with 9 mM geldanamycin, which is used as an inhibitor of the Hsp90 chaperone. Cells were incubated for one generation time, 1.5 h, at 30 °C. Cells were subjected to the treatment at the time of the diauxic shift.

### 2.2.6.3 Torin treatments

The  $\Delta$ Snf1 strain was treated with 100 nM torin, which is used as a TOR pathway inhibitor, for 2 h before the cells were pelleted. Cells were subjected to the treatment at the time of the diauxic shift.

### 2.2.5 Fluorescence microscopy

#### 2.2.5.1. Flow cytometry

Flow cytometry was conducted on a Becton-Dickinson FACSCalibur model equipped with a 488 nm Argon laser and a 635 nm red diode laser.

#### 2.2.5.2 ROS measurement

To measure the presence of ROS 2',7'-dichlorofluorescein diacetate (H2DCFDA) was used. This reagent, although non-fluorescent, becomes fluorescent (green) in the presence of ROS, as oxidation converts it into 2',7'-dichlorofluorescein (DCF). This fluorescence is analyzed using Becton-Dickinson FACSCalibur model equipped with a 488 nm Argon laser and a 635 nm red diode laser.

Immediately before the flow cytometry experiment, fresh solution of H2DCFDA is prepared in either dimethylsulfoxide (DMSO) or 100% ethanol. Cells were carefully washed with PBS solution to remove any traces of the growth medium, and incubated with 10 µg/µL H2DCFDA for 120 min at 37 °C in the dark. ROS was then measured by flow cytometry using the FL1 channel (green fluorescence), and the collected data analyzed using FlowJo software. Results are expressed as the mean fluorescence of 10,000 cells.

#### 2.2.5.3 Measurement of Mitochondrial Mass

In order to measure the mitochondrial mass, 10-N Nonyl acridine orange (NAO) was used, a green fluorescent dye. NAO specifically binds to the mitochondrial inner membranes, more specifically to cardiolipin, a phospholipid present on the inner mitochondrial membrane, and is, therefore, used as a marker of the mitochondrial membrane surface per unit of cell mass (Maftah et al., 1989).

$1 \times 10^6$  cells/mL were resuspended in 1mL of the growth medium containing 100 nM NAO, and were incubated at 30 °C with shaking in the dark. After the incubation period, the cells were analyzed using FACSCalibur flow cytometer at FL1-height. The data obtained by flow cytometry was analyzed using FlowJo software version 7.2.5 to determine the mean green fluorescence intensity after each treatment.

#### 2.2.5.4 Assessment of mitochondrial membrane potential

The mitochondrial membrane potential (MMP) together with the proton gradient forms the mitochondrial transmembrane potential that is harnessed to form ATP. The changes in the MMP are monitored as a key indicator of mitochondrial function and cell health (Sakamuru et al., 2016). In order to measure the variations of the mitochondrial transmembrane potential, a cell membrane permeable fluorescent dye 3, 3'-dihexyloxacarbocyanine iodide (DiOC6(3)) was used.  $1 \times 10^6$  cells/mL were resuspended in 1 mL of the growth medium containing 40 nM DiOC6(3), and were incubated at 30 °C with shaking in the dark. The membrane potential-related fluorescence of DiOC6(3) was measured using FL1-height of the FACSCalibur flow cytometer. Data obtained was analyzed using FlowJo software to determine the mean green fluorescence intensity after each treatment. The results are expressed as % of mean fluorescence of the control strain. As a negative control of the experiment, cells were incubated with 100  $\mu$ M carbonyl-cyanide 4-(trifluoromethoxy) - phenylhydrazone (FCCP) in order to collapse the mitochondrial membrane potential. After its collapse, the dye remains in the cytoplasm, in contrast to healthy cells, where the dye accumulates in the mitochondria.

#### 2.2.5.5 Overexpression level measurement

The expression levels of each studied chaperone in the enriched strains was measured by flow cytometry, with the mean fluorescence from over 10000 cells. The conditions for the expression level measurements are listed in the Table 4. Obtained signals were normalized to the mean endogenous expression level of each chaperone. The internal expression levels for the Lhs1 and Egd2 chaperones were obtained by the flow cytometry measurements based on the signal of green fluorescent protein (GFP) fusions (Thermo Fisher Scientific), while the conditions for the measurements of the expression levels for the Ssc1 and Tcpl are listed in the Table 4.

Before the expression level measurements, the cells were fixed following a procedure described in 2.2.1.5. After that, cells were blocked with 5% BSA in 10 mM PBS for 30 min. The primary and secondary antibodies were diluted in blocking buffer, and incubated for 1 h at room temperature. After being thoroughly washed, cells were subjected to the flow cytometry, as described in 2.2.5.1.

### 2.2.6 Imaging

#### 2.2.6.1 Microscope slide preparation

Agarose solution was prepared using the appropriate growth media and 2% (w/v) agarose. The solution was heated to allow for the agarose to completely dissolve. 50  $\mu$ L of the agarose solution was placed on a preheated microscope slide, and it was allowed to cool before placing yeast cells in a monolayer.

3 mL of the yeast cultures used for microscope slides were previously centrifuged at 4000 rpm for 3 min, and were resuspended in 50  $\mu$ L of the appropriate growth media.

#### 2.2.6.2 Live cell imaging and analysis

Regardless of the object imaged, the same general setup was used. The slide was mounted on the Volocity software (version 6.3; Perkin Elmer) driven, temperature-controlled Nikon Ti-E Eclipse inverted/UltraVIEW VoX (Perkin Elmer) spinning disc confocal setup. Images were recorded through 60xCFI PlanApo VC oil objective (NA 1.4) using coherent solid state 488 nm/50 mW diode laser with DPSS module, and 1000x1000 pixels 14 bit Hamamatsu (C9100-50) electron-multiplied, charge-coupled device (EMCCD). The exposure time was 150 ms, and 5-10% laser intensity was used. The images were analyzed by using Image J software.

#### 2.2.7 Statistical analysis

All represented values are mean values normalized to experimental controls from three experimental and three biological replicates. All results were analyzed using R v2.15.3 (*CRAN*, <http://cran.r-project.org>) and RStudio for Windows, v 0.97 (<http://www.rstudio.com/>). All groups were tested for normality of distribution using Shapiro-Wilk test. Since analyzed data followed normal distribution, differences of means were considered statistically significant if they passed thresholds calculated using Student's two-tailed t-test for two-parameter comparisons, and parametric one-way ANOVA, followed by Tukey's *post-hoc* test for multi-parametric comparisons. For all tests significance level was set at  $p < 0.05$ , and significance was indicated as \*\*\* $P < 0.001$ ; \*\* $P < 0.01$ ; \* $P < 0.05$ .



### 3. RESULTS

#### 3.1 Part I: Mild proteotoxicity ensuing chaperone deletions leads to cross-organelle stress response (CORE) resulting in lifespan extension

This part of thesis has been published in Scientific Reports (Perić, M., Dib, P. B., Dennerlein, S., Musa, M., Rudan, M., Lovrić, A., ... Kriško, A. (2016). Crosstalk between cellular compartments protects against proteotoxicity and extends lifespan. *Scientific Reports*, (December 2015), 1–12. <https://doi.org/10.1038/srep28751>).

##### 3.1.1 Chaperone deletion in any cellular compartment induces cell-wide protein stress

With the intention to investigate the cell-wide effects of compartmentalized proteostasis failure, imbalance of protein homeostasis was provoked in specific intracellular compartments by deletion of genes encoding for a specific protein chaperone. Three chaperones localized in three distinct cellular compartments were chosen for this purpose: SSC1 gene encoding for Ssc1 chaperone (mitochondrial HSP70), EGD2 gene encoding for nascent polypeptide-associated complex NAC, and LHS1 gene encoding for Lhs1 chaperone (endoplasmic reticulum HSP70).

To confirm stress induced upon chaperone deficient strains, levels of key stress response chaperone, HSP90, were measured. Results indicate increase in the cytosolic HSP90 levels in all of the three mutant strains, without regard to the compartment of chaperone deficiency, thus verifying induced protein stress (Figure 26).

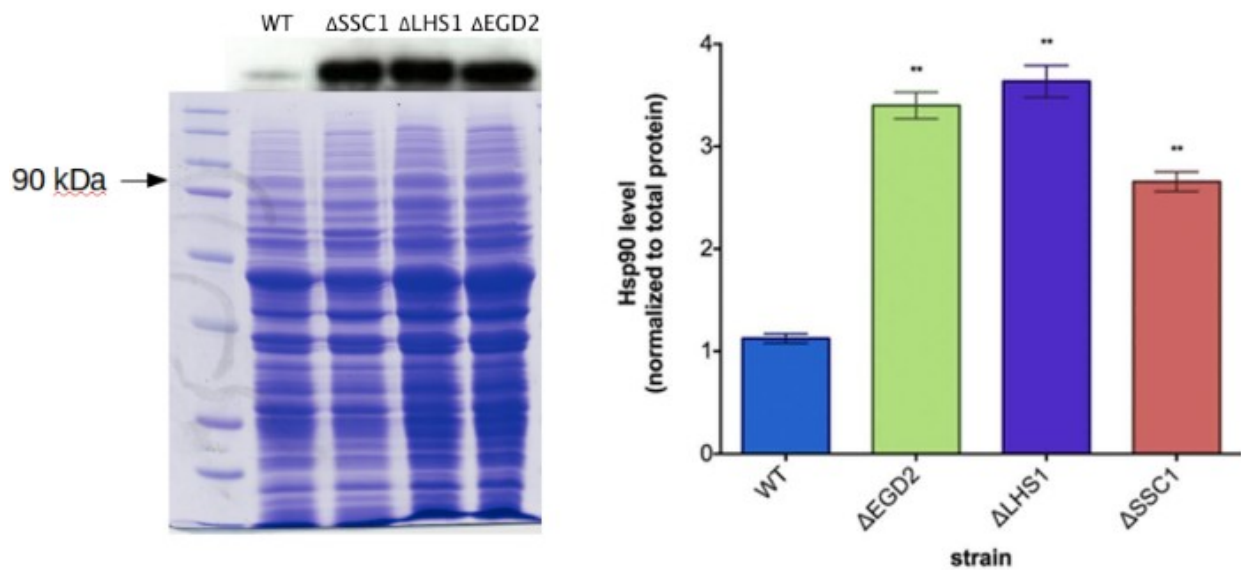


Figure 26| **Deletion of chaperones induces protein stress characterized by increased HSP90 levels.** (A) Western blotting of HSP90 chaperone in WT and deletion background strains (left). Band intensities from the western blot assay (top left) were normalized to the band intensities of total protein from the Coomassie-stained SDS-polyacrylamide (bottom left). Images shown are representative of experimental replicates. (B) Quantification of HSP90 band intensities from the western blot assay analysis (right). Results indicate increase in HSP90 level in deletion background strains in comparison to the WT strain. Asterisks indicate significant difference between samples. Data are represented as mean  $\pm$  SD from three experimental replicates. \*\* $p < 0.01$  (ANOVA plus post hoc).

### 3.1.2 Compartmentalized failure of proteostasis results in respiration decline

In order to evaluate the consequence of protein stress on cellular performance, mitochondrial respiration of chaperone deficient strain was studied, as it is generally a critical component of stress responses. Oxygen consumption rate was firstly measured, which showed a substantial decrease in comparison to the wild type (WT) strain (Figure 27).

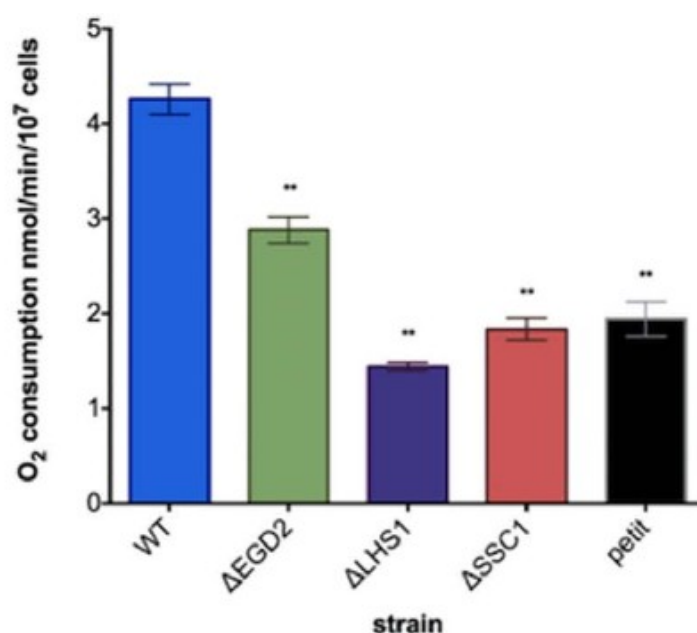


Figure 27| **Induced protein stress leads to a decline in respiration.** Oxygen consumption rate measured polarographically using a Clark electrode. The results indicate decreased oxygen consumption rate of chaperone deficient strains compared to the WT strain. Asterisks indicate significant difference between samples. Data are represented as mean  $\pm$  SD from three experimental replicates. \*\* $p < 0.01$  (ANOVA plus post hoc).

Since oxygen consumption rate of chaperone deficient strain corresponds to that of respiratory-incompetent petite strain (introduced as a negative control, Figure 27), it was important to rule out a possible respiratory chain defect resembling to the petite yeast. To eliminate this option, mutant strains were grown on YPEG media containing nonfermentable carbon source (3% ethanol, 3% glycerol) as respiratory-incompetent strains are unable to grow on it (Figure 28A). Considering that the observed growth showed no discrepancy in comparison to the WT strain, it suggests that the characterized decrease in oxygen consumption is not due to the defective respiratory chain (RC) components. To further support the absence of respiratory chain deficit, mitochondrial protein complexes of the oxidative phosphorylation (OXPHOS) system were resolved using BN-PAGE. The results showed no difference in the level of mitochondrial complexes between the studied strains, thereby eliminating the likelihood of RC defect (Figure 28B).

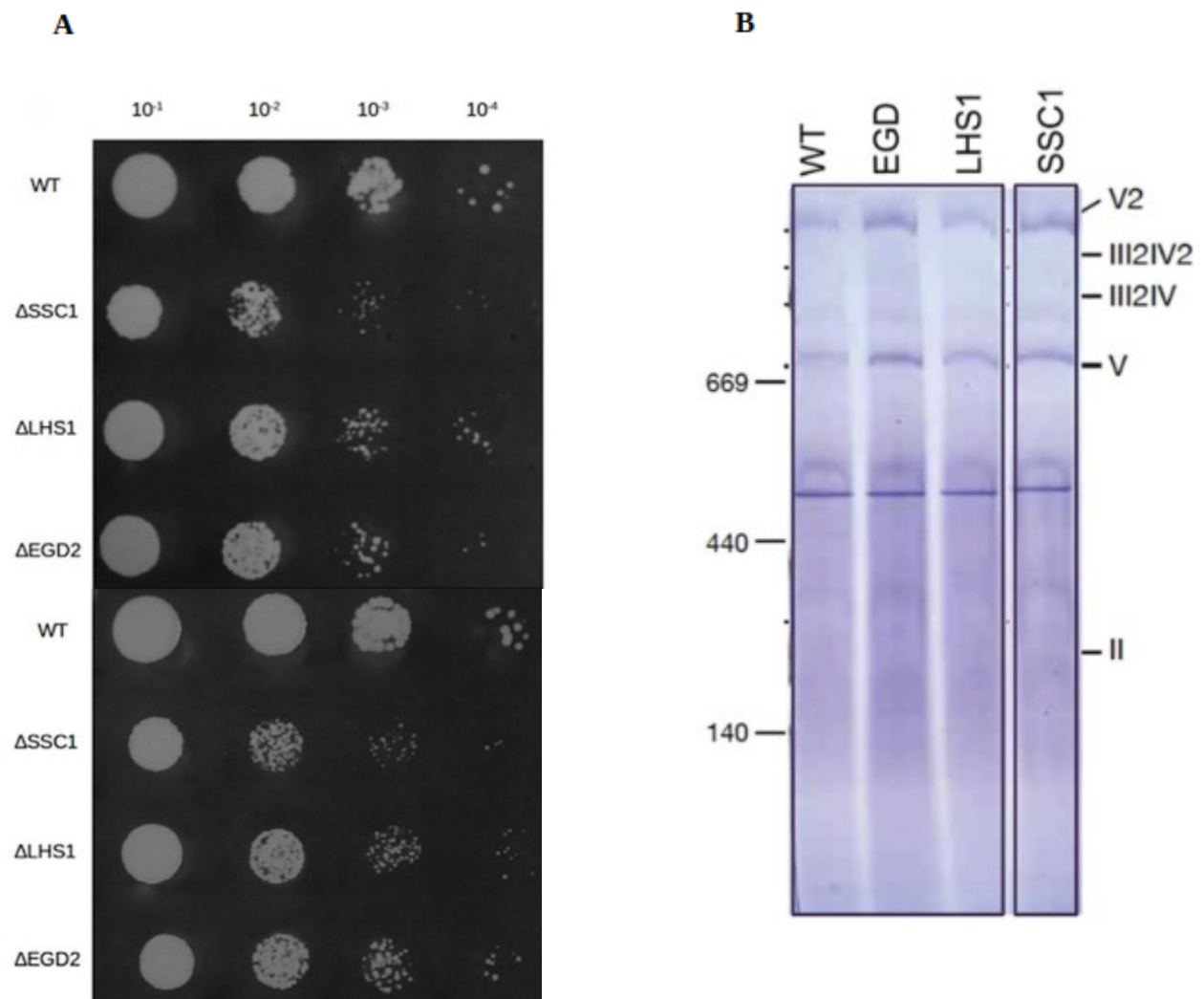


Figure 28| **Decline in respiration is not a result of defective RC complexes.** (A) Spot test analysis on YPEG medium revealed no difference in the growth rate between for both exponential (top plate) and stationary (bottom plate) growth phases. Relative number of spotted yeast cells is indicated. (B) BN-PAGE gel displaying II, IV and V of the mitochondrial OXPHOS complexes. The results presented show no difference in band intensities, and therefore, no difference in the respiratory chain configuration.

Next decision was to determine whether the declined oxygen consumption is the direct consequence of decreased mitochondrial mass. To test this, NAO fluorescent probe was used which binds to cardiolipin in the inner mitochondrial membrane, and as such, is a reliable indicator of mitochondrial mass. The fluorescent signal showed no change between the studied strains, denoting no modification in mitochondrial mass of mutated strains (Figure 29).

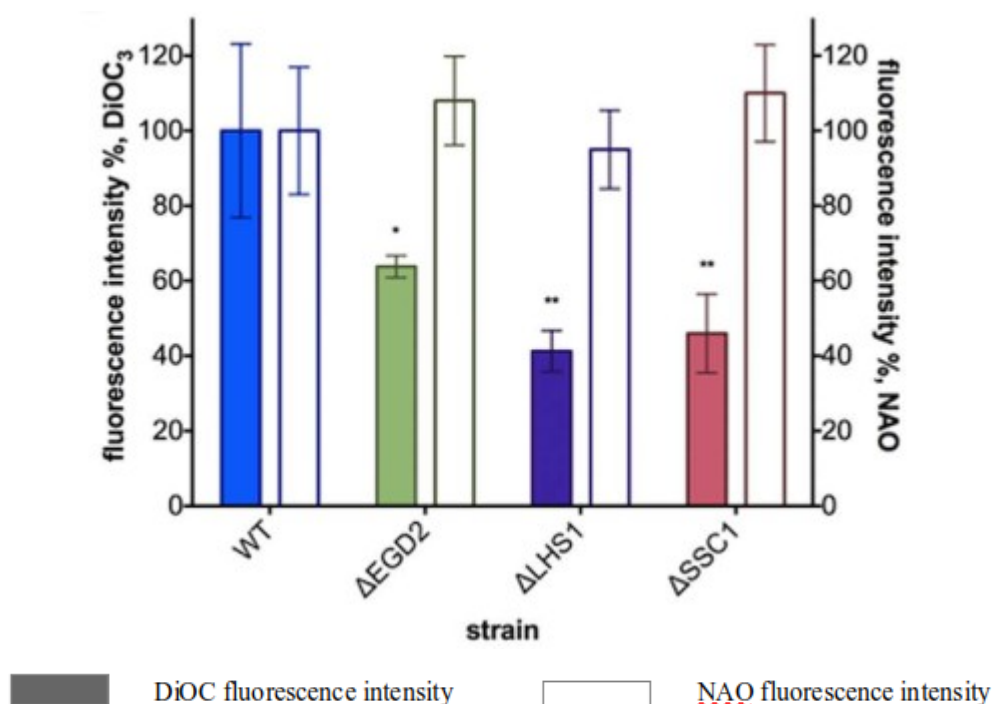


Figure 29| **Chaperone deficient strains exhibit a decline in MMP.** Mitochondrial membrane potential measurement using positively charged green fluorescent probe DiOC<sub>6</sub>(3) indicated membrane depolarization upon chaperone deletions. The analysis of the mitochondrial mass was obtained using a green fluorescent mitochondrial dye NAO, and the results show no change in the mitochondrial biomass of mutant strains in comparison to the control. Values are the mean  $\pm$  standard deviation of two technical replicates from three independent cultures \*\*\* $p < 0.001$ ; \*\* $p < 0.01$  (ANOVA plus post hoc).

Having analyzed oxygen consumption rate of the chaperone deficient strains, other core parameter of OXPHOS were evaluated – the mitochondrial membrane potential (MMP). The DiOC<sub>6</sub>(3) staining of mitochondria indicated the decline of the MMP (Figure 30A). Since MMP pertains to cells' aptitude to generate ATP, the measurements of ATP levels displayed predictable decrease in chaperone deficient strains compared to the control, while ROS levels remained unaltered (Figure 30B).

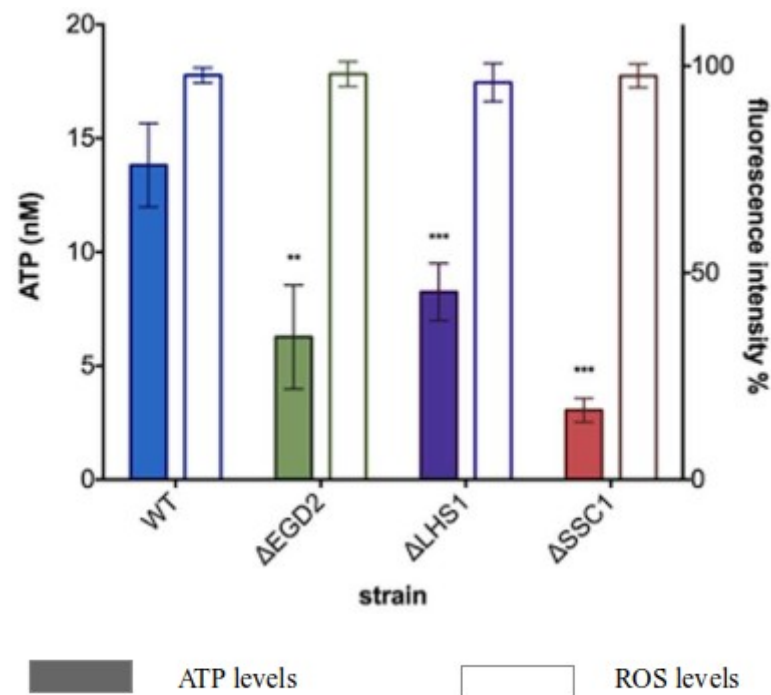


Figure 30| **Chaperone deletion induces a decrease in ATP levels without affecting the production of ROS.** Quantification of ATP in deletion background strain compared to WT determined by using fluorometric assay and quantified relative to the standard curve. Results indicate decrease in levels of ATP produced by the chaperone deficient strains. ROS production measurement. Carboxy-H2DCFDA probe was used to determine the production of ROS in flow cytometer. Results denote no change in the fluorescence intensity or ROS production. Values are the mean  $\pm$  standard deviation of two technical replicates from three independent cultures \*\*\* $p < 0.001$ ; \*\* $p < 0.01$  (ANOVA plus post hoc).

### 3.1.3 Compartmentalized proteotoxicity mediates a cell-wide response

The aforementioned decline in respiration prompted us to consider transcript levels of several conventional stress response pathways affiliated with all three compartments of chaperone deficiency: ERAD, cytosolic heat shock response, and the mitochondrial retrograde response. Gene expression was analyzed using qPCR, and the most outstanding characteristic of the chaperone deficiencies is observed in the cytosolic stress response pathway, more precisely in the upregulation of the cytosolic sHSP HSP26 (Figure 31A). The cytosolic constituent of the chaperone family HSP26 is found active exclusively under stress conditions, and its predominant function is prevention of protein aggregation (Haslbeck et al., 1999). Considering that its upregulation suggests recognition of cytosolic stress, it is rather unexpected that the levels of

HSP42, sHSP from the same family with a comparable function as HSP26, and levels of HSP70 (SSA1), a constitutively expressed chaperone induced under stress conditions, remain unaffected (Figure 31A).

Regarding ERAD mechanism components, analysis of the transcript levels indicates the increased expression of protein chaperones facilitating ER protein folding, which include KAR2, PDI1 and SEC62 (Figure 31B). On the other hand, chaperones involved in the degradation machinery of ER, such as DER1, HRD1 and UBC1, mainly remain unchanged (Figure 31B).

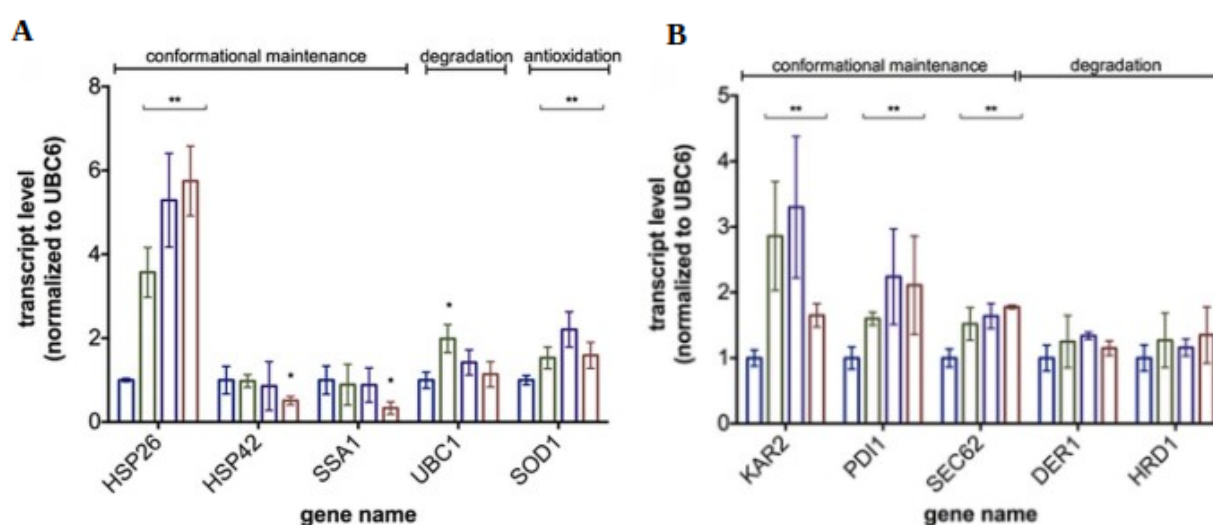


Figure 31| **Expression levels of indicated genes** were analyzed by qPCR and normalized using UBC6 as a reference gene. The examination was performed in (A) cytosol and (B) ER of WT control and chaperone deficient strains. The blue, green, purple and red bars in each graph represent WT,  $\Delta$ EGD2,  $\Delta$ LHS1 and  $\Delta$ SSC1 respectively. Values are the mean  $\pm$  standard deviation of three technical replicates from three independent cultures \*\*\* $p < 0.001$ ; \*\* $p < 0.01$  (ANOVA plus post hoc).

Since retrograde response, an intracellular compensation pathway, is triggered by the loss of membrane potential and is known to elicit cellular effect comparable to the one indicated in deletion background strains, its implication had to be eliminated. The examination of the transcript levels revealed the unchanged expression of the peroxisomal citrate synthase encoded by *CIT2* gene (Figure 32A). Taking into the account that the *CIT2* activation is a diagnostic for

retrograde response, its absence rules out the involvement of mitochondrial compensation pathway in cellular response of chaperone deficient strains.

Further examination of the mitochondrial genes demonstrated the absence of the mtUPR response, noted from the levels of chaperone used for recognition of mtUPR activation – HSP60, while the steady levels of Lon protease encoded by *PIMI* gene indicate that the degradation of oxidized proteins has not been activated (Figure 32A). Continued analysis revealed the upregulation of mitochondrial citrate synthase encoded by *CITI* and the downregulation of isocitrate dehydrogenase encoded by *IDHI* (Figure 32A). Mitochondrial citrate synthase catalyzes the first reaction of the tricarboxylic acid (TCA) cycle in which oxaloacetate and acetyl CoA react to form citrate, while isocitrate dehydrogenase converts isocitrate to  $\alpha$ -ketoglutarate generating NADH in the third reaction of the TCA cycle (Lee et al., 2007). Taken together, these results suggest a possible accumulation of citrate. To further elaborate on this hypothesis, NADP<sup>+</sup>/NADPH ratio needed to be measured.

The findings show a significant decrease in the NADP<sup>+</sup>/NADPH ratio in chaperone deficient strains relative to the control, implying an increase in the reducing power in the cytosol (Figure 32B).



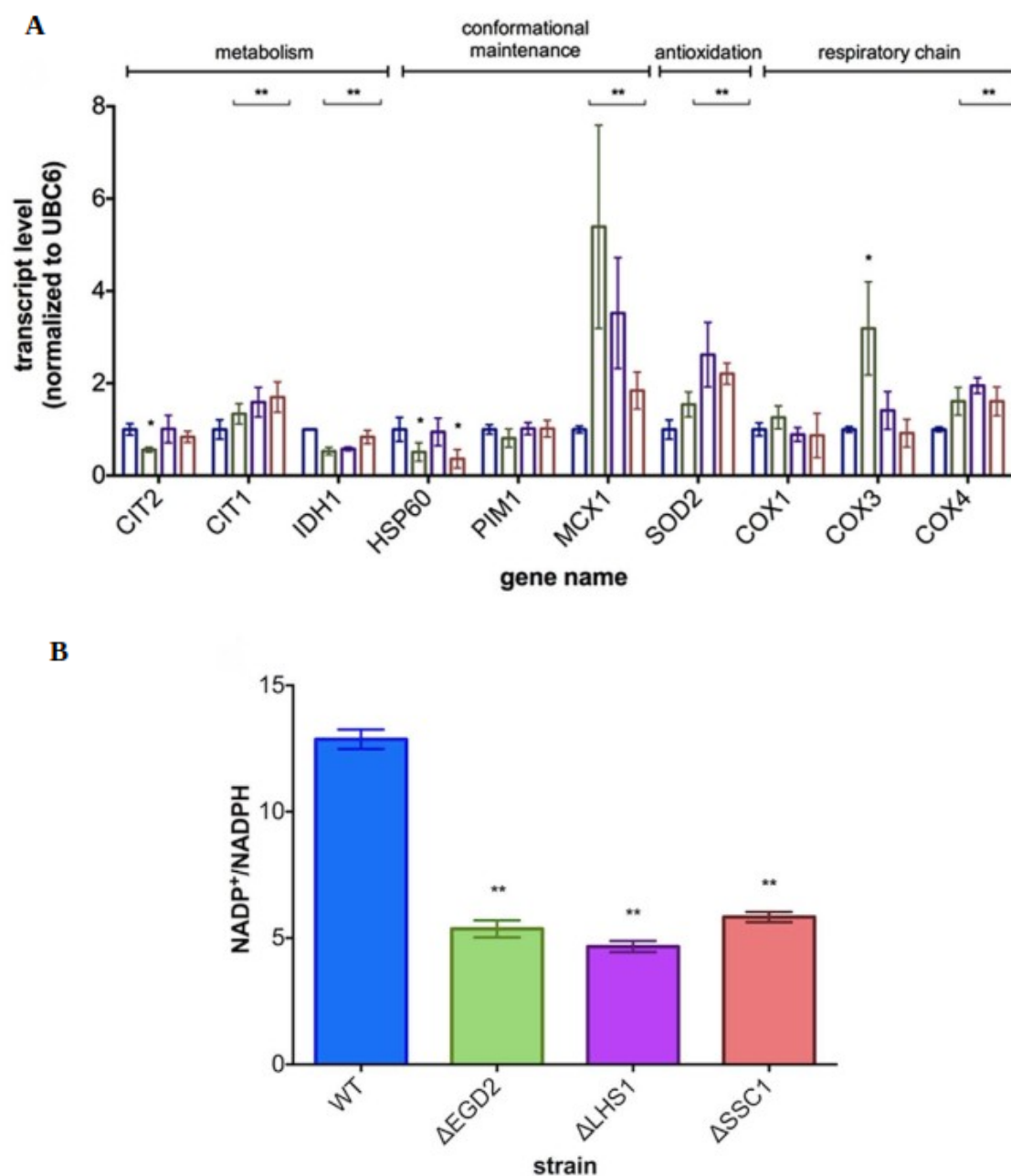


Figure 32| **Compartmentalized proteotoxicity mediates a cell-wide response.** (A) Expression levels of indicated genes were analyzed by qPCR and normalized using UBC6 as a reference gene. The examination was performed in mitochondria of WT control and chaperone deficient strains. The blue, green, purple and red bars in each graph represent WT,  $\Delta$ EGD2,  $\Delta$ LHS1 and  $\Delta$ SSC1 respectively. (B) Determination of NADP<sup>+</sup>/NADPH redox ratio by colorimetric detection. The results disclose a significant decrease in deletion strains compared to the WT control. Values are the mean  $\pm$  standard deviation of three technical replicates from three independent cultures \*\*\* $p < 0.001$ ; \*\* $p < 0.01$  (ANOVA plus post hoc).

Collectively, these results indicate that, thus far, compartmentalized proteotoxicity mediates a cell-wide response comprising of metabolic changes and the activation of conformation maintenance machinery. This prompted us to denominate the cellular response as the cross-organelle stress response (CORE).

### 3.1.4 CORE pathway induces a variable change in the components of the RC complexes

Further examination of the mitochondrial health as well as its involvement in the observed CORE pathway was desirable. It was, therefore, decided for the steady-state levels of mitochondrial respiratory chain enzyme subunits to be determined (Figure 33). For this measurement, several subunits of Complex III, including Qcr8 and Rip1; several subunits of the Complex IV, including Cox1, Cox5, and the assembly factors Coa3 and Cox15; as well as the one subunit of Complex V – Atp5 were examined. As visible from the results, the levels of Cox1 and Coa3 increased, while those of Rip1, Cox15 and Atp5 remained unchanged in all of the deletion background strains (Figure 33). Partial change was observed with the Cox5 and Qcr8, as their levels increased only in the EGD2 and SSC1 deficient strains.

Additionally, the steady-state levels of subunits of the translocase of inner mitochondrial (TIM) membrane Tim21 and Tim23, as well as that of the translocase of the outer mitochondrial (TOM) membrane Tom40 were measured. The results point to no variations in their levels compared to the WT control (Figure 33).

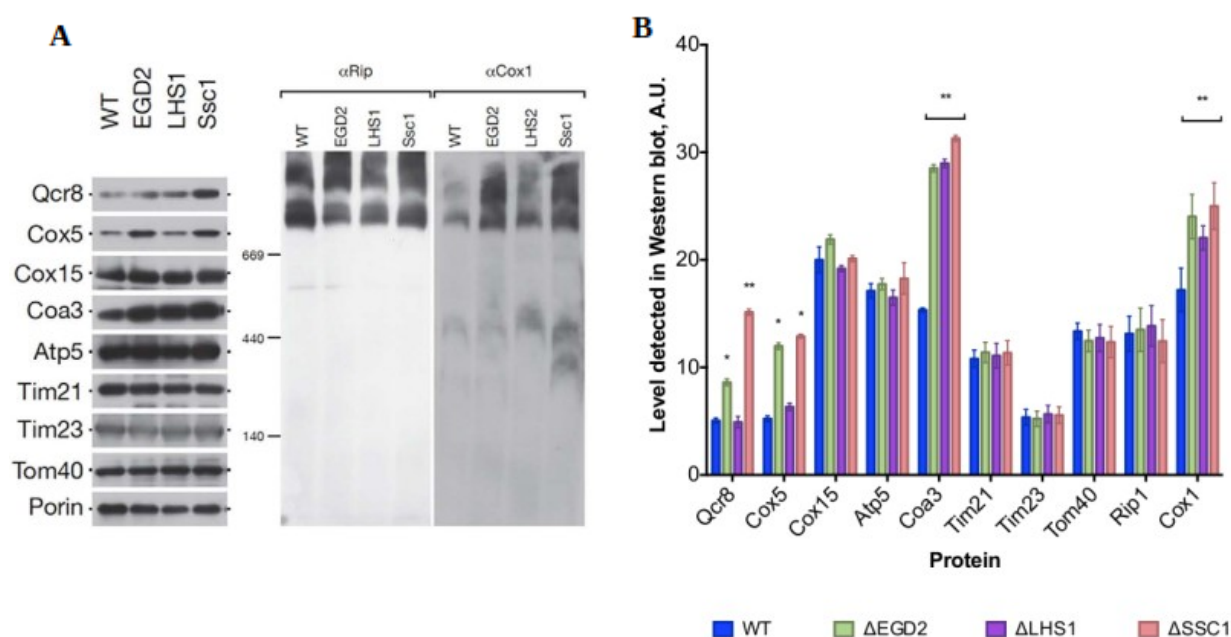


Figure 33| **CORE pathway induces a variable change in the components of the RC complexes.** (A) Western blot examination of steady-state levels respiratory chain components. Porin was used as a mitochondrial loading control. (B) Quantification of western blot analysis of steady-state levels respiratory chain components. All levels were normalized to the band intensity of porin, used as a mitochondrial loading control. \*\*\*  $p < 0.001$ ; \*\*  $p < 0.01$ ; \*  $p < 0.05$  (ANOVA plus post hoc).

### 3.1.5 Chaperone deletion results in mitochondrial fragmentation

Next, mitochondrial network morphology and its protein import ability were characterized and quantitatively measured. For that, the cells were assayed *in vivo* using MitoLoc, which contains fluorescent protein markers preSu9-GFP and preCox4-mCherry (Vowinckel et al., 2015). MitoLoc plasmid was introduced into WT and chaperone deficient strains, and the subsequent analysis of obtained images indicated mitochondrial fragmentation of the deletion background strains (Figure 34A). Unlike the tubular mitochondria observed in the WT control, chaperone deficient strains exhibited smaller and rounded mitochondria, characteristic of mitochondrial fragmentation. Further assessment of mitochondrial fragmentation using a *MitoMap* analysis software as an ImageJ plugin confirmed the detected fragmentation by reduced volume of mutant strains (Figure 34B).

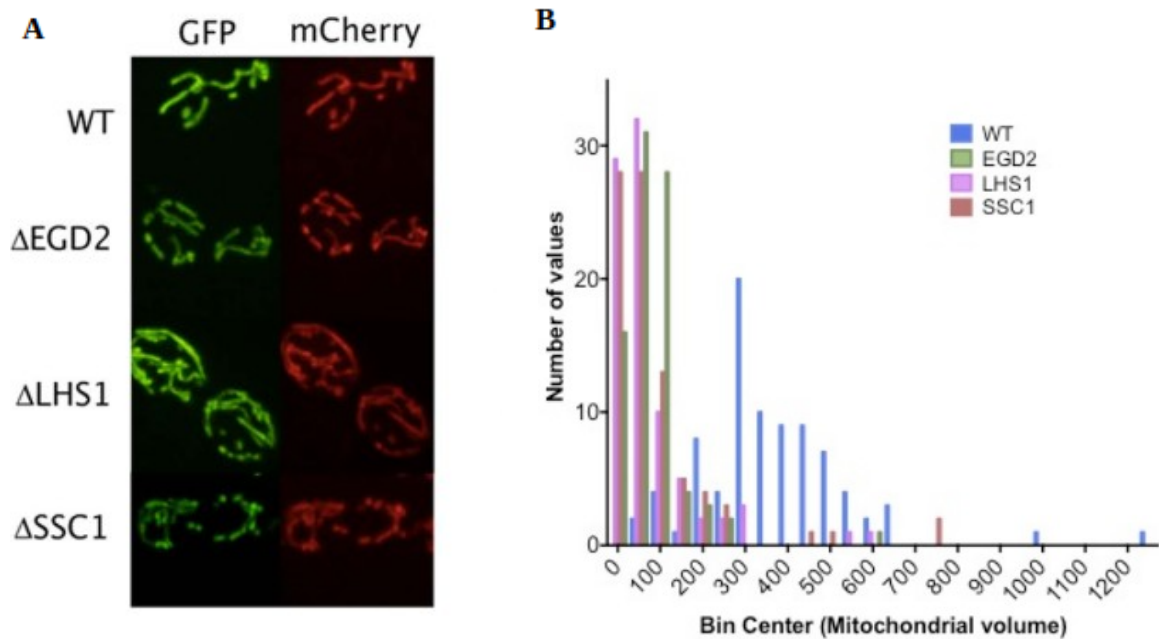


Figure 34| **Chaperone deficient strains exhibit mitochondrial fragmentation.** (A) The mitochondrial structures on the image are identified by preSU9-GFP (green) and COX4-mCherry (red), and both show mitochondrial localization. The results reveal mitochondrial fragmentation in chaperone deficient strains. Image is the representative example from more than 300 visualized cells from two biological replicates (B) Mitochondrial volume assessment, calculated by two parameters of mitochondrial surface area and volume, using ImageJ plugin, indicate decreased volume in studied strains.

To assess the mitochondrial protein import efficiency, the accumulation of COX4-mCherry in chaperone deficient mutants was analyzed and compared to the WT control. The results revealed no increase in the accumulation of the COX4-mCherry protein, suggesting successful localization in the inner mitochondrial membrane, and thus an effective translocation of COX4 across the membrane (Figure 35). Additionally, consistent co-localization of both fluorescent proteins in all studied strains makes the defective mitochondrial protein import an improbable explanation of observed partial upregulation of cytosolic chaperones.

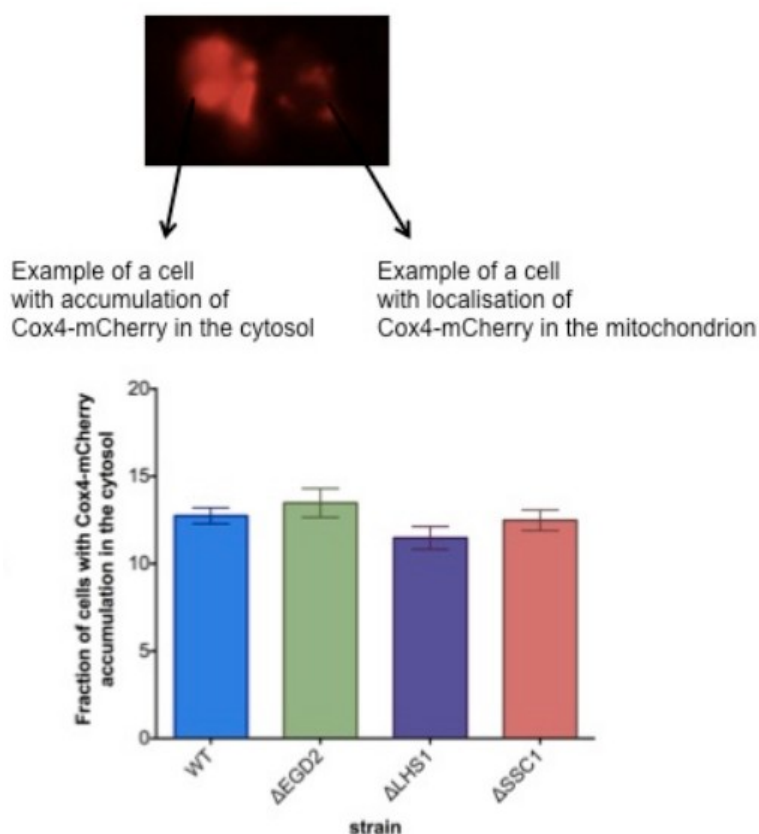


Figure 35| **Chaperone deficient strains' mitochondrial protein import is not defected.** Example of a cell with accumulation of COX4-mCherry in the cytosol, vs its localization in the mitochondrion (top). Quantification of cells which show COX4-mCherry localization within the cytosol across all the studied strains (bottom), dismissing the possibility of defected protein import. Values are the mean  $\pm$  standard deviation of more than 300 cells from three independent cultures \*\*\* $p < 0.001$ ; \*\* $p < 0.01$  (ANOVA plus post hoc).

Nevertheless, the option of defected mitochondrial protein import was further reviewed. To accomplish that, transcript levels of CORE pathway related components were investigated in two yeast strains:

- respiratory-deficient strain with the inactivated *COA3* gene whose activity is critical for cytochrome oxidase biogenesis and, hence, function of the respiratory chain;
- wild type strain treated with carbonyl cyanide *m*-chlorophenylhydrazone (CCCP) is mitochondrial oxidative phosphorylation uncoupler that prevents translocation of proteins across the inner mitochondrial membrane (Yaffe & Schatz, 1984).

The results indicated a partial overlap of the expression of targeted genes in the above-mentioned strains compared to the effect observed from the activated CORE pathway in the chaperone deficient strains (Figure 36A). The respiratory-deficient COA-null mutant shared only the upregulation of HSP26 expression level compared to the chaperone deficient strains, while, along with the upregulation of HSP26 chaperone, also resulted in the upregulation of protein disulfide isomerase (*PDII*) and isocitrate dehydrogenase (*IDHI*). The CCCP uncoupling of the respiratory chain from oxidative phosphorylation, on the other hand, had more changes of the transcript level in common. These include the upregulation of *PDII*, citrate synthase (i) and *HSP26* chaperone (Figure 36A). It did, however, result in other changes that were not witnessed with the mutant background strains, such as upregulation of *IDHI* and mitochondrial *HSP60*, and down-regulation of *SOD1* and ERAD constituents such as *KAR2* and *SEC62* (Figure 36A). To further elucidate the involvement of respiratory chain uncoupling in the detected CORE response, the levels of the HSP90 chaperone that was markedly elevated in the chaperone deficient strains were measured. WT strain treated with CCCP, however, showed no change in comparison to the control (Figure 36B). These results confirm once again that a defected mitochondrial protein import or defected respiratory chain is a highly unlikely rationale for the observed effect of chaperone deficient strains.

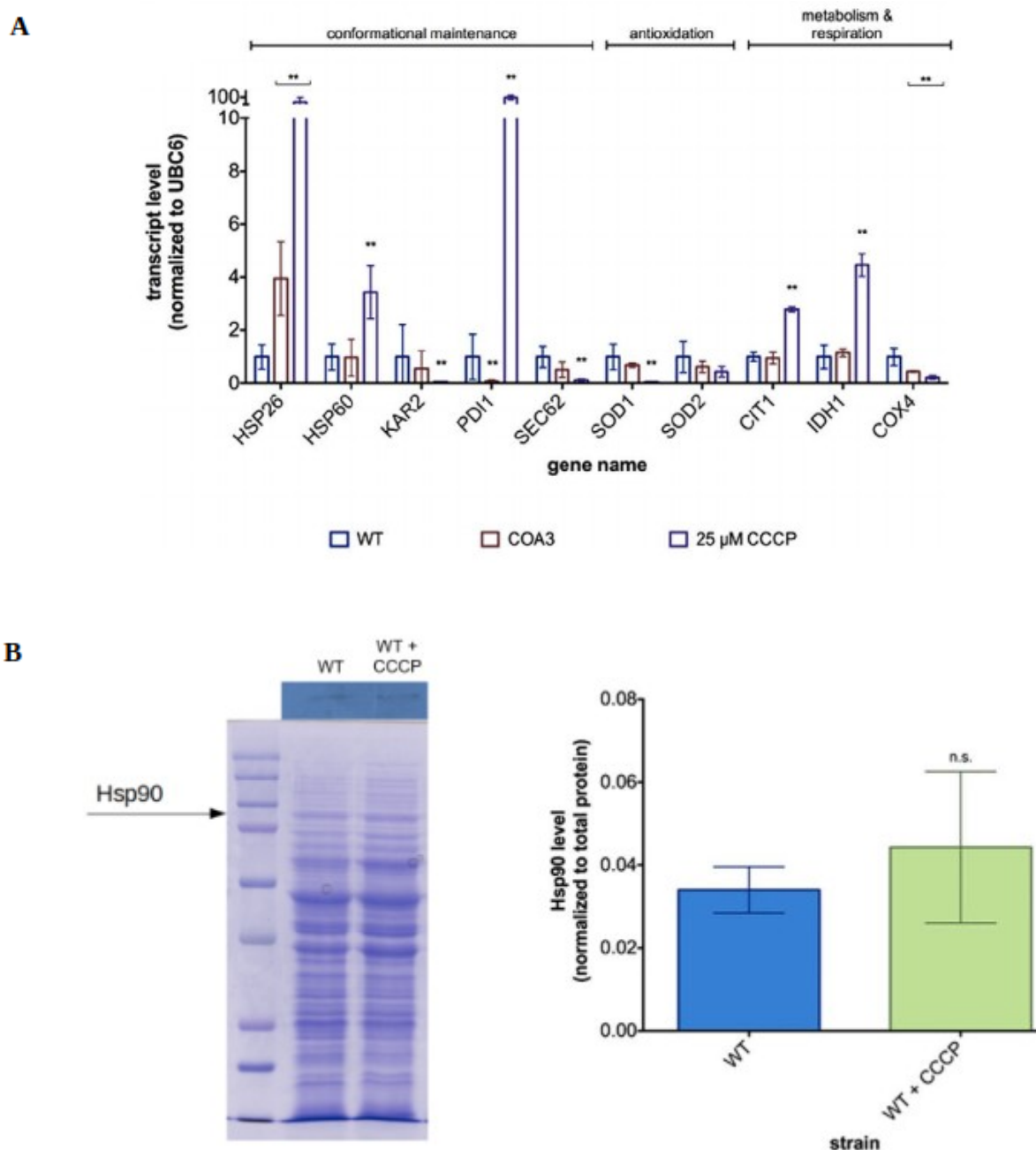


Figure 36| **Transcript levels of COA3-null mutant and WT treated with CCCP show a partial overlap with the chaperone deficient strains.** (A) WT strain was treated with 25  $\mu$ M CCCP for 2 hr during the phase of exponential growth, while COA3-null mutant was constructed as described by (Mick et al., 2010). UBC6 was used for normalization. (B) HSP90 level measurement in WT treated with 25  $\mu$ M CCCP. Protein extracts, 50 $\mu$ g, were separated by standard SDS-PAGE succeeded by Western blot analysis using antibodies against HSP90

(bottom left). Band intensities from the western blot assay (top left) were normalized to the band intensities of total protein from the Coomassie-stained SDS-polyacrylamide gel (bottom left). Quantification of HSP90 band intensities from the western blot assay analysis (right). Results indicate no change in HSP90 level in WT treated with CCCP in comparison to the control strain. Data are represented as mean  $\pm$  SD from three biological and two technical replicates. \*\*\*P < 0.001; \*\*P < 0.01; (ANOVA plus post hoc)

### 3.1.6 Hsf1 incompletely involved in regulation of the CORE pathway

Next, in order to elucidate if Hsf1 plays a role in the regulation of CORE response, the transcript levels of target genes were examined, whose expression was altered in chaperone deficient strains, in double deletion mutants of Hsf1 and each studied chaperone individually. The results show that the deletion of Hsf1 in chaperone deficient strains precludes upregulation of HSP26 (Figure 37A) and HSP90 (Figure 37B). Interestingly, the metabolic changes and the oxygen consumption remained unchanged, indicating that Hsf1 regulation does not mediate this part of the CORE response.



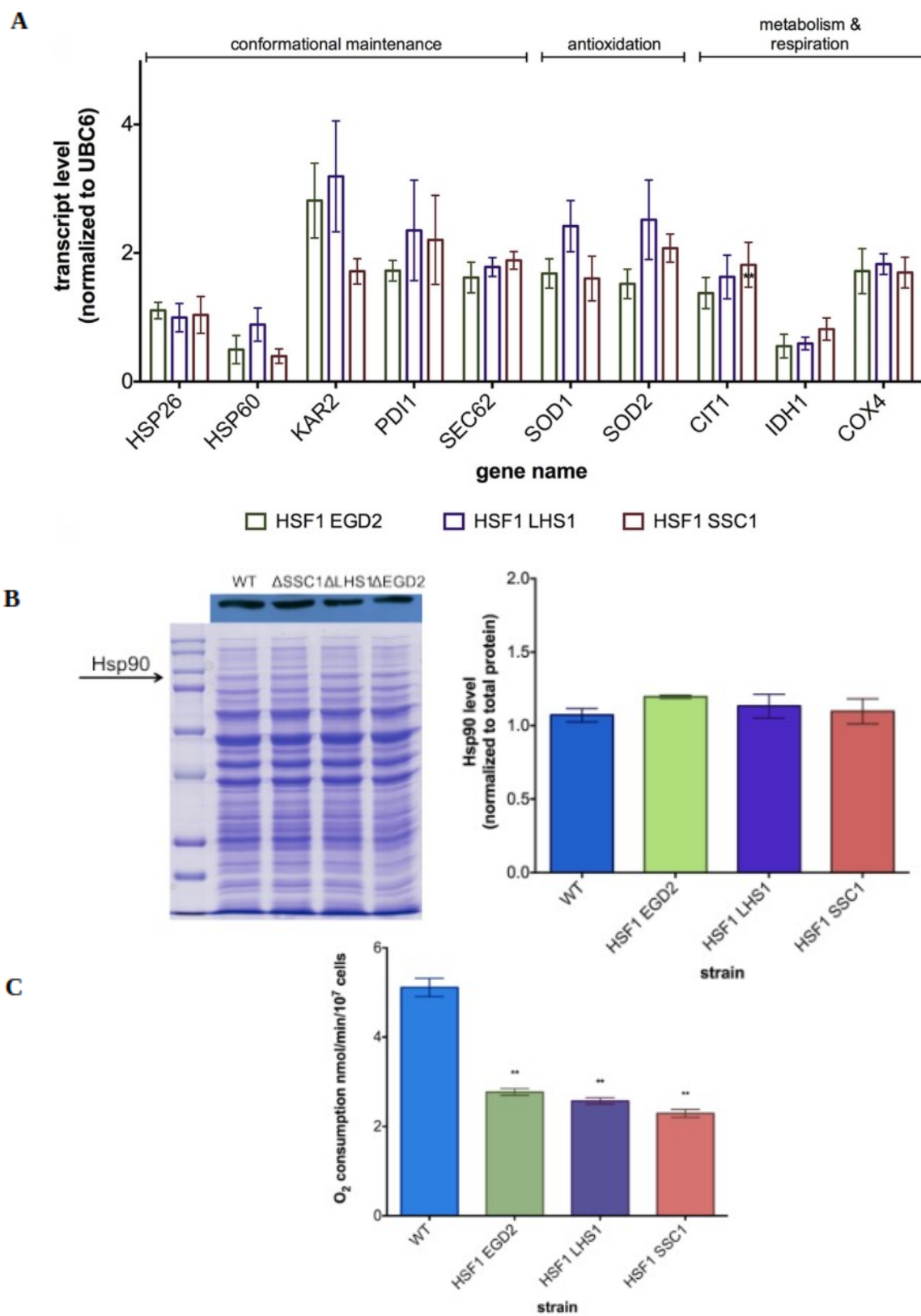


Figure 37| **Hsf1 incompletely involved in regulation of the CORE pathway.** (A) Transcript levels of targeted genes obtained by qPCR. UBC6 was used for normalization. (B) HSP90 level measurement in double deletion strains compared to the WT control. Protein extracts, 50µg, were separated by standard SDS-PAGE succeeded by Western blot analysis using antibodies against HSP90 (bottom left). Band intensities from the western blot assay (top left) were normalized to the band intensities of total protein from the Coomassie-stained SDS-polyacrylamide (bottom left). Quantification of HSP90 band intensities from the western blot assay analysis (right). Results indicate no change in HSP90 level in Hsf1 deletion of chaperone deficient strains in comparison to the control strain. Data are represented as mean  $\pm$  SD from three biological and two technical replicates. (C) Oxygen consumption rate of each yeast strain was measured polarographically using a Clark electrode. The results indicate decreased oxygen consumption rate of Hsf1 deletion in chaperone deficient strains compared to the WT strain. Data are represented as mean  $\pm$  SD from three biological and two technical replicates. **\*\*p < 0.01** (ANOVA plus post hoc).

### 3.1.7 Chaperone deficient strains evince extended lifespan

Intrigued by the cell-wide impact of the activated CORE pathway, learning the possible effect it might have on the lifespan of studied strains was necessary. As mentioned previously, mild stress conditions exert beneficial consequences on cellular longevity, which in yeast can be measured in both replicative and chronological manner. As the RLS of yeast is defined as the number of daughters produced by the mother cell before reaching senescence, mother cells need to be monitored in order to separate and enumerate the generated buds. This is performed using a manual dissection microscope referred to as the micromanipulator. The maximum RLS of the chaperone deficient strains is significantly longer than that of WT control (Figure 38). Deletion of EGD2 and SSC1, encoding a subunit of nascent polypeptide associated complex (NAC) and mtHSP70 respectively, resulted in the most prominent lifespan extension, with the maximum RLS from 19 to 26 generations, or 40% increase compared to the WT control. Following was the deletion of LHS1, encoding for erHSP70, which resulted in the increase of maximum RLS from 19 to 24 generations, or 30% increase compared to the WT control.

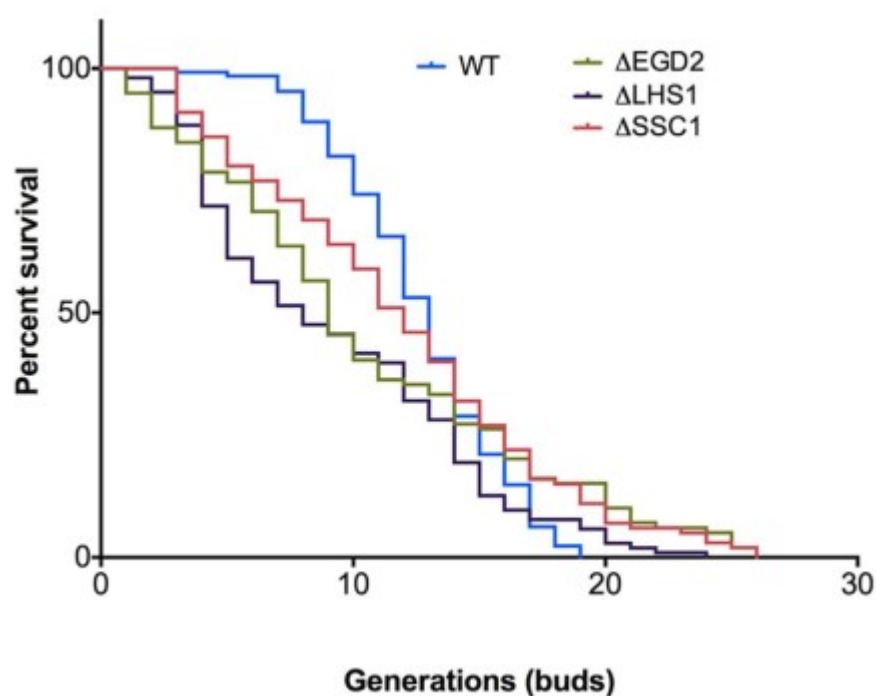


Figure 38| **CORE pathway activation elicits replicative lifespan extension** Survival curves for chaperone deletion strains compared to WT control determined by micromanipulation. Data presented are pooled from two independent experiments, totaling WT (n=104),  $\Delta$ EGD2 (n=117),  $\Delta$ LHS1 (n=115) and  $\Delta$ SSC1 (n=121) mother cells. Significance of the results was tested with log-rank test, p-values < 0.05.

Although two models of aging in yeast, RLS and CLS, were considered to be quite divergent, certain overlaps were recently identified. We, therefore, wanted to test whether activation of the CORE pathway in the chaperone deficient strains also leads to the extension of chronological lifespan. CLS is defined as the length of time yeast cells survive in the non-dividing state. The measurements revealed the extension of CLS similar to the one observed in RLS measurements (Figure 39). Deletion of LHS1 gene resulted in ~40% increase in lifespan compared to the WT control, while deletion of EGD2 and SSC1 genes resulted in 25% and 15% increase in lifespan compared to the control.

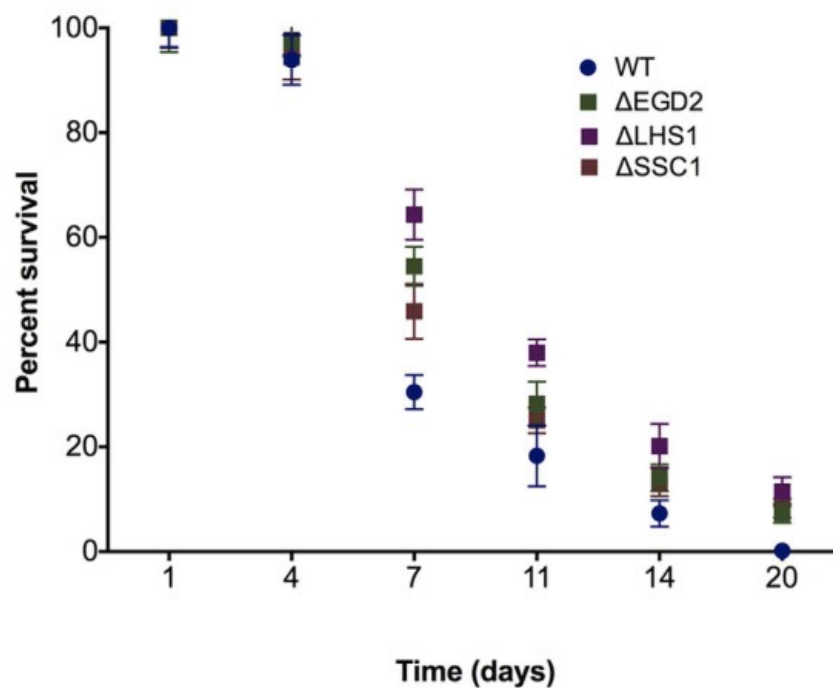


Figure 39| **CORE pathway activation leads to chronological lifespan extension.** Colony establishment was determined from day 1, and every 3 days thereafter. 3 independent experiments were performed, and their mean and standard deviation is presented in the results.

## 4.1 DISCUSSION PART I

Results from our study reveal the existence of cross-organelle response (CORE), an unprecedented pathway which allows for communication between distinct cellular compartments and actuation of cell wide stress response following the exertion of a mild proteotoxic stress succeeding compartmentalized deletion of chaperones. CORE response is activated in all studied strains irrespective of the compartmentalized origin of proteostasis failure, and it encompasses the modification of genes involved in cellular maintenance and metabolism as well as the reduction of respiration.

### 4.1.1 CORE pathway elicits upregulation of cellular maintenance genes

Mild compartmentalized failure of proteostasis triggers the upregulation of genes involved in the conformational maintenance, more specifically HSP90 and HSP26 molecular chaperones. HSP90 is a cytosolic cytoprotective molecular chaperone essential for maintaining the conformational stability of nascent polypeptides and refolding misfolded proteins. Its expression is modulated by cellular stress and is used as a reliable parameter of proteotoxic response. HSP26, the most distinguished member of the small HSP (sHSP) family, inhibits protein aggregation by trapping misfolded proteins in soluble state (Haslbeck et al., 2005). The observed upregulation of the two chaperones indicates the detection of proteostasis failure and the subsequent reciprocation by entrapping and refolding the damaged proteins, thus promoting restoration of cellular health. The identified alteration of molecular chaperone gene expression revealed the dependence on HSF1, as the cross-organelle response was absent in chaperone deficient strains lacking HSF1. HSF1 belongs to the family of heat shock transcription factors (HSFs), which are promoter regulators that mediate the expression of heat shock genes in response to stimulation by various stressors (Verghese et al., 2012). On the other hand, another prominent hallmark of HSR - the upregulation of HSP70 chaperone, was not observed in the chaperone deficient strains, suggesting that the HSR is not activated in the conventional manner. Further review of the gene expression levels revealed the upregulation of folding maintenance component of the ER, notably the *KAR2*, *SEC62*, and *PDII* genes, and mitochondria, in

particular the *MCX1* gene. Secreted proteins are subjected to the ER quality control (ERQC) mechanisms upon entering ER, which promote native structure conformation and prevent protein aggregation (Marco Sandri, 2014). ER-associated degradation (ERAD) is the resulting process of ERQC which targets and retrotranslocates aberrant or damaged proteins that accumulate within the ER lumen back into the cytosol, where they are marked for degradation or refolding (Brodsky et al., 1999; Verghese et al., 2012). One of the key chaperones aiding the retrotranslocation process is KAR2, which detects and interacts with misfolded proteins assisting in ER stress alleviation. It has also been shown that KAR2 is essential for proper folding of proteins in the ER (Kimata et al., 2003; Liu & Chang, 2008; Simons et al., 1995). Considering that KAR2 is a known target and is induced by constitutively active Hsf1, the chaperone deficient strains lacking HSF1 predictably showed no change in the expression of KAR2 (Liu & Chang, 2008). Upregulation was also observed with the ER membrane translocon encoded by *SEC62*. The transmembrane protein, Sec62, plays a pivotal role in translocation machinery upon forming a dimeric complex with Sec63. The complex regulates the import of newly synthesized proteins into the ER lumen. Besides this conventional role, it was showed recently that Sec62, in separation from Sec63, is involved in mitigation of ER stress resulting from perturbations of ER proteostasis (Fumagalli et al., 2016; Linxweiler et al., 2017).

Besides *KAR2* and *SEC62*, upregulation was noted with *PDII* gene encoding for the protein disulfide isomerase 1. PDI1 chaperone promotes aggregation prevention and catalyzes the formation and rearrangement of disulfide bonds which maintain protein's tertiary and quaternary conformation (Verghese et al., 2012; Wilkinson & Gilbert, 2004).

As for the mitochondrial input in proteostasis maintenance, the *MCX1* gene encoding for the mitochondrial ClpX (Mcx1) was upregulated in the chaperone deficient strains. Mcx1 belongs to the Hsp100/Clp protein family and is localized to the mitochondrial matrix. Although its function still remains to be elucidated, it was shown that it is a non-proteolytic protein with unfoldase properties (Chen et al., 2015; Dyck et al., 1998).

On the contrary, the degradation components of the ERAD pathway remained unaltered by the mild proteotoxicity, in particular genes encoding for Der1, Hrd1, and Ubc1. Ubiquitin protein ligase Hrd1 acts together with Ubc1 and Der1 to detect proteins with misfolded luminal domains and mediate their degradation within the ER. ER-associated Ubc1 provides Hrd1 with an

ubiquitin, while the accessory factor Der1 forms complex with Hrd1 required for the ERAD-luminal (ERAD-L) degradation (Kanehara & Ng, 2010).

These results suggest that the CORE pathway activation leads to cells alleviating stress by protecting and restoring the cell-wide folding environments. The detected upregulation of SOD1 and SOD2 in response to detected proteotoxicity further confirms the protective stress mitigation. The cytosolic copper-zinc superoxide dismutase (Sod1) and the mitochondrial manganese superoxide dismutase (Sod2) protect the cells from oxidative damage by converting the superoxide anion to molecular oxygen and hydrogen peroxide (Nedeva et al., 2004).

#### 4.1.2 CORE pathway alters the expression of metabolic genes

The most outstanding changes in the expression of genes involved in metabolism include the upregulation of CIT1 together with the downregulation of IDH1. Both genes encode for enzymes taking part in one of the most quintessential metabolic pathway - the TCA cycle. Tricarboxylic acid (TCA) cycle is considered to be the central respiratory pathway involved in oxidation of acetyl-CoA obtained from oxidation of pyruvate in the glycolysis pathways. Citrate synthase (CS), encoded by CIT1, and isocitrate dehydrogenase, encoded by IDH1, are involved in the initial steps of the TCA cycle that result in the formation of  $\alpha$ -ketoglutarate (Liu & Chang, 2008). CS, as the name suggests, is involved in the production of citrate, while IDH1 takes part in its breakdown (Anoop et al., 2003). Thus the observed increased expression of CIT1, together with the decreased expression of IDH1 most likely leads to the accumulation of citrate in mitochondria (Figure 40).

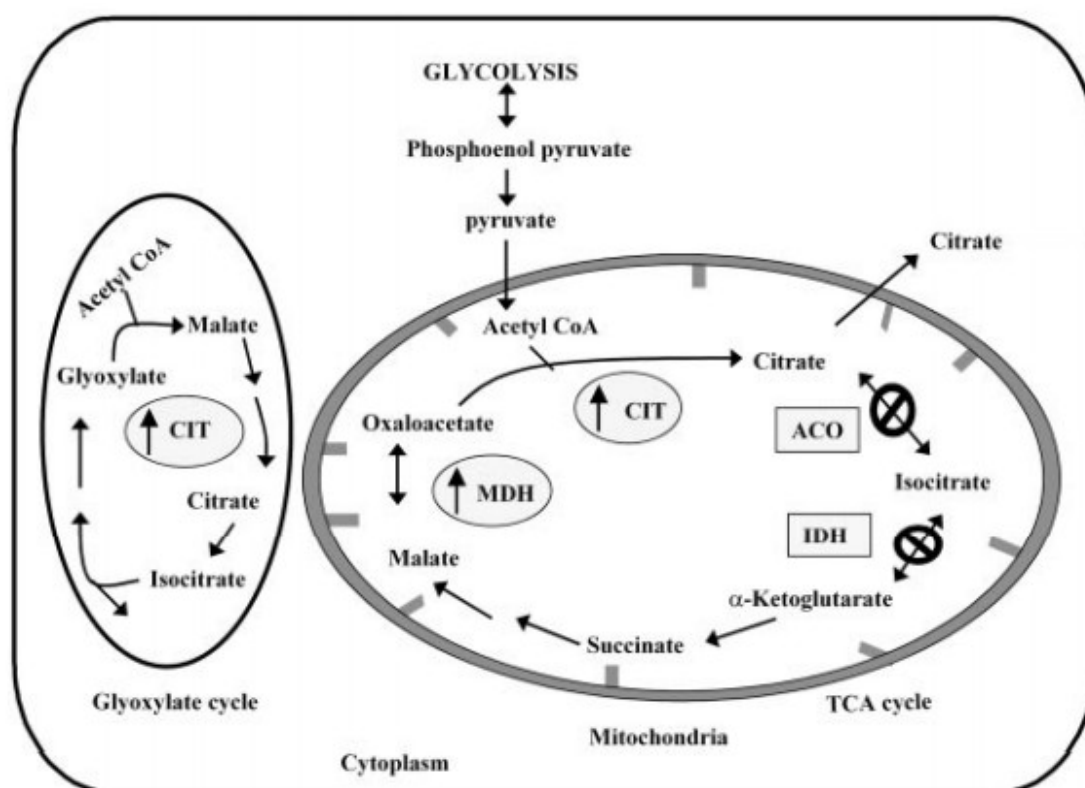


Figure 40| **Diagram illustrating the changes in gene expression that results in the modification of the citrate production.** The upregulation of genes (indicated with  $\uparrow$ ) and the downregulation of genes (indicated with  $\emptyset$ ) would lead to an increased production of citrate, and ultimately its accumulation (Anoop et al., 2003).

There was a possibility that the accumulated citrate is exported from mitochondria to the cytosol via mitochondrial citrate transporter (CIC), with the intent to increase the NADPH reducing power in the cytosol (Catalina-Rodriguez et al., 2012; Gnoni, Priore, Geelen, & Siculella, 2009). CIC is a member of a carrier protein family located in the inner mitochondrial membrane. These mitochondrial carriers catalyze the translocation of substrates, providing a crucial connection with the cytosol as they supply the intermediates of the TCA cycle. In particular, CIC facilitates the export of citrate in exchange for malate. The flux of citrate from mitochondria to the cytosol supports  $\beta$ -oxidation of fatty acids and amino acid synthesis, while high levels of cytosolic citrate blunt glycolysis by directly inhibiting PhosphoFructoKinase 1 (PFK1), an essential



glycolytic enzyme (Catalina-Rodriguez et al., 2012; Palmieri et al., 2006). The citrate translocation also supplies the glycolysis with the  $\text{NAD}^+$  while providing the cell with NADPH, which could be utilized for synthesis of important cellular antioxidants which help the cell cope with mild stress conditions (Castegna et al., 2010). It was the observed decrease of  $\text{NADP}^+/\text{NADPH}$  ratio in the chaperone deficient strains that strongly supported the hypothesis of citrate accumulation and its subsequent translocation to cytosol that is directly influenced by the activation of CORE pathway.

#### 4.1.3 CORE pathway activation results in impaired mitochondria

As the mitochondrion is deemed the core of cellular metabolism, perturbed proteostasis induced by chaperone deletions could lead to alterations in its performance. Indeed, the activation of the CORE pathway provoked a decline in respiration of the chaperone deficient strains. In addition to lowered respiration, chaperone deficient strains also demonstrated a decline in the mitochondrial membrane potential (MMP). MMP, or  $\Delta\Psi_M$ , is essential for maintaining physiological mitochondrial functions which involve production of ATP, as well as the import and synthesis of mitochondrial proteins (Zorova et al., 2018). The electron transport chain (ETC) of the inner mitochondrial membrane generates two gradients:

- the electrochemical gradient, composed of the  $\Delta\Psi_M$  and pH gradient, formed by a series of redox reactions
- proton gradient formed by proton pumping of complexes I, III and IV (Marchi et al., 2012; Zorova et al., 2018).

Together, the two gradients form the transmembrane potential which acts as an intermediate form of energy depot that drives the synthesis of ATP (Joshi & Bakowska, 2011). Hence, the noted decrease of ATP levels in the deletion strains following a decline in the  $\Delta\Psi_M$  comes as no surprise. Furthermore, given that the import of proteins into the mitochondria is dependent on the MMP, it was necessary to test the mitochondrial import capacity, as well as to understand whether the observed response is a consequence of a faulty import.

#### 4.1.4 CORE pathway activation is an improbable response to faulty protein import

Although mitochondria are capable of protein synthesis, they are largely dependent on importing the vast majority of required proteins. These proteins, synthesized on the cytosolic ribosomes are imported into the mitochondria across mitochondrial membranes predominantly via the members of the translocases of the outer membrane (TOM) and the members of translocases of the inner membrane (TIM) (Chacinska et al., 2014). Consequently, the observed steady state levels of TOM40 and TIM21 and TIM23 have failed to reveal a defected mitochondrial protein import. Nonetheless, it was important to further investigate the possibility of a malfunctioning protein import in mitochondria considering that it alone could be accounted for the witnessed response of chaperone deficiency. In pursuit of this, the mitochondrial protein import was impeded by two disparate mechanisms:

- dissipation of the inner mitochondrial membrane potential (“uncoupling of mitochondria”) by carbonyl cyanide 3-chlorophenylhydrazone (CCCP)
- dissolution of the inner MMP via COA3 gene deletion.

In the presence of the uncoupling reagent, CCCP, the electrochemical potential of the inner mitochondrial membrane is abolished due to the translocation of the protons across the membrane. This abolishment further leads to the inhibition of protein import into mitochondria (Kasianowicz et al., 1984; Martin et al., 1991). The COA3-null mutants, on the other hand, exhibit a defected protein import into mitochondria by the dissipation of the inner MMP (Mick et al., 2010). The expression levels of the COA3-null mutants and the CCCP treated cells revealed a fractional degree of similarity to the expression levels observed in the chaperone deletion strains, suggesting that the CORE pathway activation is an improbable response to faulty mitochondrial protein import.

Finally, decision was made to examine the protein import in mitochondria using a dual reporter MitoLoc. MitoLoc is a fluorescence microscopy-based system comprising of a plasmid which allows for localization analysis of two mitochondrial fluorescent proteins: GFP and mCherry. GFP is fused with F<sub>0</sub>-ATPase subunit 9 (preSU9) of *Neurospora crassa*, which allows for MMP-independent import and mitochondrial localization, robustly labeling mitochondrial structures.

The second marker, mCherry, is generated by cytochrome C oxidase 4 (COX4) fusion, whose mitochondrial localization, unlike that of GFP-tagged preSU9, is MMP dependent. Co-localization of the two markers allows for mitochondrial protein import analysis (Vowinckel et al., 2015). The results indicated no protein accumulation, suggesting a functioning protein import into mitochondria. This all led us to conclude that the witnessed response following the activation of cross-organelle response (CORE) is not attributable to an impaired protein import into the mitochondria.

#### 4.1.5 CORE pathway activation results in lifespan extension

The lifespan extension, both replicative and chronological, has been observed in all of the studied chaperone deficient strains. As mentioned previously, replicative lifespan is assessed as the total number of daughter cells produced by the mother cell, while the chronological lifespan is measured as the time span non-dividing cells can survive in a stationary phase (Fabrizio & Longo, 2003). In this study, both replicative and chronological lifespan extension has been observed in all of the studied chaperone deficient strains, possibly due to a minor proteotoxic stress exerted by the deletion of various chaperones. Mild mitochondrial impairment has previously been implicated in lifespan extension conserved across eukaryotic species through a hormetic mechanism termed mitohormesis (Merkwirth et al., 2016; Yun & Finkel, 2014). Hormesis, a concept studied since 19<sup>th</sup> century, can be defined as an adaptive response to mild and transient disruption of homeostasis with frequent beneficial implications (Calabrese & Baldwin, 2002). Similarly, mitohormesis is identified as a comprehensive cytoprotective state ordained by cytosolic and nuclear response to a moderate mitochondrial stress (Figure 41) (Yun & Finkel, 2014). This mild mitochondrial stress, signaled by change in the mitochondrial membrane potential or ROS levels, elicits cellular responses, such as deviated chaperone expression or increased antioxidant production, whose compounding impact results in lifespan extension. It is also presumed that other organelles within the cells, such as ER, could sense organelle-specific stress and signal the nucleus (Yun & Finkel, 2014). This would explain the response observed in all of our studied strains regardless of the origin of deleted chaperone. How mitochondria, or other organelles, signal the perceived stress to the nucleus is still not fully understood, but it is studied considerably regarding retrograde response.

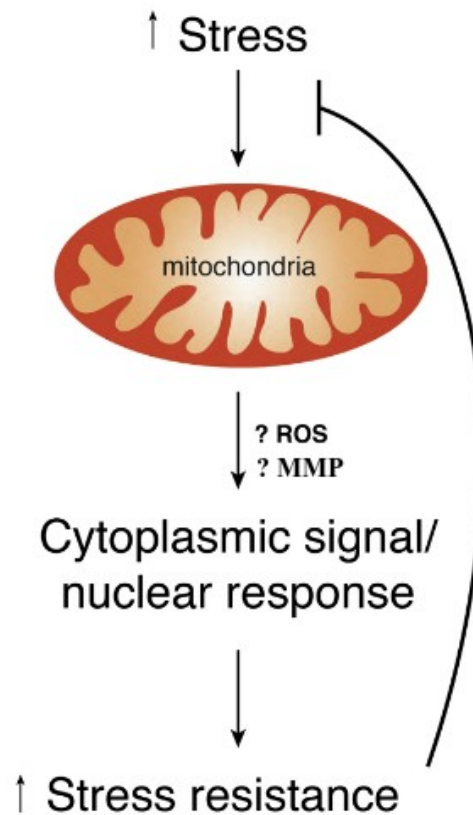


Figure 41| **Fundamentals of mitohormesis** (adapted from Yun & Finkel, 2014)

#### 4.1.6 CORE pathway activation does not result in retrograde response nor the HSR activation

Retrograde response pathway is a programmed form of inter-organelle communication following a stress signal generated by impaired mitochondria to the nucleus (Jazwinski, 2013; Miceli et al., 2012). As a result of mitochondrial dysfunction detection, Rtg3 protein translocates to the nucleus upon phosphorylation by Rtg2 protein, and binds to GTCAC sequence in the promoter of the retrograde response genes (Jazwinski, 2013). It has been suggested that mitochondrial impairment is sensed by disrupted MMP or by decreased cellular ATP levels, and that the subsequent activation of retrograde response pathway results in lifespan extension in yeast (Jazwinski, 2013; Jiang et al., 2016; Trendelewa & Zvyagilskaya, 2018). Given that the studied chaperone deficient strains exhibited disrupted MMP, decreased cellular ATP levels and extended lifespan, there was a potential that the activation of CORE pathway leads to enablement of the retrograde response. To test this hypothesis, the expression levels of peroxisomal citrate synthase (CIT2), considered being a core diagnostic gene for retrograde response, were measured (Miceli

et al., 2012). The results showed no change in its expression levels, deeming the observed alterations in mutant strains unlikely to be caused by retrograde response induction.

Additionally, chaperone deletion strains did not display the conventional activation of heat shock response (HSR). Recent finding shows that mitochondrial damage abolishes HS response, and consistent with this, the levels of Hsp70 in this research remained unaltered upon proteostasis disruption. Upregulation of Hp70 could exacerbate stress by promoting folding, which would impact the degradation of cytosolic proteins (Wang & Chen, 2015).

In summary, failure of proteostasis upon deletion of compartmentalized chaperones evokes a cell-wide response that culminates in lifespan extension (Figure 42). Presumably, deletion of some chaperones is discerned as mild decline in proteostasis and it leads to a decrease in mitochondrial function, i.e., decline in oxygen consumption and MMP. Concurrently, cellular metabolic activity is altered, collectively resulting in extension of both chronological and replicative lifespan. Although the two lifespan models were deemed independent of each other, new data implies that it might not be the case as some inherent aging processes do, in fact, partially coincide. Interestingly, those exact concurring processes are considered to hold the key to unlocking the enigma of aging process in humans (Janssens & Veenhoff, 2016; Kaeberlein et al., 2007; Zimmermann et al., 2018).

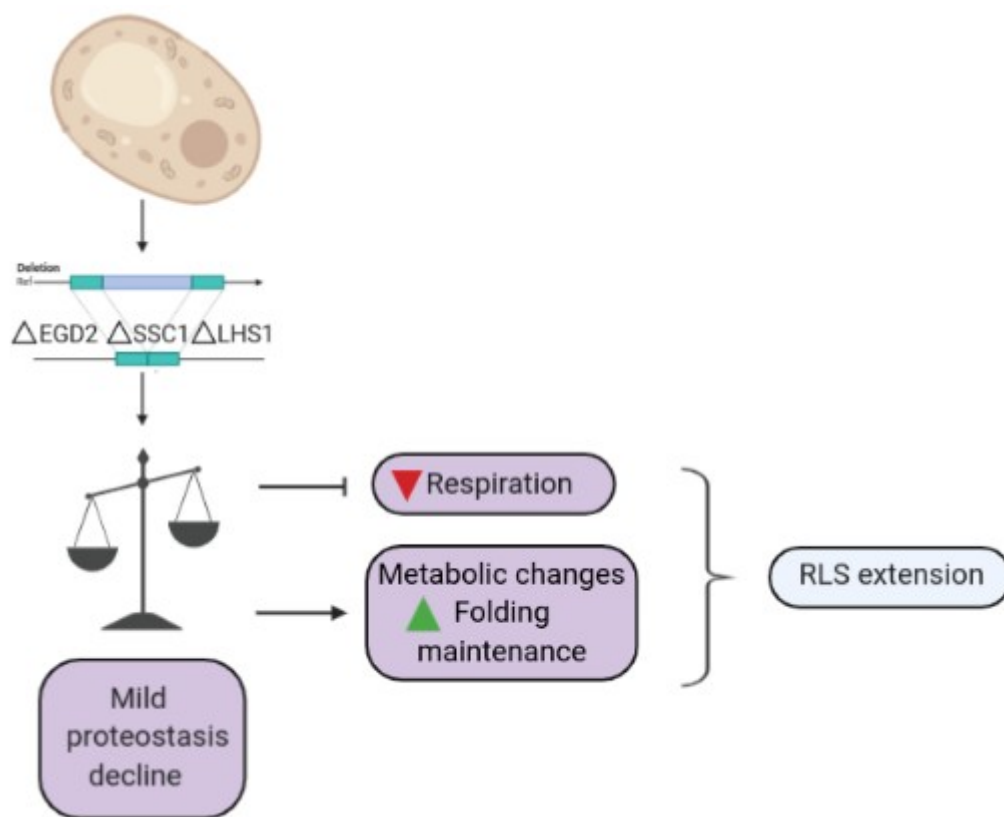


Figure 42| **Illustration depicting sequence of events following chaperone deletions in yeast *Saccharomyces cerevisiae*** (created with “BioRender.com”).

### 3.2 Part II: Mild proteotoxicity ensuing chaperone overexpressions leads to glucose starvation-like response resulting in lifespan extension

This part of thesis has been published in *Aging Cell* (Perić, M.\*, Lovrić, A.\*, Musa, M., Dib, P. B., Rudan, M., Nikolić, A., ... Kriško, A. (2017). TORC1-mediated sensing of chaperone activity alters glucose metabolism and extends lifespan. *Aging Cell*, 994–1005. <https://doi.org/10.1111/accel.12623> \*equal contribution).

Having examined the cell-wide effect of failed proteostasis induced by deletions of chaperones, studying the cellular response to improved proteostasis resulting in reduction of protein misfolding became intriguing. With the intention to provoke alleviation of proteotoxicity within the yeast cell, molecular chaperones found in distinct cellular compartments were autonomously overexpressed: mitochondrial HSP70 chaperone (Ssc1), nascent polypeptide-associated complex (NAC), endoplasmic reticulum HSP70 chaperone (Lhs1), and cytosolic T-complex chaperone (Tcp1). The strains with the overexpressed chaperones will be referred to as the chaperone-enriched strains (ChESs). The analysis by flow cytometry confirmed the degree of chaperone overexpression to be 3-fold for Lhs1, Tcp1 and NAC, and 2.5-fold for Ssc1 (Figure 43).

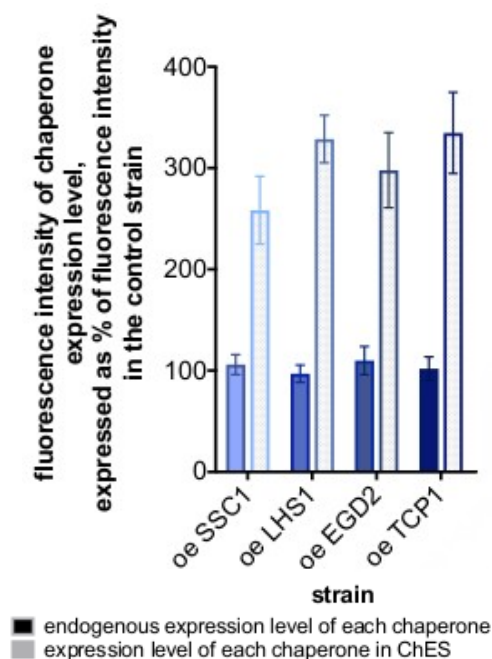


Figure 43| **Overexpression levels of chaperones verified by flow cytometry.** Magnitude of expression in ChES was compared to the basal levels of endogenous chaperone in the control. Results indicate an approximate 3-fold increase in expression of each chaperone. Control is wild-type yeast with an empty vector. Data are mean  $\pm$  SD from at least three independent cultures, each performed in triplicate. \*\*\* $P < 0.001$ ; \*\* $P < 0.01$ ; \* $P < 0.05$  (ANOVA plus post hoc)

### 3.2.1 Chaperone enrichment leads to the alleviation of protein misfolding

It became essential to determine whether chaperone enrichment elicits protein misfolding abatement. It has been recognized that aberrant proteins are particularly susceptible to oxidative damage, predominately by baring the, otherwise concealed, hydrophobic regions of polypeptides (Dalle-Donne et al., 2006; Dukan et al., 2000). This predisposition serves as a marker of protein folding quality, i.e. protein misfolding (Krisko & Radman, 2019). To assess the folding nature of the proteome, a type of irreversible protein oxidation – protein carbonylation (PC) was measured. The results show, on average, a 40% reduction of PC in the ChESs, confirming the alleviation of protein misfolding compared to the WT (Figure 44A).

This is validated further by a substantial downregulation of Hsp90 chaperone (Figure 44B). Downregulation of Hsp90 chaperone was additionally substantiated by differential gene expression analysis, along with downregulation of Hsp150 and Hsp26 chaperones, all of which are indicative of reduced proteotoxic stress (Figure 44C). Moreover, enzymes involved in regulation of cellular ROS levels, cytosolic copper–zinc superoxide dismutase (SOD1), and mitochondrial manganese superoxide dismutase (SOD2) were both considerably downregulated in ChES relative to the control. These results imply reduction of cellular ROS, and to corroborate this declaration, the conversion of H2DCFDA into green fluorescence in presence of ROS was monitored, and the results showed, on average, a 40% reduction of intracellular ROS compared to the control ( Figure 44C).



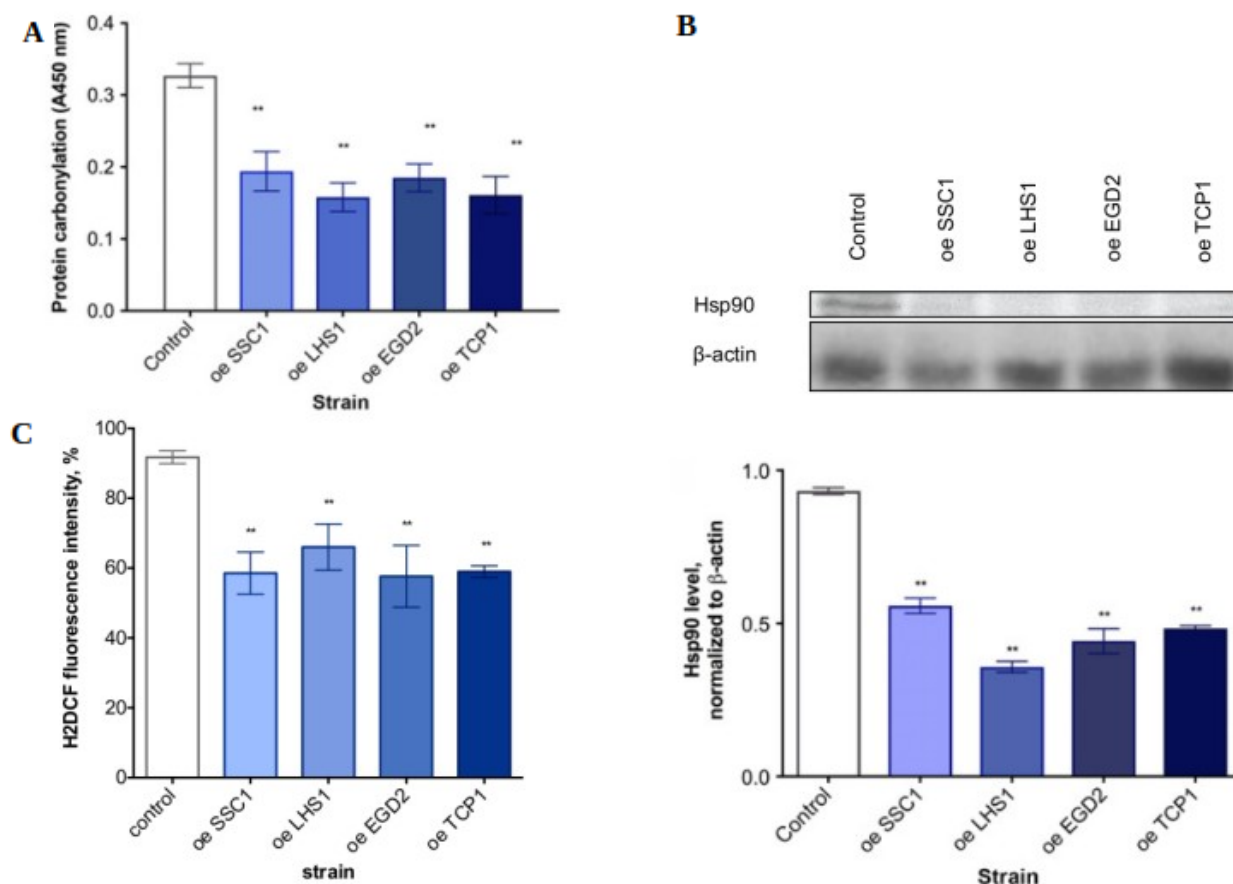


**Figure 44| ChES exhibit alleviation of protein misfolding.** (A) Levels of protein carbonylation in ChES were compared to levels in the control strain. Results revealed reduced protein carbonylation in chaperone-enriched strains compared to the control. (B) Levels of Hsp90 in ChES were compared to levels in the control strain. Results revealed reduction in Hsp90 levels in chaperone-enriched strains compared to the control. Control is wild-type yeast with an empty vector. Data are mean  $\pm$  SD from at least three independent cultures, each performed in triplicate. \*\*\* $P < 0.001$ ; \*\* $P < 0.01$ ; \* $P < 0.05$  (ANOVA plus post hoc). (C) H2DCF probe was used to determine the production of ROS in flow cytometer. Levels of H2DCF in ChES were compared to levels in the control strain. The results indicate decrease in ROS levels compared to the WT control. The results are expressed as the mean fluorescence of the 10,000 cells. \*\*\* $P < 0.001$ ; \*\* $P < 0.01$ ; \* $P < 0.05$  (ANOVA plus post hoc).

The improvement of proteostasis upon chaperone overexpression was further confirmed by a consistent mitigation of Hsp104-dependent protein aggregates in ChESs compared to the control (Figure 45). These data indicate a significant reduction of protein misfolding induced by overexpression of molecular chaperone irrespective of the cellular compartments subjected to the overexpression.

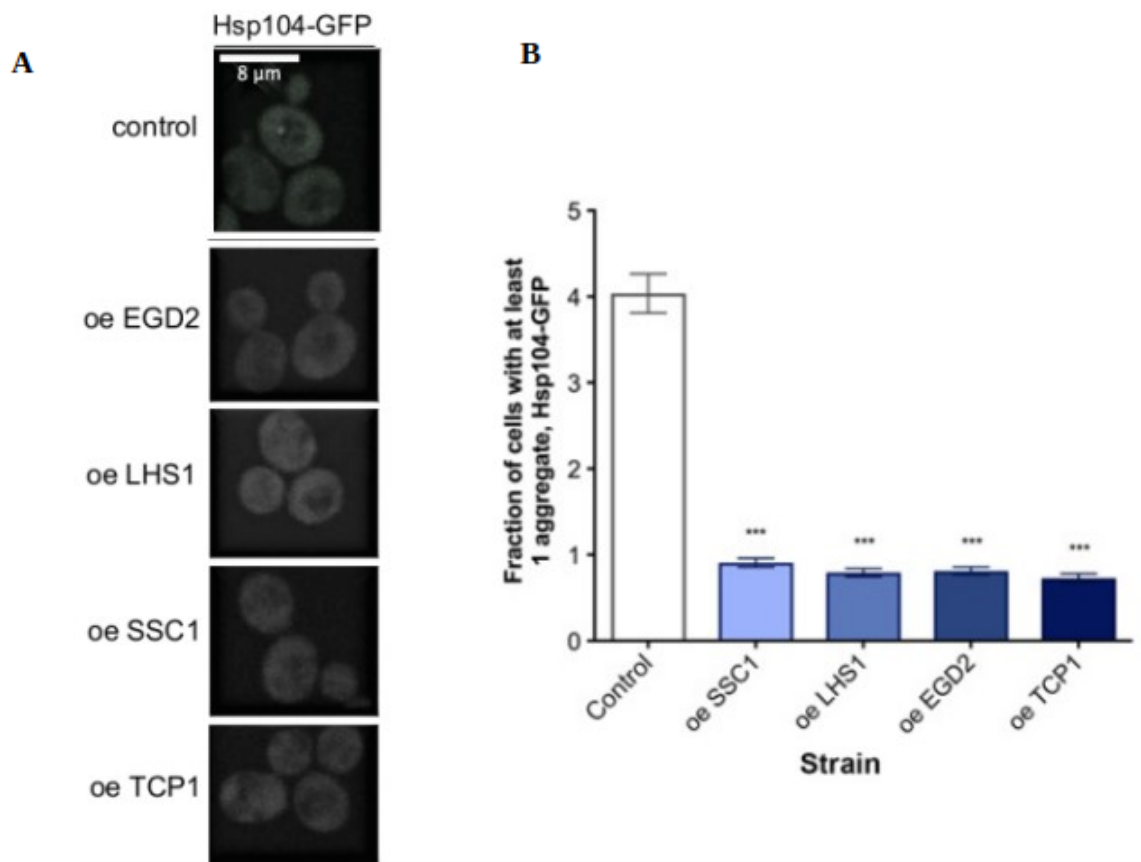


Figure 45| **ChES exhibit decreased tendency for protein aggregation.** ChESs are marked by having a reduced tendency to form protein aggregates. This was revealed in cell screening experiment, where protein aggregation tendency is stated as the fraction of cells having one aggregate at a minimum. (A) Representative image of cells with HSP104-GFP tagged protein aggregates. More than 1000 cells screened for aggregates starting from two independent exponential yeast cultures for each strain. Control is wild-type yeast with an empty vector. (B) Quantification of HSP104-GFP tagged protein aggregates. P values were calculated using ANOVA plus post hoc. \*\*\*P < 0.001; \*\*P < 0.01; \*P < 0.05

Results obtained in the aforementioned experiments were compared to an additional control of strains enriched with inactivated versions of molecular chaperones used for this research (iChESs) as an added validation. Conversely, iChESs exhibited an increase in protein carbonylation level of 15% and an increase of Hsp104-dependent protein aggregates of 3-4% compared to the ChESs (Figure 46).

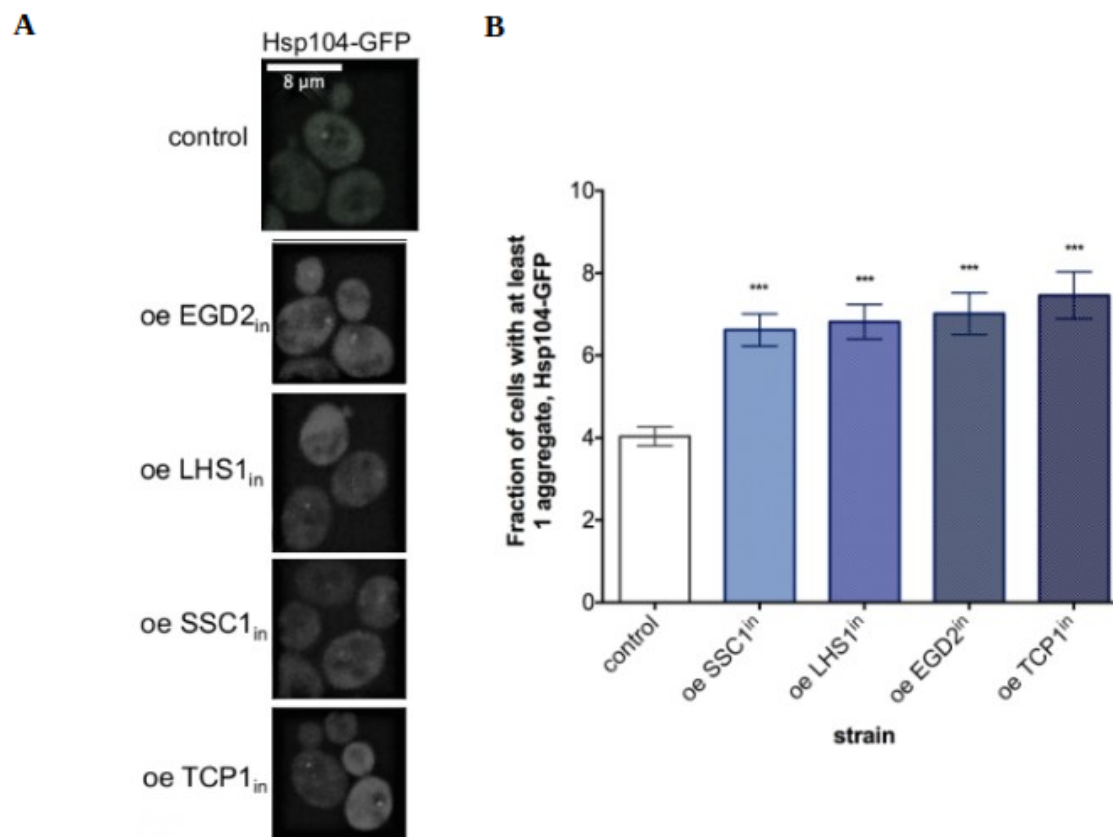
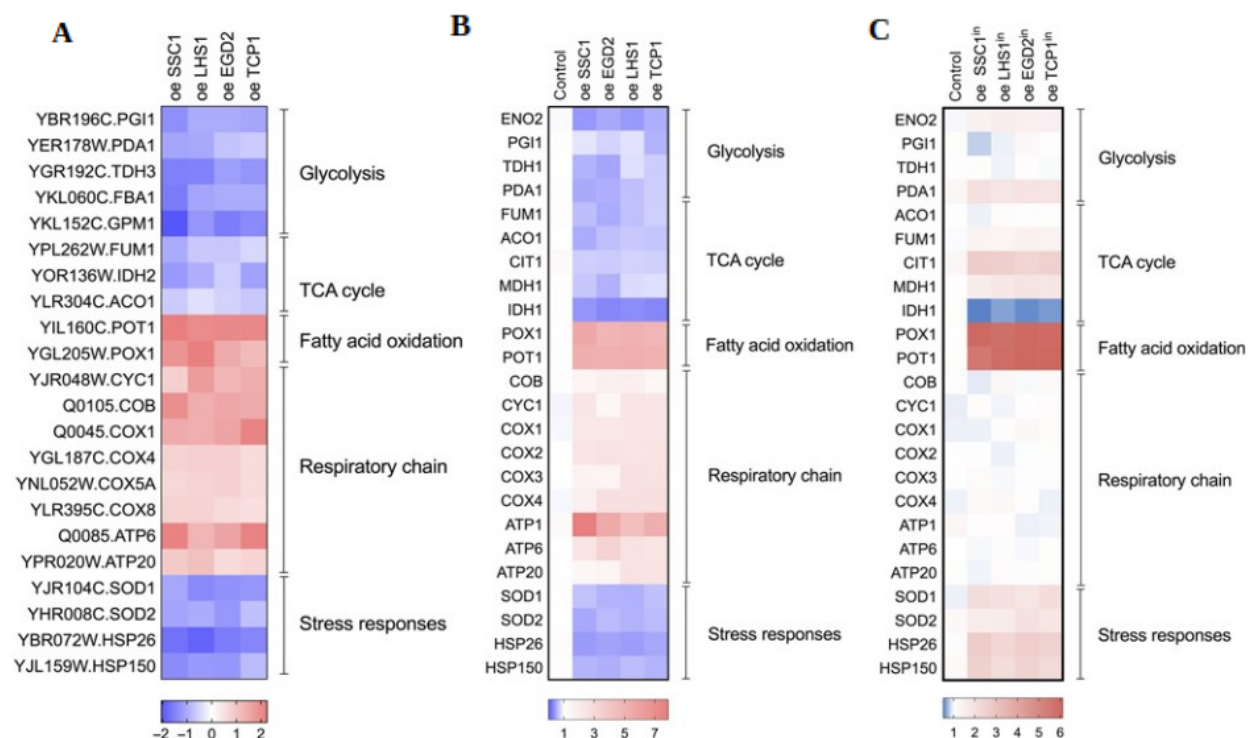


Figure 46| **iChES exhibit increased tendency for protein aggregation.** Introduction of inactivated chaperones has annulled lowered propensity of ChES to form protein aggregates. This was revealed in cell screening experiment, where protein aggregation tendency is stated as the fraction of cells having one aggregate at a minimum. (A) Representative image of cells with HSP104-GFP tagged protein aggregates. More than 1000 cells screened for aggregates starting from two independent exponential yeast cultures for each strain. Control is wild-type yeast with an empty vector. (B) Quantification of HSP104-GFP tagged protein aggregates. P values were calculated using ANOVA plus post hoc. \*\*\* $P < 0.001$ ; \*\* $P < 0.01$ ; \* $P < 0.05$

### 3.2.2 Chaperone enrichment induces a glucose starvation-like response

RNA sequencing (RNASeq) was implemented with the intent to look into the possible deviations of gene expression patterns in ChESs compared to the controls. The results revealed downregulation of several pivotal enzymes involved in the glycolysis and the TCA cycle on the one hand as well as the upregulation of the subunits from the respiratory chain complexes (Figure 47A). Together, these results firmly indicate the repression of glycolysis and the TCA cycle in conjunction with intensified respiration in ChES.

These results were further corroborated by qPCR which displayed comparable tendencies of target genes to the ones observed in RNASeq (Figure 47B). It is evident from the obtained differential gene expression of the studied strains that chaperone enrichment instigates a glucose starvation-like response (Lin et al., 2002).



**Figure 47| Chaperone enrichment induces a glucose starvation-like response** (A) Heat map of differential gene expression in ChES reveals a phenocopy of glucose starvation, characterized by downregulation of TCA cycle and glycolysis and upregulation in respiratory chain. (B) qPCR evaluation of differential gene expression confirms the obtained results of starvation-like response induction in ChES. (C) Heat map of iChES reveals absence of a response observed in ChES. Color of the squares on the heat map corresponds to the mean value of the log fold change from three biological and three technical replicates. UBC6 was used for normalization. Control is wild-type yeast with an empty vector.

Contrarily the iChES, enriched with the inactivated form of studied chaperone, display unaltered expression of genes involved in neither glycolytic and TCA cycle nor respiratory chain components (Figure 47C). Collectively, these findings signify that the observed response is dependent on enhanced chaperone activity.

Moreover, RNASeq results show marked upregulation of enzymes involved in peroxisomal fatty acid  $\beta$ -oxidation including POX1 (encoding for fatty-acyl coenzyme A oxidase) and POT1

(encoding for 3-ketoacyl-CoA thiolase) (Figure 47A). These findings denote a shift of preferred carbon source from glucose to fatty acids. However, this alteration is likewise noted in the iChES, suggesting that the favored utilization of fatty acid is not associated with increased chaperone activity (Figure 47C).

### 3.2.3 ChES display enhanced oxygen consumption resulting from increased mitochondrial mass

Given the results obtained from ChES transcriptome regarding the increased expression of respiratory chain components, oxygen consumption of aforementioned strains was looked into. According to the results acquired from respiration measurement, it was found that all the studied ChESs revealed, on average, doubled  $O_2$  consumption as compared to the control strain, with EGD2 strain having the most notable change (Figure 48A). Respiration deficiency was observed in petite, a respiratory-incompetent strain, used as a negative control (Figure 48A). Additionally, inactivated chaperone strains (iChES) showed no change in oxygen consumption, indicating that the increased respiration identified in ChES emanates from the overexpression of active chaperones (Figure 48B).

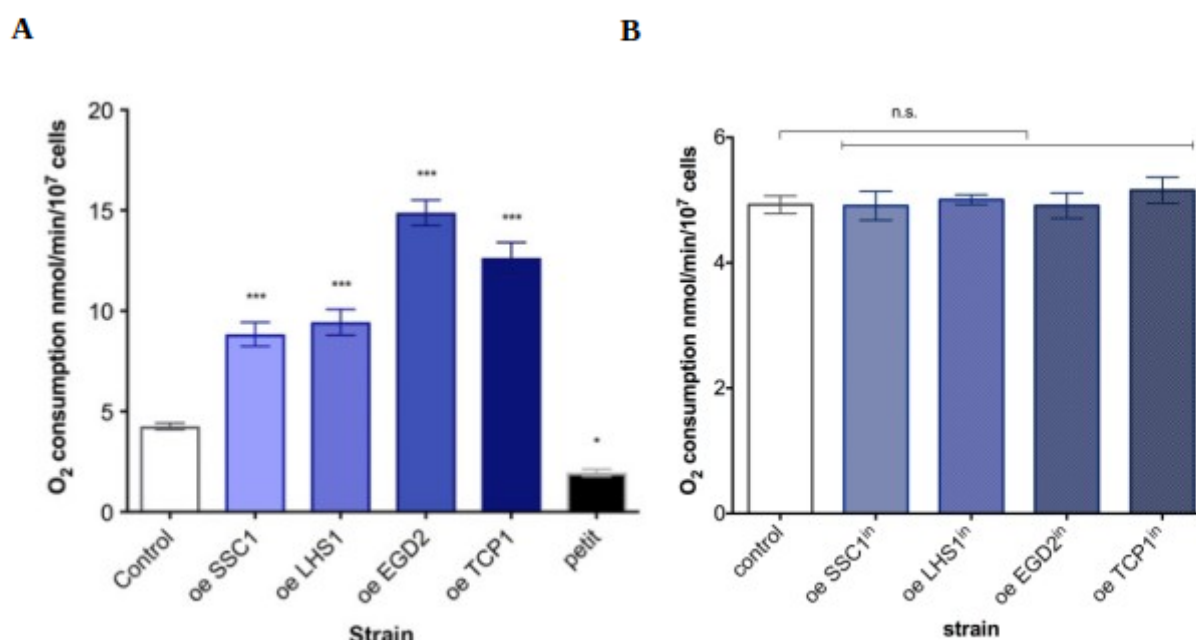


Figure 48| **Chaperone enrichment induces increased oxygen consumption in ChES.** (A) Oxygen consumption was measured in ChES and compared to the wild-type control and respiration-deficient petite strain. Results indicate increased oxygen consumption in all studied ChES. (B) Oxygen consumption was measured in iChES and compared to the wild-type control.

Results show constant oxygen consumption between iChES and the control suggesting that increased respiration emanates from the overexpression of active chaperones. Control is wild-type yeast with an empty vector. Data on the graph are mean  $\pm$  SD from three biological and three technical replicates. P values were calculated using ANOVA plus post hoc. \*\*\*P < 0.001; \*\*P < 0.01; \*P < 0.05

Recognizing that the mechanism underlying increased respiration could potentially originate upon enlarged mitochondrial aptitude, mitochondrial mass was assessed using 10-N-Nonyl acridine orange (NAO) fluorescence. The NAO fluorescent probe adheres to cardiolipin located in the inner mitochondrial membrane, and as such, is an indicator of mitochondrial mass. The fluorescent signal showed an increase, thus suggesting an increased mass in ChES compared to the control (Figure 49A).

Subsequently, the mitochondrial membrane potential (MMP) was evaluated using the DiOC6(3) fluorescent staining of mitochondria. The results failed to reveal any alteration of MMP in ChES compared to the control (Figure 49B).

Moreover, the modification of mitochondrial morphology of the ChES was further verified by preSU9-GFP marker of the MitoLoc plasmid, which revealed a substantial increase in the mitochondrial volume (Figure 49C).

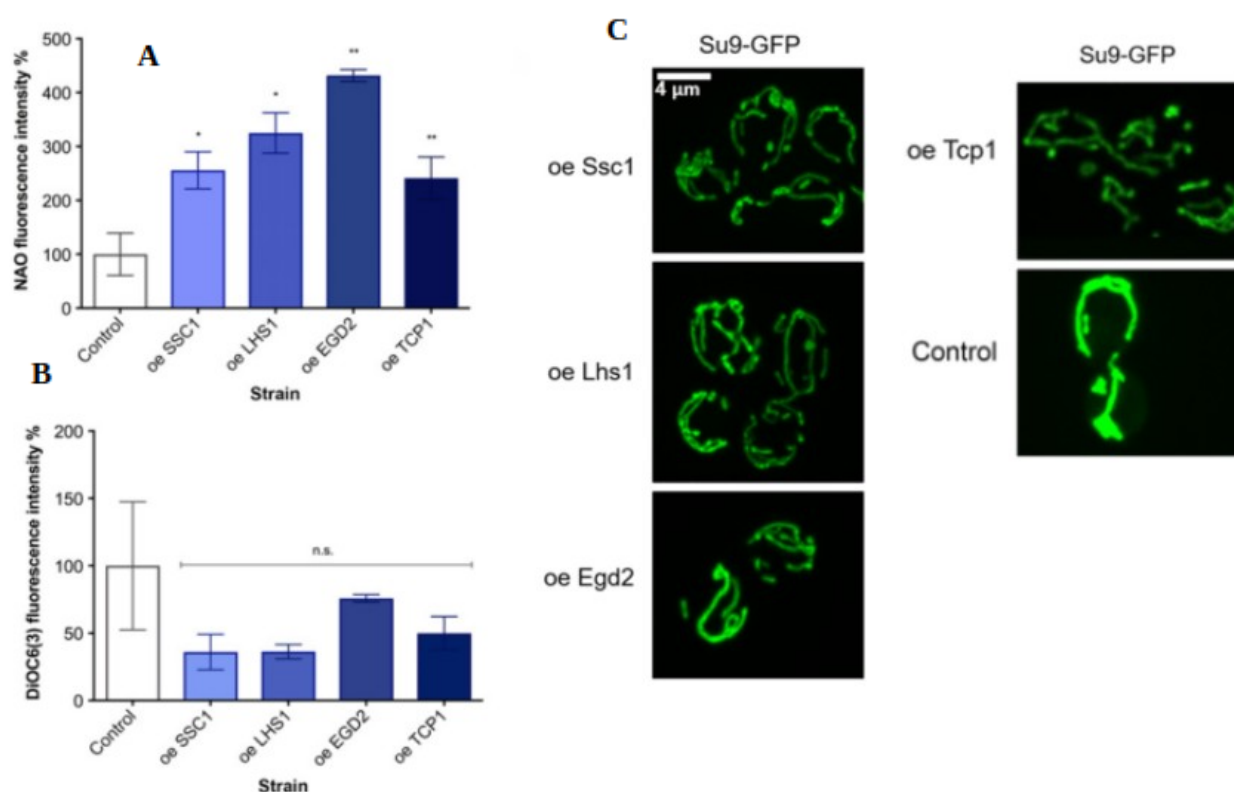


Figure 49| **Oxygen consumption eventuated from increased mitochondrial mass.** (A) The analysis of the mitochondrial mass was obtained using a green fluorescent mitochondrial dye NAO, and the results show increase in the mitochondrial biomass of ChES in comparison to the control. (B) Mitochondrial membrane potential measurement using positively charged green fluorescent probe DiOC6(3) reported no membrane depolarization upon chaperone enrichment. Control is wild-type yeast with an empty vector. Data on the graph are mean  $\pm$  SD from three biological and three technical replicates. P values were calculated using ANOVA plus post hoc. \*\*\*P < 0.001; \*\*P < 0.01; \*P < 0.05 (C) The mitochondrial structures on the image are identified by preSU9-GFP (green), and the results reveal increase in mitochondrial volume in ChES. More than 300 cells from two biological replicates were inspected, and the images here display representative examples.

Lastly, the subunit composition of mitochondrial protein complexes of the oxidative phosphorylation (OXPHOS) system and their respective *in vitro* activities were examined using BN-PAGE analysis. The results showed no difference in the level of mitochondrial complexes between the studied strains compared to the control, further confirming that the observed increase in oxygen consumption originates exclusively from mitochondrial mass expansion (Figure 50).



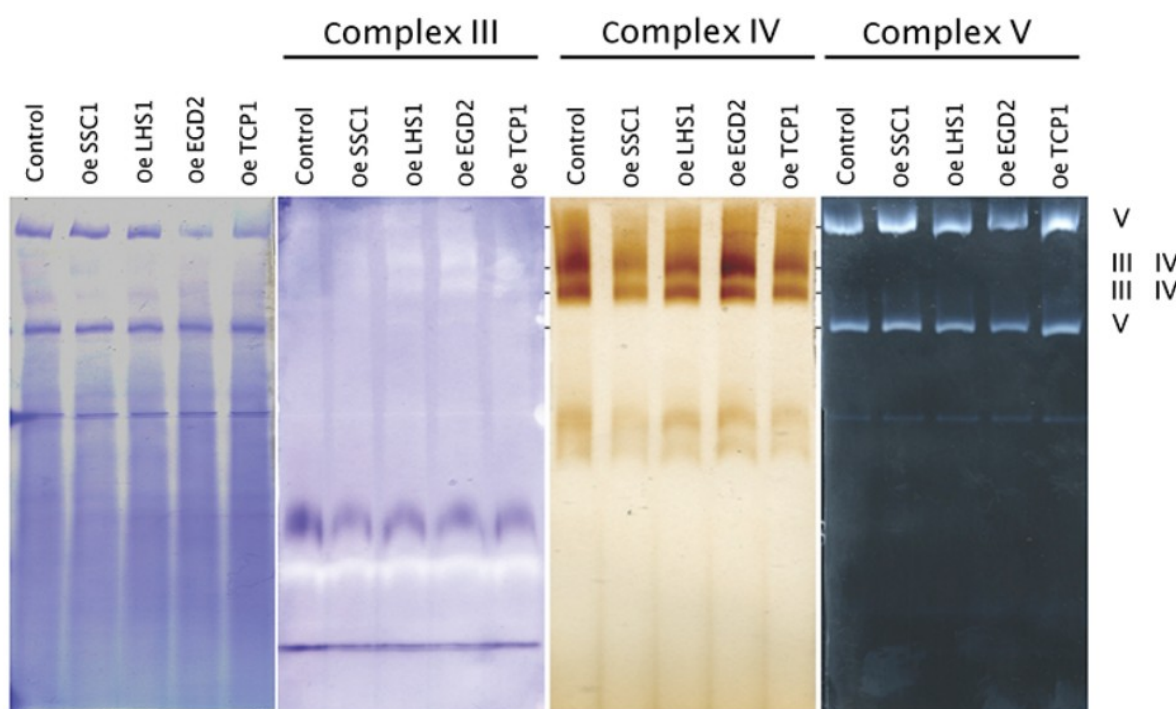


Figure 50| **Respiratory chain complexes remain unchanged in ChES.** BN-PAGE displaying III, IV and V of the mitochondrial OXPHOS complexes. The results presented show no difference in band intensities, and therefore, no difference in the respiratory chain configuration.

### 3.2.4 Snf1 activation is required for observed glucose starvation-like response in the ChES

Reviewing the literature concerning the glucose starvation-like phenotype exhibited by the studied chaperone overexpression strains, it became apparent that Snf1, a pivotal protein kinase implicated in regulation of metabolic functions, could be held accountable for the ascertained response in ChES (Hedbacker, 2008). Western blot analysis of phosphorylated Snf1 levels demonstrated a significant increase in the studied strains compared to the control (Figure 51A), indicating its increased activity.

To further investigate involvement of Snf1 protein kinase in the noted glucose starvation-like response, all four chaperones in the Snf1 deletion background were overexpressed, and gene expression was subsequently measured using qPCR. Aside from various alterations in gene expression commonly affiliated with the absence of Snf1, such as considerable upregulation of enzymes involved in glycolysis and TCA cycle, as well as the respiratory chain components, the



glucose starvation-like response recognized in ChES was inexistent in the Snf1-deficient background (Figure 51B) (Nicastro et al., 2015).

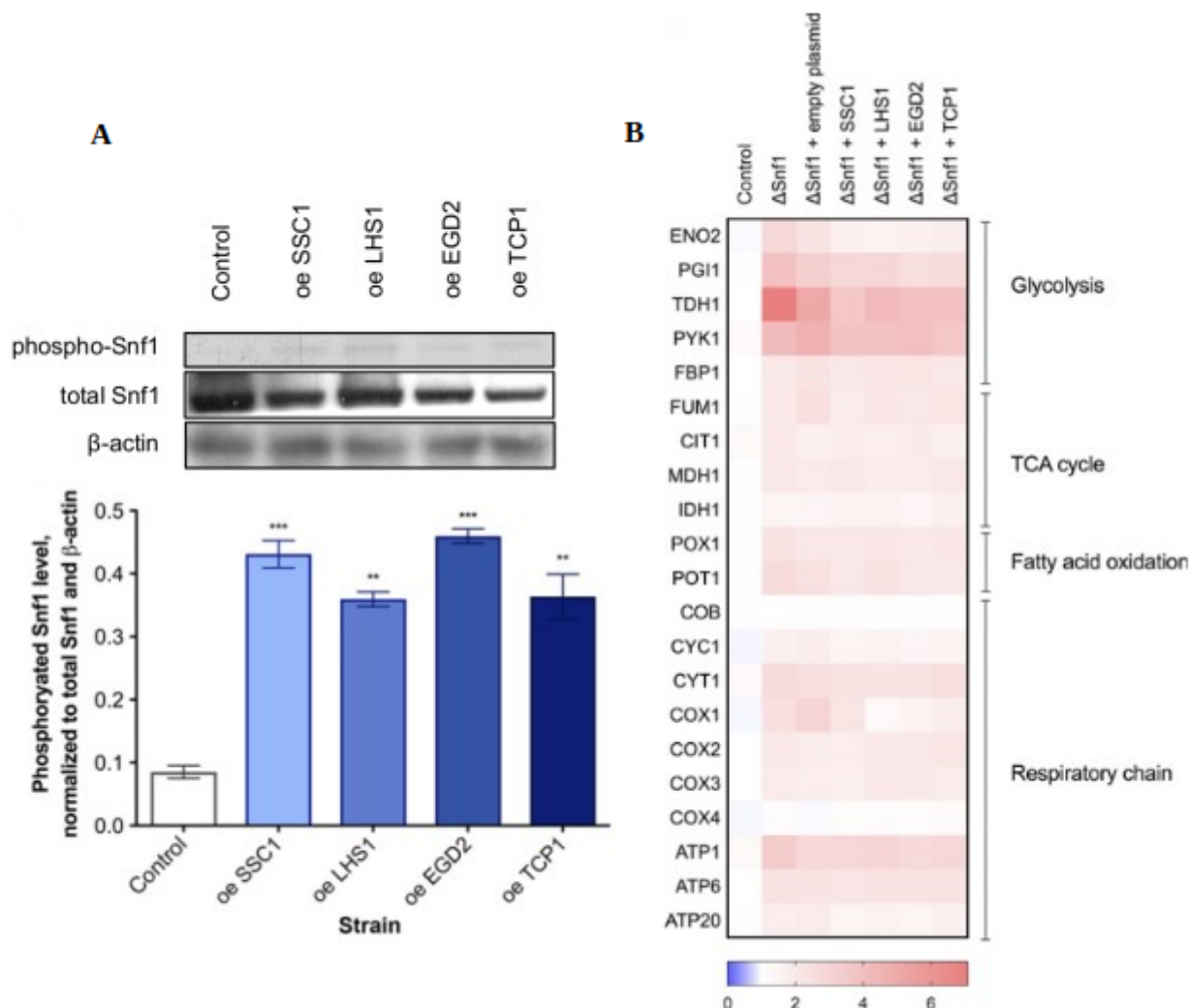


**Figure 51| ChES display a significant increase in Snf1 levels.** (A) The quantification (bottom left) of Western blot analysis (top left) of phosphorylated Snf1 levels in ChES revealed a substantial increase when compared to the control strain. Data represent quantification (ImageJ) of Western blot results from three independent experiments. Phospho-Snf1 band intensity was normalized to the intensity of total Snf1 and  $\beta$ -actin (loading control). Control is wild-type yeast with an empty vector. Data are mean  $\pm$  SD from three independent cultures, each performed in triplicate. \*\*\* $P < 0.001$ ; \*\* $P < 0.01$ ; \* $P < 0.05$  (ANOVA plus post hoc). (B) Heat map of  $\Delta$ Snf1 and the overexpression of chaperones in the Snf1-deficient background demonstrates absence of a response observed in ChES. Color of the squares on the heat map corresponds to the mean value of the log fold change from three biological and three technical replicates. UBC6 was used for normalization. Control is wild-type yeast with an empty vector.

Complementary to previous results, oxygen consumption is unchanged in the chaperone overexpression strains lacking Snf1 (Figure 52). These results, thus, firmly imply that Snf1 activity is required for the glucose starvation phenocopy in ChES. Could the most feasible explanation for Snf1 activation in ChES be the sensing of improved proteostasis? In the affirmative, what could be attainable mechanism of conveying the information, and which cellular constituent is accountable for the sensing of ameliorated proteostasis?

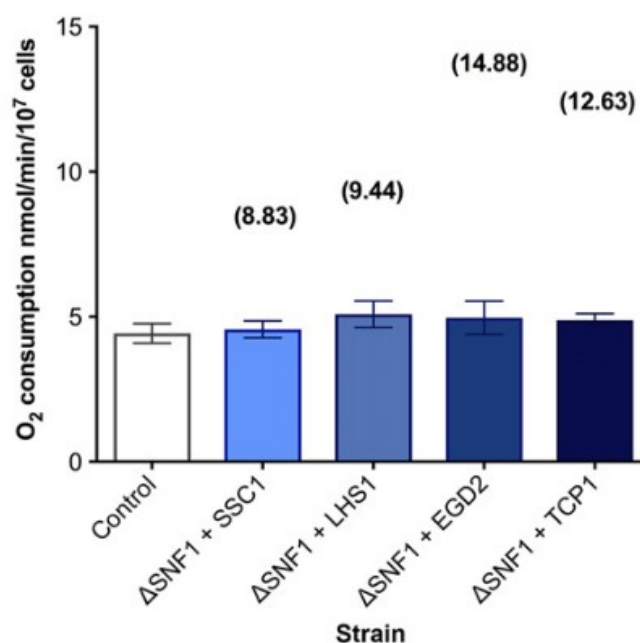
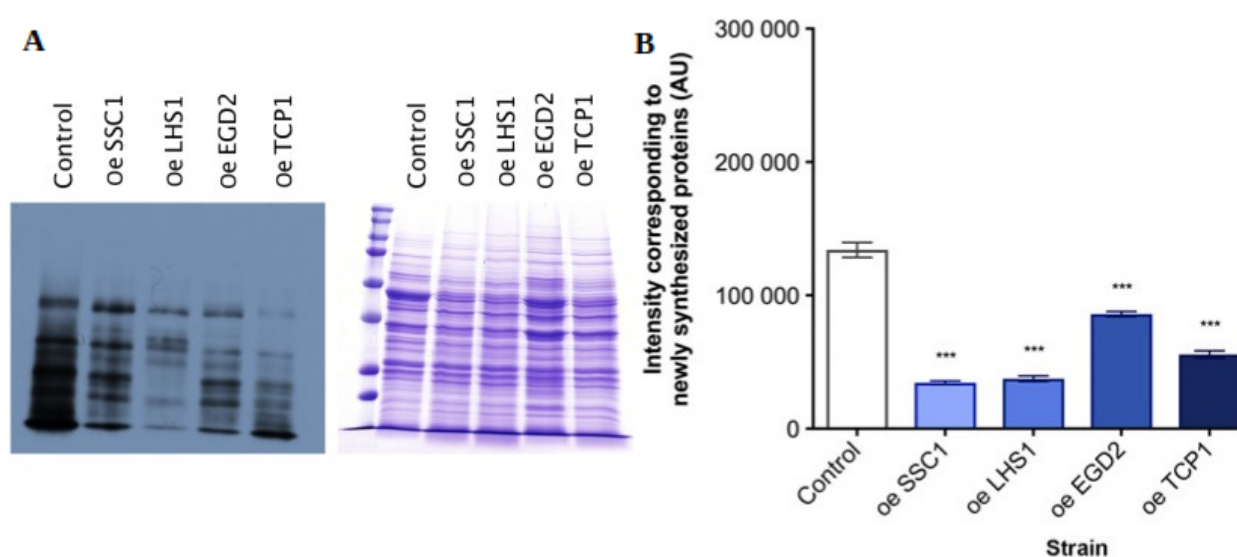


Figure 52| **Snf1 deficiency abolishes oxygen consumption increase characteristic of ChES.** Oxygen consumption was measured in Snf1-deficient chaperone overexpressions and compared to the wild-type control. Results show constant oxygen consumption between. Control is wild-type yeast with an empty vector. Data on the graph are mean  $\pm$  SD from three biological and three technical replicates. P values were calculated using ANOVA plus post hoc. \*\*\*P < 0.001; \*\*P < 0.01; \*P < 0.05

### 3.2.5 ChES response leads to the deactivation of TORC1

Since the interaction between Snf1/AMPK and TOR has been documented in numerous studies, its prospect in ChES was examined (Mei & Brenner, 2015; A. Singh et al., 2018). Furthermore, it has been recorded that TORC1, a distinct complex of TOR, performs as a sensor of proteotoxic stress (Su et al., 2016). It has become apparent that the involvement of TORC1 in sensing and

concatenating the proteostasis and metabolism in ChES could be feasible, and to test that, the activity of TORC1 was measured in ChES relative to the control. TORC1 is known to be an important regulator of translation, and this attribute can be used to determine its activity within the cell (Su et al., 2016). Therefore, the levels of newly synthesized proteins were measured during one generation time of all the studied strains. The results point to the translation reduction in ChES relative to the control indicating a mitigation of TORC1 activity (Figure 53).



**Figure 53| Amount of newly synthesized proteins is decreased in ChES.** (A) Western blot analysis of newly synthesized protein in ChES. Band intensities from the western blot assay (left) were normalized to the band intensities of total protein from the Coomassie-stained SDS-PAGE (right). (B) Quantification of newly synthesized protein levels indicates a reduction in the amount of newly translated proteins in ChES compared to the control. Data represent quantification (ImageJ) of Western blot results from three independent experiments (mean with SD). \*\*\* $P < 0.001$ ; \*\* $P < 0.01$ ; \* $P < 0.05$  (ANOVA plus post hoc).

To further substantiate the indication, the phosphorylation levels of Sch9 were measured, as its dephosphorylation and deactivation is a clear indicator of TORC1 activity. The results, in addition, confirm TORC1 deactivation as the phosphorylation levels of Sch9 were shown to be considerably reduced in ChES compared to the WT (Figure 54).

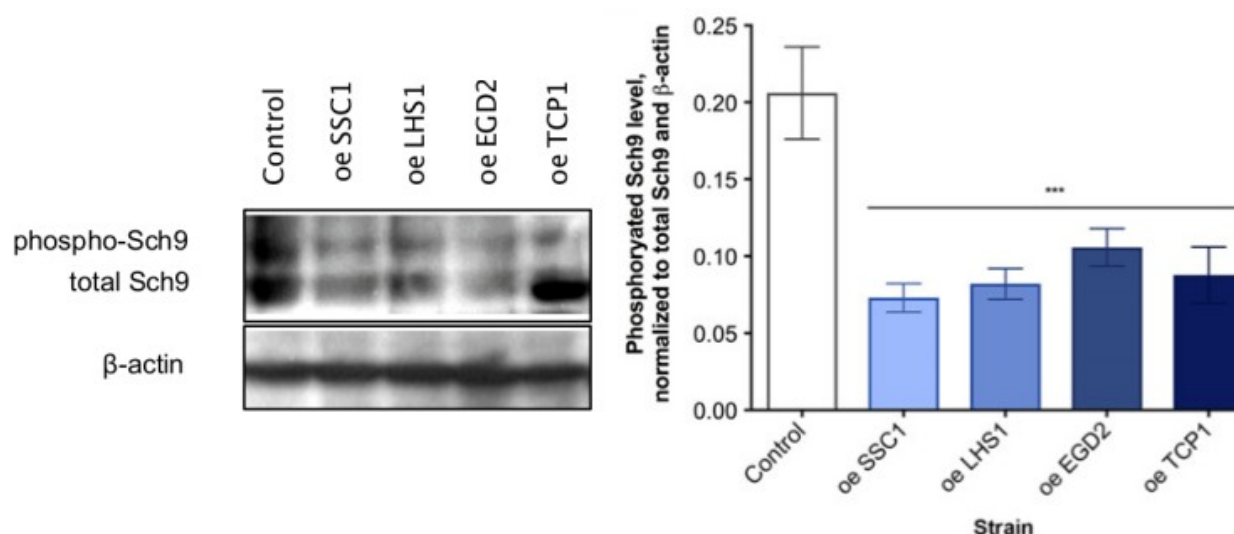


Figure 54| **Overexpression of studied chaperones leads to a reduction of phosphorylated Sch9 levels.** Western blot analysis of Sch9 phosphorylation (left) and the quantification of the band intensities (right) shows a significant reduction in phosphorylation levels of Sch9 in ChES compared to the control. Data represent quantification (ImageJ) of Western blot results from three independent experiments. Phospho-Sch9 band intensity was normalized to the total level of Sch9 and to the intensity of b-actin (loading control). Control is wild-type yeast with an empty vector. Data are mean  $\pm$  SD from at least three independent cultures, each performed in triplicate. \*\*\* $P < 0.001$ ; \*\* $P < 0.01$ ; \* $P < 0.05$  (ANOVA plus post hoc).

### 3.2.6 Snf1 activation in ChES is dependent on Tor1 deactivation

Having established the deactivation of TORC1 in ChES, the correlation of its inactivity to the response observed in the studied strains was studied. To accomplish this, I1954V mutation was inserted within Tor1 kinase, ensuring it acquires constitutive activity without the capacity to be deactivated (Hardt et al., 2011). In this research, the strain is referred to as a constitutively active Tor1 (caTor1). To validate its activity, the amount of newly translated proteins were once again measured. The findings show increased translation activity in the caTor1 strain, thus substantiating constitutive activity of the strain (Figure 55).

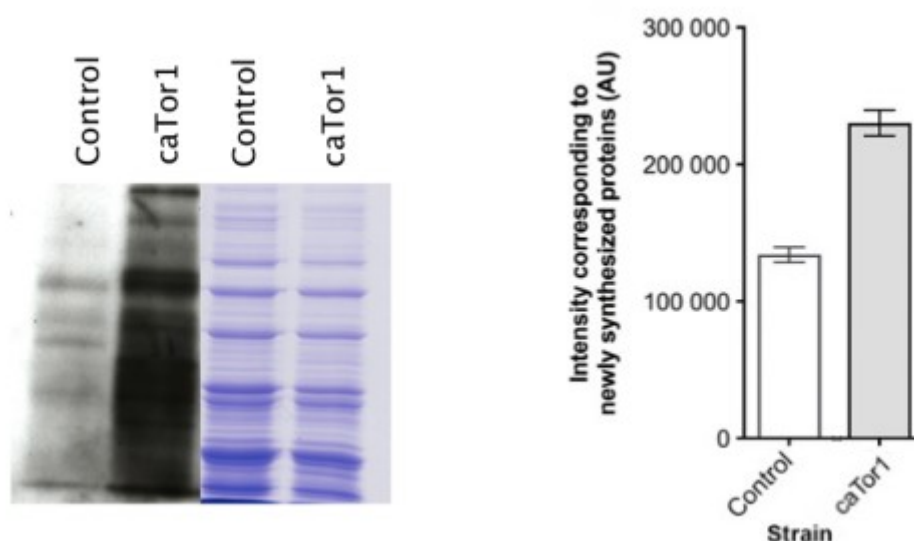


Figure 55| **Constitutive activity of Tor1 results in increased translation activity.** Western blot analysis of newly synthesized proteins in caTor1 (left) and the quantification of band intensities (right) indicate a sharp increase in the amount of newly translated proteins in ChES compared to the control. Data represent quantification (ImageJ) of Western blot results from three independent experiments (mean with SD). \*\*\* $P < 0.001$ ; \*\* $P < 0.01$ ; \* $P < 0.05$  (ANOVA plus post hoc).

It then became necessary to ascertain whether Tor1 activity influences phosphorylation levels of Snf1. The levels in the caTor1 strain were firstly measured, and the results showed a distinct decline in Snf1 phosphorylation compared to the control (Figure 56). Conversely, strain deficient in Tor exhibited a dramatic increase in Snf1 phosphorylation, a tendency repeatedly documented in previous studies (Hedbacker, 2008) (Figure 56). This disposition is denotative of the Tor1 function to serve as a negative regulator of Snf1 (Orlova et al., 2006).

Moreover, all studied chaperones were introduced into the caTor1 strain, and the phosphorylation levels of Snf1 were examined. As anticipated, Snf1 levels were analogous to the ones measured in caTor1 strain (Figure 56).

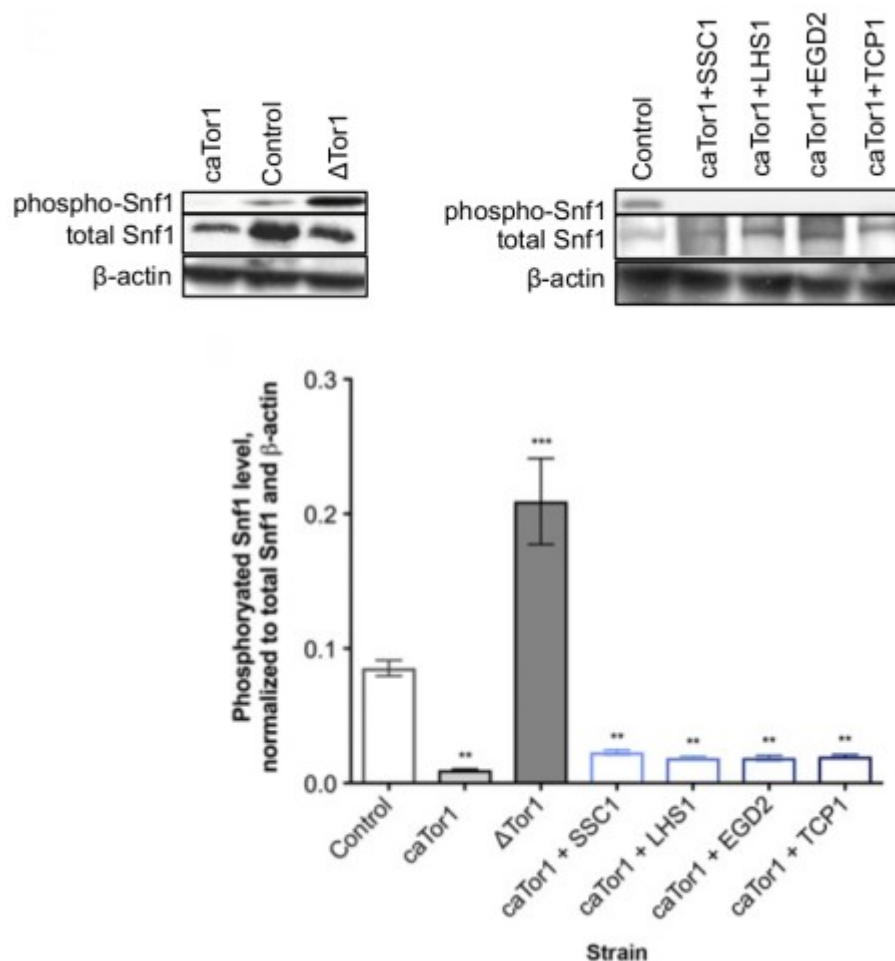


Figure 56| **Tor1 serves as a negative regulator of Snf1.** Western blot analysis of Snf1 phosphorylation levels (top) and the quantification of band intensities (bottom) indicate that inhibition of Tor1 enables Snf1 activity. Constitutive activity of Tor1 prevents Snf1 phosphorylation in the wild-type and ChES. Data represent quantification (ImageJ) of Western blot results from three independent experiments (mean with SD). \*\*\* $P < 0.001$ ; \*\* $P < 0.01$ ; \* $P < 0.05$  (ANOVA plus post hoc).

Having ascertained the increase in oxygen consumption of studied ChES as a pivotal aspect of the observed response, the consumption of oxygen in chaperone overexpression in the caTor1 background strain needed to be measured. The results denoted the invariable levels of oxygen consumption in all studied strains compared to the WT and caTor1 control strains (Figure 57A). This is indicative of certitude that Snf1 activation and the recognized response in ChES is

dependent on Tor1 deactivation. This indication is reinforced by the absence of alterations in differential gene expression confirmed in ChES shown in the figure below (Figure 57B).

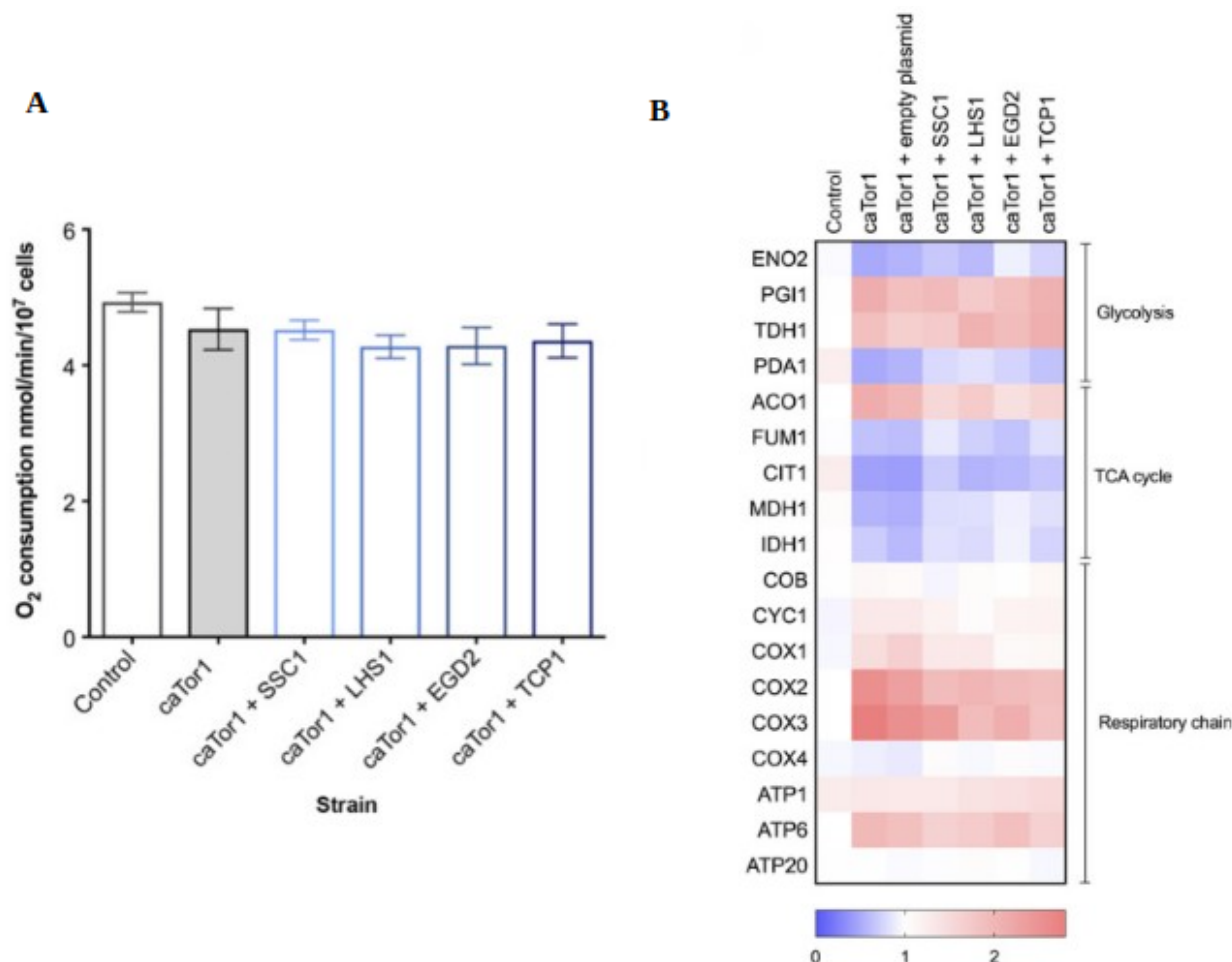


Figure 57| **Tor1 deactivation is required for a response characteristic of ChES** (A) Oxygen consumption is unchanged in caTor1 mutant as well as chaperone enriched caTor1 mutants. Control is wild-type yeast with an empty vector. Data are mean  $\pm$  SD from at least three independent cultures, each performed in triplicate. \*\*\* $P < 0.001$ ; \*\* $P < 0.01$ ; \* $P < 0.05$  (ANOVA plus post hoc) (B) Heat map of differential gene expression in caTor1 mutant and chaperone enriched caTor1 mutants fails to demonstrate a response equivalent to the one observed in ChES. This response remains constant following chaperone enrichment. Color of the squares on the heat map corresponds to the mean value of the log fold change from three biological and three technical replicates. UBC6 was used for normalization. Control is wild-type yeast with an empty vector.

### 3.2.7 Pivotal features of ChES response are evoked by Tor1 deactivation

To further resolve the role of Tor1-Snf1 interplay in mitochondrial activity, measuring oxygen consumption in  $\Delta$ Tor1 mutant was considered, and the  $\Delta$ Tor1 $\Delta$ Snf1 mutant. Regrettably, double deletion mutant was not viable and, therefore,  $\Delta$ Snf1 mutant was treated with 100 nM torin, a potent TOR inhibitor as an alternative (Huang et al., 2017). To corroborate that claim, control treated with torin was included and compared to the  $\Delta$ Tor1 mutant demonstrating equivalent oxygen consumption (Figure 58).

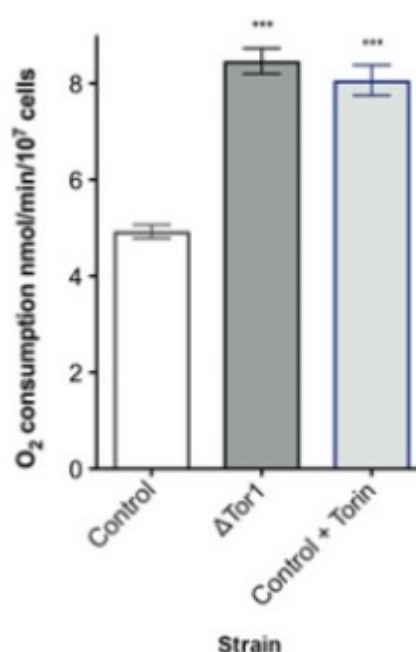
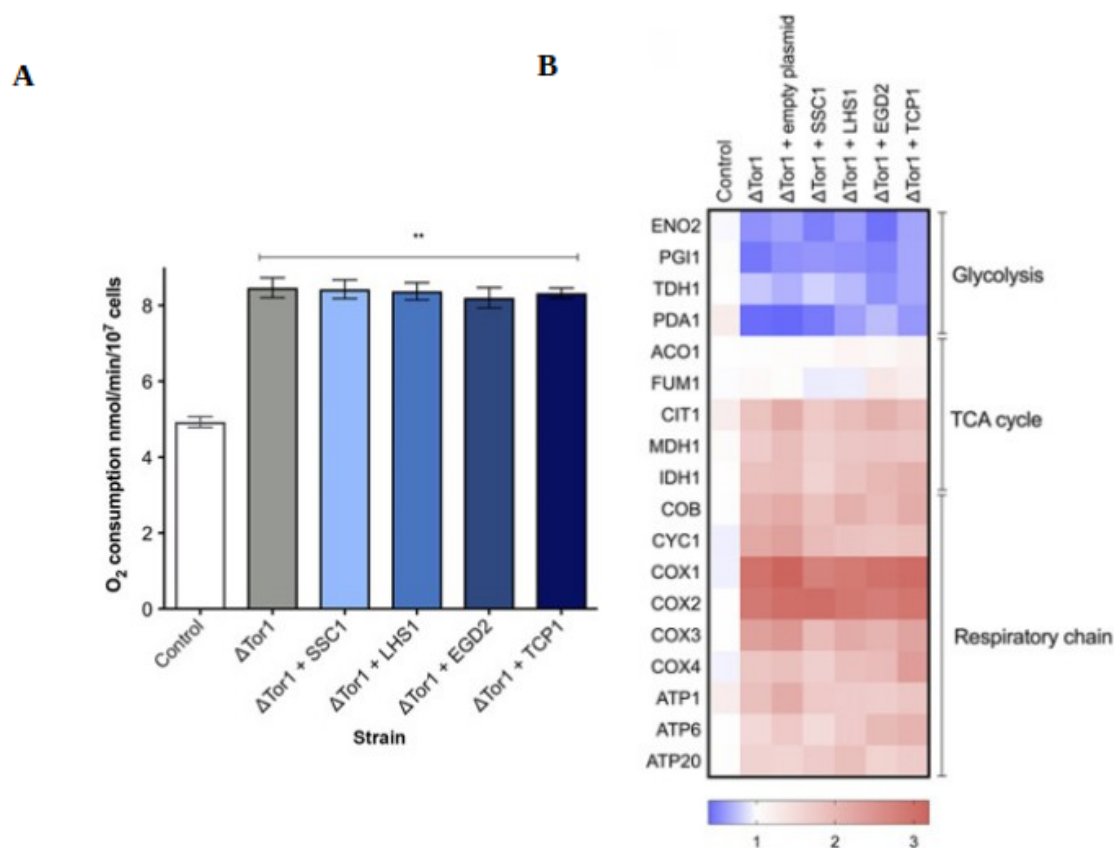


Figure 58| **Inhibition of TOR pathway results in significantly increased oxygen consumption.** Oxygen consumption is considerably increased in both  $\Delta$ Tor1 mutant and the torin treated control with inhibited TOR pathway suggesting that torin treatment is effective. Control is wild-type yeast with an empty vector. Data are mean  $\pm$  SD from at least three independent cultures, each performed in triplicate. \*\*\*P < 0.001; \*\*P < 0.01; \*P < 0.05 (ANOVA plus post hoc)

Additionally, the aforementioned oxygen consumption corresponds to the levels obtained in ChES, substantiating the claim that deactivation of Tor is necessary for ChES response (Figure 59A). Likewise, the differential gene expression analysis of torin treated control strain and the  $\Delta$ Tor1 mutant showed correspondence in core features of ChES, i.e., glycolysis repression and the elevated expression of the respiratory chain complexes (Figure 59B). Furthermore, following the introduction of studied chaperones in the  $\Delta$ Tor1 background, no alteration could be detected



in neither the gene expression nor the oxygen consumption compared to the  $\Delta\text{Tor1}$  strain, failing to generate any further change (Figure 59A B).



**Figure 59| Tor1 deactivation necessary for ChES response.** (A) Oxygen consumption is unchanged in  $\Delta\text{Tor1}$  mutant upon chaperone enrichment. Control is wild-type yeast with an empty vector. Data are mean  $\pm$  SD from at least three independent cultures, each performed in triplicate. \*\*\* $P < 0.001$ ; \*\* $P < 0.01$ ; \* $P < 0.05$  (ANOVA plus post hoc) (B) Heat map of differential gene expression in  $\Delta\text{Tor1}$  mutant shows a response equivalent to the one observed in ChES. This response remains constant following chaperone enrichment. Color of the squares on the heat map corresponds to the mean value of the log fold change from three biological and three technical replicates. UBC6 was used for normalization. Control is wild-type yeast with an empty vector.

Previously observed increase in oxygen consumption is annulled in torin treated  $\Delta\text{Snf1}$  mutants (Figure 60A). Moreover, the differential gene expression showed strong downregulation of nearly all metabolic activities, including the glycolysis, TCA cycle and respiration (Figure 60B). These results are coherent with defected fitness and arrested growth documented in these

circumstances, and they firmly imply that TORC1 activity is essential for survival of  $\Delta$ Snf1 mutant.

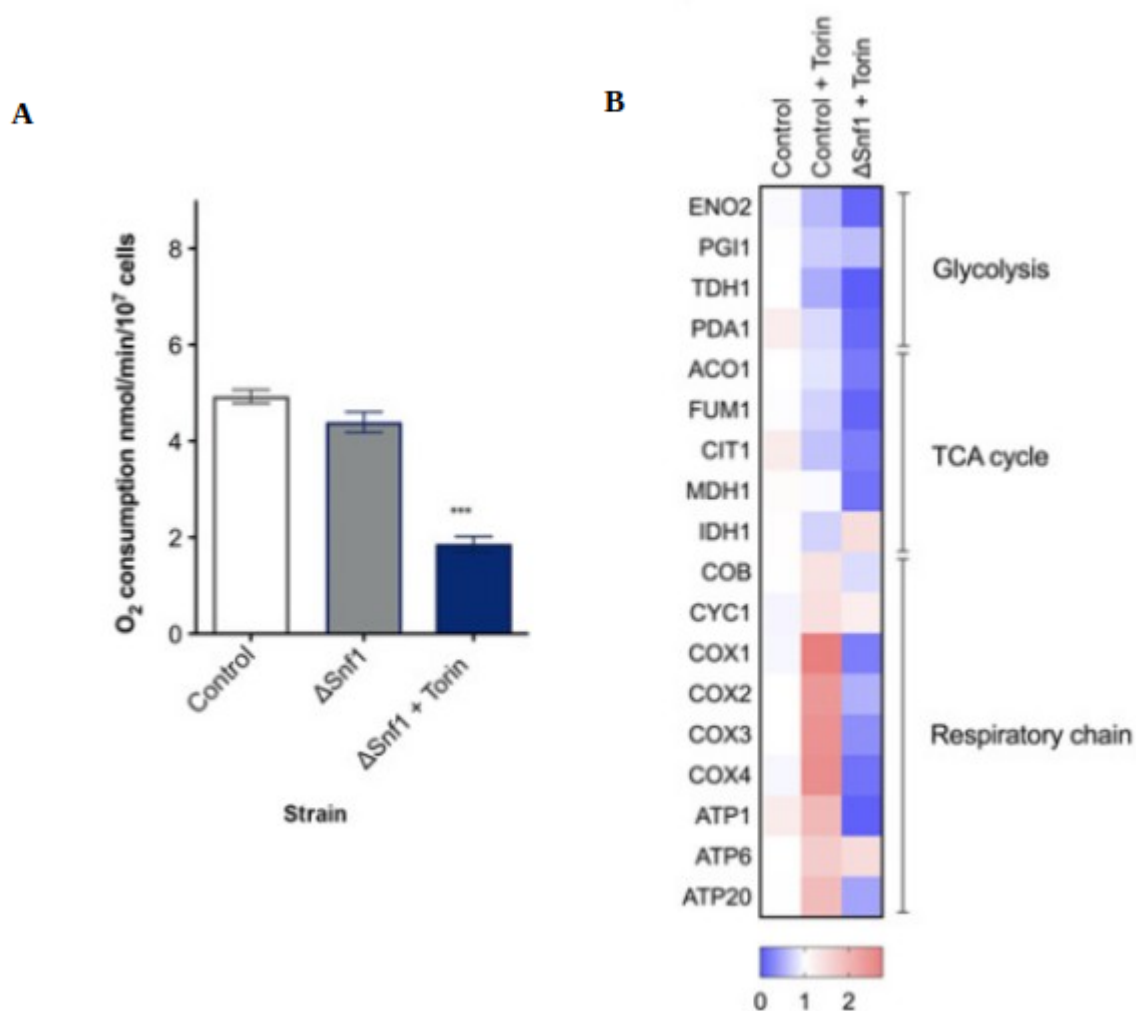


**Figure 60| Torin treated  $\Delta$ Snf1 mutant show decreased respiration and a downregulation of most metabolic activities.** (A) Oxygen consumption is considerably lowered in a mutant with inhibited Snf1 and TOR action. Control is wild-type yeast with an empty vector. Data are mean  $\pm$  SD from at least three independent cultures, each performed in triplicate. \*\*\* $P < 0.001$ ; \*\* $P < 0.01$ ; \* $P < 0.05$  (ANOVA plus post hoc) (B) Heat map of differential gene expression shows marked downregulation in important metabolic activities of mutants with inhibited Snf1 and TOR action. Color of the squares on the heat map corresponds to the mean value of the log fold change from three biological and three technical replicates. UBC6 was used for normalization. Control is wild-type yeast with an empty vector.

### 3.2.8 TORC1 is activated upon Hsp82 chaperone overexpression

Next, the hypothesis that TORC1 senses and, to some extent, mediates the protein folding conditions was tested. As Hsp82 chaperone, a homologue of Hsp90, is known to be one of the most abundantly expressed cellular proteins in stress-induced circumstances, its observed downregulation came to our attention as a potential solution to our protein folding sensing challenge (Borkovich et al., 1989; Samanfar et al., 2017). Hsp90 chaperone was expressed, followed by all of the chaperones used in this study. To confirm its enrichment, the expression level of Hsp82 were measured and shown to be increased by an average of 2-fold (Figure 61A). Snf1 activity was then tested by measuring its phosphorylation levels. The characteristic increase of Snf1 activity noted in ChES was demonstrated to be lacking while Hsp82 is overexpressed (Figure 61B).

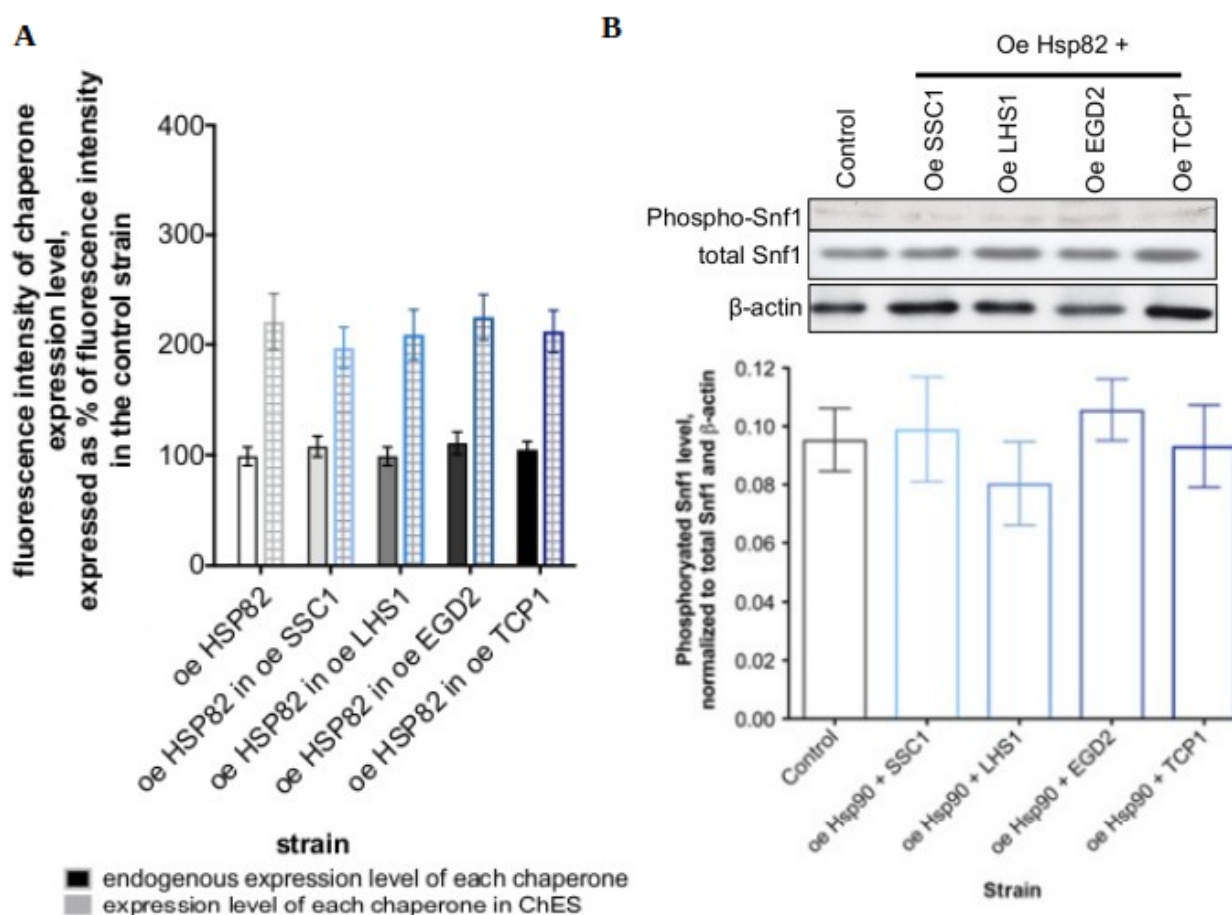


Figure 61| **Overexpression of Hsp82 chaperone in ChES eliminates the increase in Snf1 activity observed previously.** (A) Overexpression of Hsp82 chaperone is confirmed via flow

cytometry to be ~2-fold increase compared to the control. (B) Western blot analysis of Hsp82 overexpression failed to show increased Snf1 activity characteristic of ChES (top right). Data represent quantification (ImageJ) of Western blot results (bottom left) from three independent experiments. Phospho-Snf1 band intensity was normalized to the intensity of total Snf1 and b-actin (loading control). Data are mean  $\pm$  SD from at least three independent cultures, each performed in triplicate. \*\*\* $P < 0.001$ ; \*\* $P < 0.01$ ; \* $P < 0.05$  (ANOVA plus post hoc).

To determine the status of TORC1 activity in Hsp82 overexpression strain, the amount of newly synthesized proteins was assayed. The results showed a minor increase in the extent of newly translated proteins, unlike the typical decrease that was observed previously (Figure 62). Also, this inclination was not modified upon introduction of studied chaperones (Figure 62). This finding suggests not only that TORC1 is activated providing that Hsp82 chaperone is overexpressed, but that Tor1 kinase might sense the protein folding conditions by detection of cellular Hsp82 levels. Furthermore, it is implicated that TORC1 might play the part of mediating the folding status and the metabolism via negative regulation of Snf1.

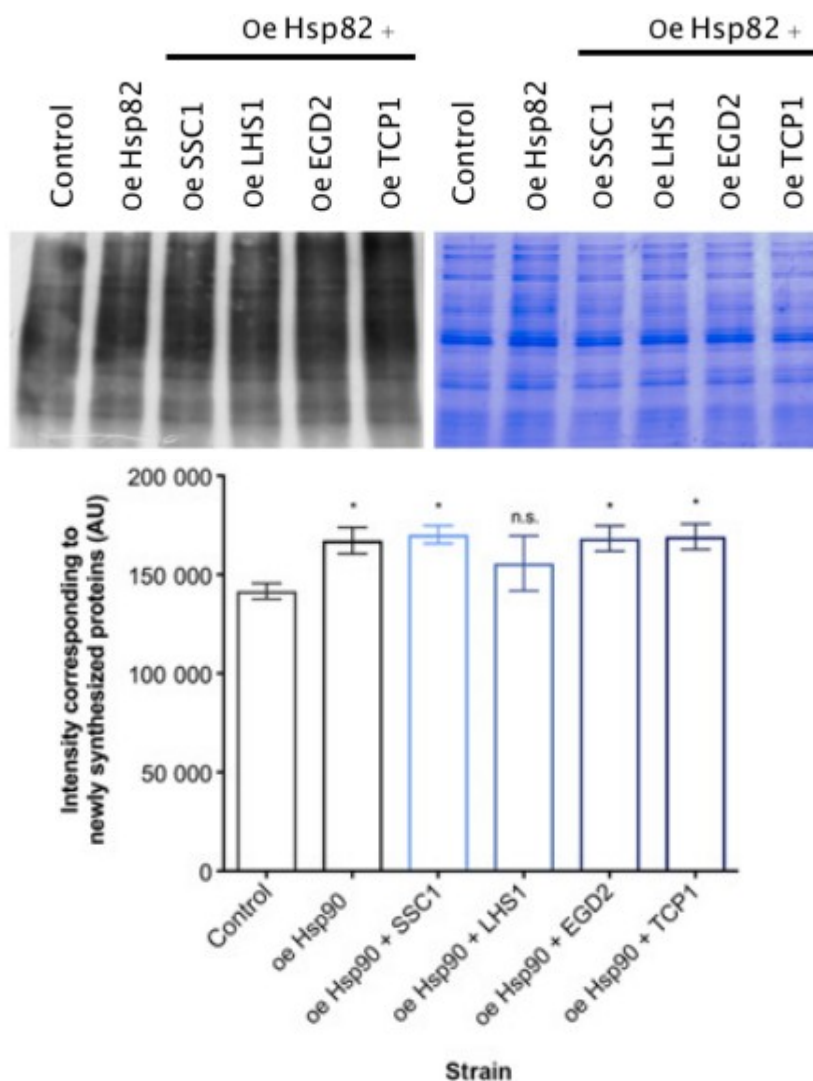


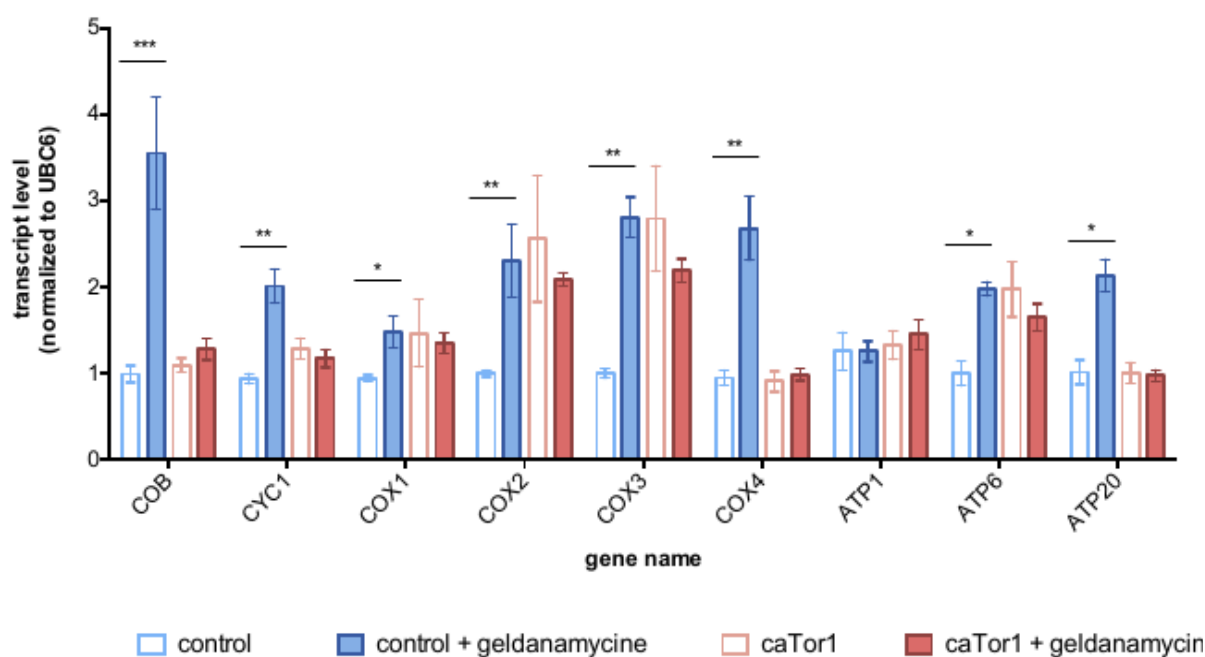
Figure 62| **Overexpression of Hsp82 does not lead to an increase in protein translation observed in ChES.** Western blot analysis of newly synthesized proteins in oeHsp82 (top) and the quantification of band intensities (bottom) indicate that a failure to downregulate Hsp82 in ChES results in a minor increase in the amount of newly synthesized proteins atypical of ChES. This response is constant following overexpression of studied chaperones. Data represent quantification (ImageJ) of Western blot results from three independent experiments (mean with SD). \*\*\* $P < 0.001$ ; \*\* $P < 0.01$ ; \* $P < 0.05$  (ANOVA plus post hoc).

### 3.2.8 Hsp82 chaperone downregulation is the initiating event preceding chaperone enrichment

To further test the involvement of downregulated Hsp82 in TORC1-related chaperone activity sensing, Hsp82 was treated and inhibited using geldanamycin. Differential gene expression analysis revealed comparable shifts in gene expression to those noted in the ChES, consisting of respiration activation and repression of glycolysis and TCA cycle (Figure 63). These data imply that the downregulation/inhibition of Hsp82 could be imminent occurrence in the signaling cascade underlying the observed ChES response.

Contrarily to the trend observed in ChES, considerable upregulation of enzymes involved in peroxisomal fatty acid  $\beta$ -oxidation, notably POT1 and POX1, was demonstrated by Hsp82 inhibited strain leading us to presume that fatty acid oxidation is not interrelated to the chaperone enrichment and reduction of Hsp82 levels in the studied strains (Figure 63).

H



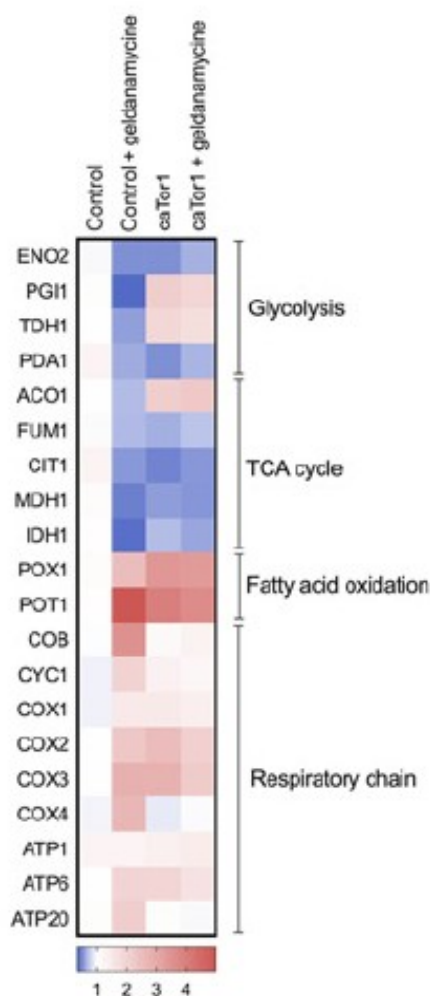


Figure 63| **Inhibition of Hsp82 chaperone leads to differential gene expression shifts comparable to ChES.** Transcript levels (top) and their representative heat map (bottom) indicate gene expression characteristic of ChES. Geld stands for geldanamycin. Color of the squares on the heat map corresponds to the mean value of the log fold change from three biological and three technical replicates. UBC6 was used for normalization. \*\*\* $P < 0.001$ ; \*\* $P < 0.01$ ; \* $P < 0.05$  (ANOVA plus post hoc).

Furthermore, the notion of Hsp82 chaperone downregulation being the proximal element of the cascade is additionally substantiated by increased oxygen consumption of geldanamycin treated wild-type strain, amounting to the tendency demonstrated in the ChES (Figure 64).

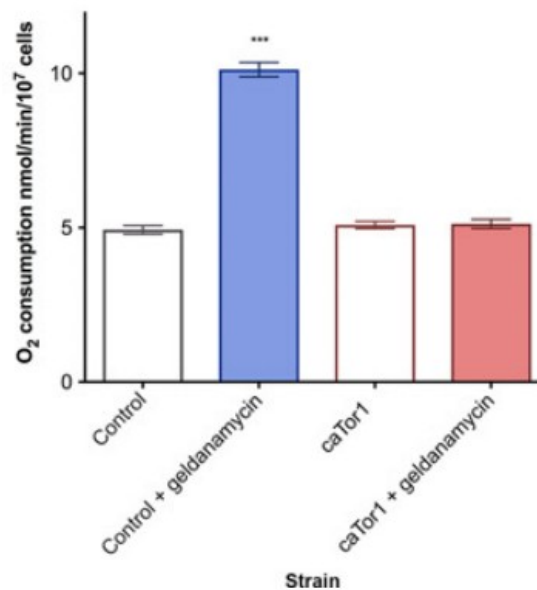


Figure 64| **Inhibition of Hsp82 chaperone leads to increased respiration.** Oxygen consumption is increased in control strain treated with geldanamycin, while caTOR1 strain failed to generate increased oxygen consumption. Control is wild-type yeast. Data are mean  $\pm$  SD from at least three independent cultures, each performed in triplicate. \*\*\* $P < 0.001$ ; \*\* $P < 0.01$ ; \* $P < 0.05$  (ANOVA plus post hoc).

To investigate the sequence of events following chaperone enrichment, Hsp82 chaperone was inhibited in the caTOR1 strain. Intriguingly, suppression of Hsp82 along with constitutive activation of Tor1 failed to generate increased oxygen consumption compared to the control strains (Figure 64). This is an added confirmation that Hsp82 downregulation is indeed an initiating event resulting in deactivation of TORC1, activation of Snf1 and the resultant glucose starvation-like phenotype observed in ChES. Moreover, the emphasis was consistently given to the significance of TORC1 deactivation in the noted signaling cascade preceding chaperone enrichment.

### 3.2.9 Chaperone enrichment leads to the extension of RLS

Since involvement of TOR and caloric restriction in lifespan extension has been extensively documented in numerous studies, the effect of chaperone enrichment on the replicative lifespan



of studied strains was examined (Bitterman et al., 2003; Johnson et al., 2013). The results showed a drastic prolongation of RLS in all of the investigated strains (Figure 65). The extent of lifespan extension of strains with overexpressions of nascent polypeptide-associated complex (NAC), cytosolic T-complex (Tcp1), ER Hsp70 chaperone (Lhs1) and mitochondrial Hsp70 (Ssc1) were demonstrated to be 67%, 61%, 56%, and 33% respectively. Median lifespan was left unaffected by chaperone enrichment as it remained ~12 generations for each strain (Figure 65).

With the intention to eliminate the possibility that the observed lifespan extension was resulting from sporadic tenacious cells not succumbing to death, the area under the curve (AUC) corresponding to the final lifespan phase ( $AUC_{late}$ ) was measured. The measurement for the  $AUC_{late}$  was normalized to the area of the entire curve ( $AUC_{total}$ ) revealed that 0.66% of the studied WT control population remains alive until the late life phase, while 4-10% of the ChES population reaching the same life stage.

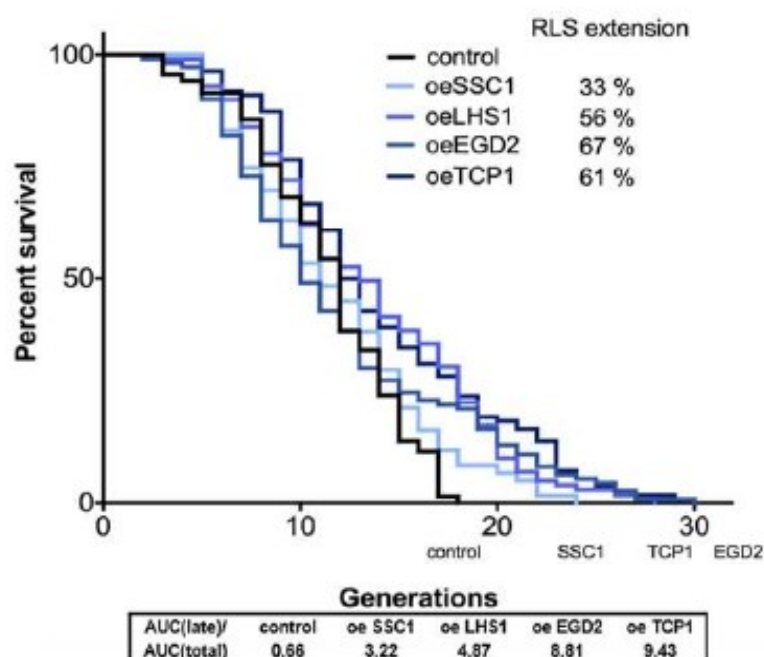


Figure 65| **Chaperone enrichment leads to replicative lifespan extension.** Survival curves determined by micromanipulation. Number of cells used for this experiment Control (n=103), oe SSC1 (n=120), oe LHS1 (n=112), oe EGD2 (n=129) and oe TCP1 (n=127). P values are 0.0009 (LHS1 and EGD2), 0.0004 (TCP1), and 0.0081 (0.SSC1). The data shown are pooled from three independent experiments for each strain. Oe stands for overexpression. Significance of the results was tested with log-rank (Mantel–Cox) test. Table under the graph demonstrates the percentage of the studied population that is still alive in the late life stage of the RLS.

### 3.2.10 Snf1/AMPK activation is required for chaperone-mediated RLS extension

To further elucidate the mechanisms responsible for the observed lifespan extension, the involvement of features characteristic of ChES: Snf1 activation, Tor1 deactivation and respiration increase was resolved to be studied.

Firstly, RLS in  $\Delta$ Snf1 mutant was measured and compared to the chaperone enriched strains in  $\Delta$ Snf1 genetic background. The results disclosed replicative lifespan of chaperone-enriched Snf1 deficient strains to be corresponding to replicative lifespan of the control strain, ie., Snf1 activation is necessary to attain RLS extension (Figure 66A).

Secondly, RLS was measured in constitutively active Tor1 strain (caTor1) and compared to the chaperone enriched strain in caTor1 genetic background. The results revealed replicative lifespan of chaperone-enriched caTor1 strain to be comparable to the RLS of the control strain, ie., Tor1 kinase deactivation is essential for RLS extension to be achieved (Figure 66B).

Lastly, the effect increased respiration has on the observed lifespan extension in the studied strains needed to be expounded. To examine this, RLS was measured in respiration-deficient petite strain and compared to chaperone-enriched petite strain. The results exhibit RLS in chaperone-enriched petite strain to be equivalent to the control strain, i.e., respiration increase is crucial for RLS extension observed in ChES (Figure 66C).

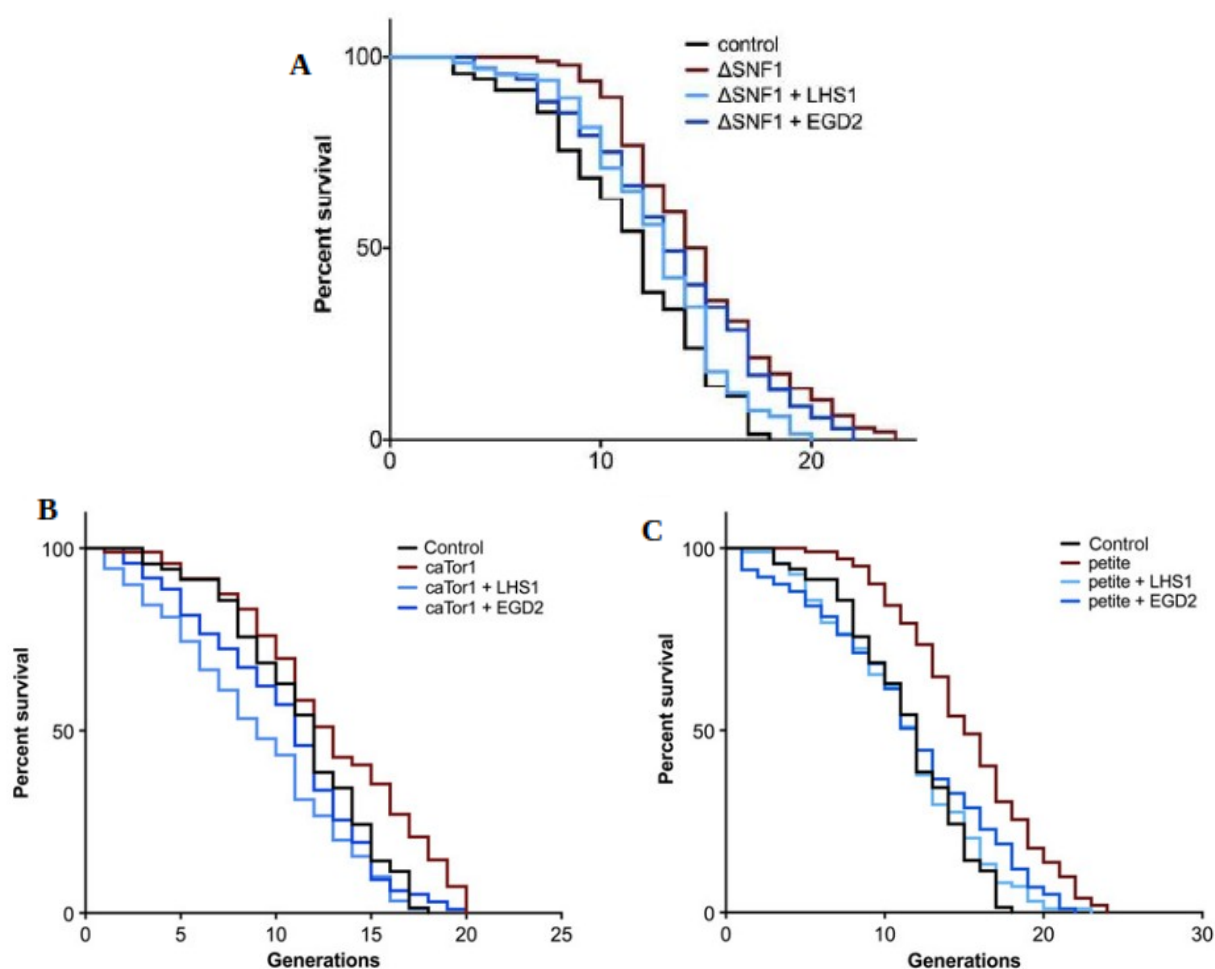


**Figure 66| RLS extension is contingent on Snf1 activation and TOR deactivation, and is attributable to respiration increase in ChES** Survival curves were determined by micromanipulation. (A) Replicative lifespan extension annulled in the absence of Snf1. Number of cells used for this experiment Control (n=103),  $\Delta$ Snf1 (n=95),  $\Delta$ Snf1 + LHS1 (n=79) and  $\Delta$ Snf1 + EGD2 (n=95). P value for  $\Delta$ Snf1 relative to control RLS is  $<0.0001$ . P values for  $\Delta$ Snf1+LHS1 and  $\Delta$ Snf1+EGD2 relative to the control are  $>0.05$ . (B) Replicative lifespan extension is absent in ChES with activated TOR. Number of cells used for this experiment Control (n=103), caTor1 (n=94), caTor1 + LHS1 (n=89) and caTor1 + EGD2 (n=94). P values for the RLS of caTor1, caTor1+LHS1, and caTor1+EGD2 compared to the control are  $>0.05$ . (C) Replicative lifespan extension is eliminated in respiration-deficient ChES. Control (n=103), petite (n=100), petite + LHS1 (n=97) and petite + EGD2 (n=99). P value for the petite strain relative to control is  $<0.0001$ . P values for petite+LHS1 and petite+EGD2 relative to control are 0.048 and 0.044, respectively. The data shown are pooled from three independent experiments for each strain. Significance of the results was tested with log-rank (Mantel–Cox) test.

## 4.2 DISCUSSION PART II

### 4.2.1 Enrichment of studied chaperones elicits mitigation of protein misfolding

Functional capability of a protein depends on their accurate folding. However, as a consequence of cellular/environmental stress, mutations, aging or disease, accuracy of protein folding decreases leading to accumulation of misfolded proteins and increase in proteotoxicity (Higgins et al., 2018; Vashist et al., 2010). It is well documented that misfolded proteins have an increased propensity to be carbonylated, and this tendency can, hence, be used as a marker of oxidative damage as well as a measure of protein misfolding (Dukan et al., 2000; Nystrom, 2005; Krisko & Radman, 2019). This study showed that chaperone enrichment in distinct cellular compartments has led to a marked reduction of protein carbonylation, amounting to 40% decrease compared to the control (Figure 44A). Another propensity misfolded proteins possess is to form protein aggregates. These aggregates can further generate damage and be detrimental to the cellular health. To quantitatively analyze formation of protein aggregates in ChES, cellular positioning of intrinsic GFP-tagged Hsp104 protein-disaggregase was examined. Hsp104 was C-terminally tagged with GFP without obstructing its activity, and its tendency to explicitly associate with protein aggregates is utilized as an indicator of endogenous protein aggregation (Saarikangas & Barral, 2015; Specht et al., 2011). Upon the introduction of studied chaperone, examination of Hsp104-associated chaperones revealed a significant decrease of intrinsic protein aggregates compared to the control (Figure 45). Another reliable indicator of folding accuracy of a proteome and cellular proteotoxicity is Hsp90 chaperone. It consists of two isoforms: stress-inducible Hsp82 and intrinsically expressed Hsc82 and its expression levels correlate with the amount of abrogated proteins and failure of proteostasis (Girstmair et al., 2019). In ChES, levels of Hsp90 were substantially lowered compared to the control (Figure 44B). Moreover, ChES demonstrated decreased levels of antioxidant enzymes, SOD1 and SOD2, together with reduced levels of cellular ROS (Figure 44C and 47). Considering that the controls enriched with inactivated versions of each of the studied chaperones (iChES) displayed results contradictory to ChES, all these results are indicative of alleviation of protein misfolding and accomplishment of proteostasis ensuing chaperone enrichment.

#### 4.2.2 ChES display metabolic paradigm suggestive of glucose-starvation response

Differential gene expression analysis revealed substantial alteration of genes characteristic of cellular response to glucose starvation, including suppression of glycolysis and TCA cycle as well as increased expression of subunits of the OXPHOS complexes (Figure 47) (Choi et al., 2018; Ocampo et al., 2012). Glucose is a primary source of energy, a pivotal contributor to the carbon skeleton of majority of biomolecules, and a superior choice of carbon source for budding yeast (Rødkaer & Faergeman, 2014). The sensing and uptake of glucose from the environment is accompanied by the repression of genes involved in regulation of metabolism on alternative energy sources, such as deactivation of Snf1 kinase (Kim et al., 2013). Conversely, limited glucose availability or disrupted glucose sensing ability is chaperoned by Snf1 activation, reduction of Tor1 signaling and increased respiration (Bonawitz et al., 2007; Pan & Shadel, 2009). Being cognizant of this, the involvement of aforementioned changes upon glucose starvation in ChES was studied.

In accordance with the previously mentioned effects glucose starvation has on the cellular metabolism, ChES demonstrated an equivalent paradigm. Complementary to glucose starvation response, our studied chaperone enriched strains displayed increased oxygen consumption (Figure 48). This increase was shown to be resultant from increased mitochondrial mass, as indicated by analysis of NAO and MitoLoc (Figure 49A C). NAO is a fluorescent probe which binds to a polyunsaturated acidic phospholipid, cardiolipin, located entirely in mitochondrial and bacterial membranes, and as such, is a dependable marker of mitochondrial mass (Jacobson et al., 2002). Mitochondrial volume parameter is assessed by software calculations upon introduction of MitoLoc plasmid and quantification of its reporter marker preSU9-GFP, which almost exclusively localizes to mitochondria (Vowinckel et al., 2015). Interestingly, it was shown that mitochondrial volume increases with the shift from glucose metabolism to other alternative sources; i.e., from fermentative to oxidative metabolism (Egner et al., 2002). This enables cells to increase their respiratory capacity characteristic of a switch to alternative carbon source metabolization, and further supports our findings that ChES indeed display a phenocopy of glucose starvation response (Rolland et al., 2002).

In addition to that, activation of Snf1 was likewise exhibited by the ChES (Figure 51). Snf1 has a major role governing cellular metabolism by controlling expression of glucose-repressed genes

following glucose starvation (Hahn & Thiele, 2004; Jiang et al., 2016). It is generally activated by phosphorylation upon glucose depletion in the media. Our further findings on gene expression and oxygen consumption of ChES in Snf1 null background indicate that activation of Snf1 kinase by phosphorylation is essential for the observed ChES response as it is absent in cells with inactivated Snf1 (Figure 52).

Lastly, this research showed that TORC1 is deactivated in ChES and that its inactivation is essential for the observed ChES response as chaperone enrichment in constitutively activated Tor1 background did not result in Snf1 activation or rise in oxygen consumption (Figure 56).

#### 4.2.3 Snf1 kinase is negatively regulated by Tor1

TOR regulates cell growth predominantly by affecting the rate of translation, and inhibition of TORC1, a distinct signaling complex of TOR, has been shown to negatively influence the rate of protein translation (Bonawitz et al., 2007). This property was used to test for TORC1 activity, and analysis of the amount of newly translated proteins in ChES displayed a significant decrease indicating inactivation of TORC1 (Figure 53). Another characteristic associated with reduced TOR signaling is downregulation of Sch9 (Pan & Shadel, 2009). Sch9 kinase is a TORC1 substrate and its activation depends on direct phosphorylation by TORC1 (Urban et al., 2007). Analysis of Sch9 phosphorylation levels in ChES revealed decreased levels, further corroborating inactivation of TORC1 (Figure 54). As an additional control, Tor1 was constitutively activated in ChES by introduction of an I1954V mutation. This mutation grants activity and hyperactivation of Tor1 (Hardt et al., 2011). Analysis of oxygen consumption in caTor1 enriched with studied chaperones revealed levels of O<sub>2</sub> consumption to be comparable to wild-type control and caTor1 control, postulating that TORC1 deactivation is pivotal for ChES response (Figure 57).

Further evaluation of TORC1 involvement in ChES response demonstrated that Snf1 kinase is negatively regulated by Tor1. This was revealed by levels of phosphorylated Snf1 which were showed to be abrogated in caTor1 and ChES in caTor1 background, but also substantially increased in Tor null mutant (Figure 56). These results are consistent with previously documented findings (Orlova et al., 2006).

#### 4.2.4 ChES response relies on Tor1 deactivation

The interaction between Tor1 and Snf1 and their involvement in mitochondrial activity was further elucidated by torin treatments of  $\Delta$ Snf1 mutant. Torin is a direct TOR inhibitor that is selective for suppressing TORC1 and TORC2 complexes in different concentrations (Huang et al., 2017). Chemical inhibition of TOR in  $\Delta$ Snf1 background was selected due to the inability to produce fit/viable  $\Delta$ Tor1 $\Delta$ Snf1 double deletion mutant. This is substantiated by gene expression analysis of torin treated  $\Delta$ Snf1 mutant (corresponding to  $\Delta$ Tor1 $\Delta$ Snf1 double deletion mutant), which revealed a striking downregulation of almost all metabolic activities, implying that this mutant strain is not viable (Figure 60).

100 nM torin treatment of wild-type control resulted in oxygen consumption comparable to the  $\Delta$ Tor1 mutant, and this level of O<sub>2</sub> consumption is equivalent to the levels observed in ChES (Figure 58). Oxygen consumption together with gene expression analysis of torin treated control indicate that suppression of Tor1 is required for ChES response (Figure 59). This claim is further corroborated by introduction of studied chaperones in the  $\Delta$ Tor1 mutant, and the subsequent gene expression analysis that displayed no additional change compared to the ChES (Figures 59 and 60).

#### 4.2.5 Hsp82 chaperone mediates the proteome quality to TORC1

Our hypothesis of a communication of Tor1 with Snf1 is based, partly, on sensing and mediating the protein folding quality status of the proteome. Protein misfolding and accumulating aggregation perturb the protein homeostasis predominantly by exhausting proteostasis network capacity, specifically molecular chaperones (Liu et al., 2015). Based on this, the involvement of chaperones in the sensing of proteostasis condition was considered, notably a chaperone intricately engaged in variety of cellular processes – Hsp82. Chaperone Hsp82, an Hsp90 isoform, is involved in extensive conformational maintenance of myriad of proteins, and it also actively monitors and regulates major signaling pathways (Hartl et al., 2011; Tiroli-Cepeda & Ramos, 2011). Interestingly, Hsp82 chaperone was shown to selectively interact with a particular class of proteome, most notably protein kinases (Tiroli-Cepeda & Ramos, 2011). We, therefore, decided to analyze its association with TORC1 and contribution to sensing/mediating the cellular conditions of ChES.

ChES demonstrated marked downregulation of Hsp82 in differential gene expression analysis, it was crucial to determine whether this drop in chaperone level is directly related to the observed ChES response (Figure 44B). Overexpression of Hsp82 in ChES revoked the response observed with downregulation of Hsp82 in ChES, particularly the increase of Snf1 activity (Figure 61B).

The conception that reduction of Hsp82 activity is requisite for TORC1 deactivation and commencement of the downstream response upon enrichment of studied chaperones is validated by chemical inhibition of Hsp82 chaperone in the wild-type yeast. Wild-type yeast was treated with geldanamycin, as it leads to inhibition of Hsp82 chaperone, and the resultant gene expression analysis demonstrated response analogues to the ChES: repression of glycolysis and upregulation of respiratory chain complexes (Figure 63). This was further substantiated by an observed increase in oxygen consumption upon Hsp82 suppression (Figure 64).

Interestingly, the observed outcome was not exhibited by Hsp82 inhibition in caTor1 strain, suggesting that deactivation of TORC1 is required for transmitting the condition of protein folding through Hsp82 deactivation (Figure 64).

#### 4.2.6 Replicative lifespan extension in ChES is contingent on increased respiration

As all of the components noted in the ChES response were previously associated with the extension of replicative lifespan in yeast, most notably the deactivation of Tor1 and activation of Snf1- characteristics of glucose-starvation response, its pertinence in ChES needed to be confirmed (Bitterman et al., 2003). It was demonstrated that RLS extension in ChES is entirely dependent on increased respiration upon chaperone enrichment (Figure 66).

As mentioned previously, a shift in proteostasis occurs primarily due to accumulation of abrogated and/or aggregated proteins which, in turn, consumes all the formerly available chaperones. It is noted in the literature that this particular availability of chaperones serves as an indicator of protein homeostasis and the protein folding quality within the cell sensed by TORC1 (Qian et al., 2010). It was proposed in this study that the sensing is mediated by Hsp82 levels, and in the particular case of ChES – its decline. The suggested mechanism underlying the observed ChES response is depicted in the Figure 67. Introduction of chaperones in distinct cellular compartments, and their substituent enrichment leads to the cell wide proteostasis marked by decreased protein carbonylation, ROS and Hsp82 levels. Alleviation of protein folding is communicated to Tor1 via decline in Hsp82 levels which, in turn, gets deactivated.



Deactivation of Tor1 leads to activation of Snf1 and triggers the response comparable to glucose-starvation. Increased respiration resultant from the glucose-starvation response leads to lifespan extension in all the studied chaperone overexpression. The precise mechanistic details of Tor1-Snf1 cross-talk remain yet to be elucidated and will be the topic of future research.

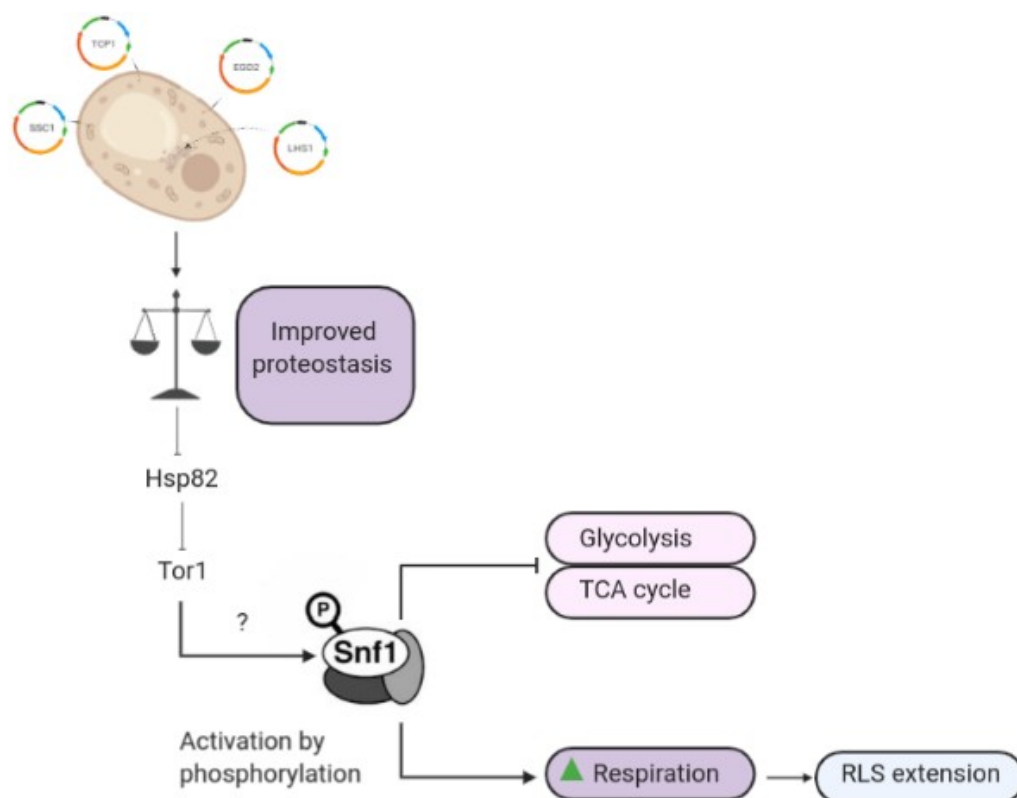


Figure 67| **Schematic representation of sequence of events following chaperone enrichment** (created with “BioRender.com”).

## 5. CONCLUSION

An intricate cellular proteostasis network (PN), comprising primarily of molecular chaperones and degradation machinery, maintains the protein homeostasis balance, a process fundamental for cell sustenance and viability. This is achieved by assiduous collaboration of extensive cellular processes most of which, if not all, are inextricably linked by molecular chaperones. Many of the central activities of chaperones involve assisting in protein folding, refolding and degrading processes as well as preventing aggregation (Hipp et al., 2014). Due to compartmentalization of eukaryotic cells, chaperones are segregated to distinct organelles. This enables cells to sustain the proteostasis by customizing regulation of the PN in response to organelle-specific perturbations, i.e., disturbed protein folding environment in the cytosol selectively activates the cytosolic heat shock response (HSR) (Yoneda, 2004). Despite the knowledge about the organelle-specific response, the existence and specificities of communication between the cellular compartments remained to be elucidated. In this study we, therefore, intended to determine the cell-wide impact of compartmentalized proteostasis decline, evoked by loss of chaperone function, and the proteostasis enhancement, evoked by enrichment of chaperones, in the mitochondria, ER, and the cytosol of the yeast *Saccharomyces cerevisiae*.

This study has demonstrated that both amelioration and mild deterioration of protein homeostasis ultimately leads to the extension of replicative lifespan through implication of hormesis (Figure 68). Hormesis is defined as an adaptive stress response to mild and transient disturbances of homeostasis, commonly with advantageous consequences to the organism (Calabrese & Baldwin, 2002). In the case of proteostasis deterioration upon chaperone deletions, beneficial extension of replicative lifespan could potentially be the result of mitohormesis, or a comprehensive cytoprotective state ordained by cytosolic and nuclear response to a moderate mitochondrial stress (Yun & Finkel, 2014). On the other hand, proteostasis amelioration upon chaperone enrichment could result in beneficial extension of replicative lifespan by hormetic effect of glucose-starvation (Masoro, 2006). The consequential effects of hormesis could promote cell's ability to cope with acute stressors that lead to damage accumulation, senescence, and ultimately, death (Masoro, 2006). Additionally, both studies revealed an intricate cross-organelle communication networking system due to which, regardless of the cellular

---

compartment the chaperone alteration originated from, effects are cell-wide and equivalent for all the studied chaperones.

Results obtained from these studies accentuate the importance of orchestrated communication between organelles and emphasize the importance of further research to recede from observing cellular responses in canonical compartmentalized manner to cell-wide approach. Furthermore, results obtained from our observations of ChES could help elucidate the obscure concept of cross-communication between nutrient-sensing pathways. These findings warrant to deepen our knowledge on cross-organelle and cross-signaling pathway communication that ensures unprecedented methodologies for future research on alleviation of aging and age-related pathologies.

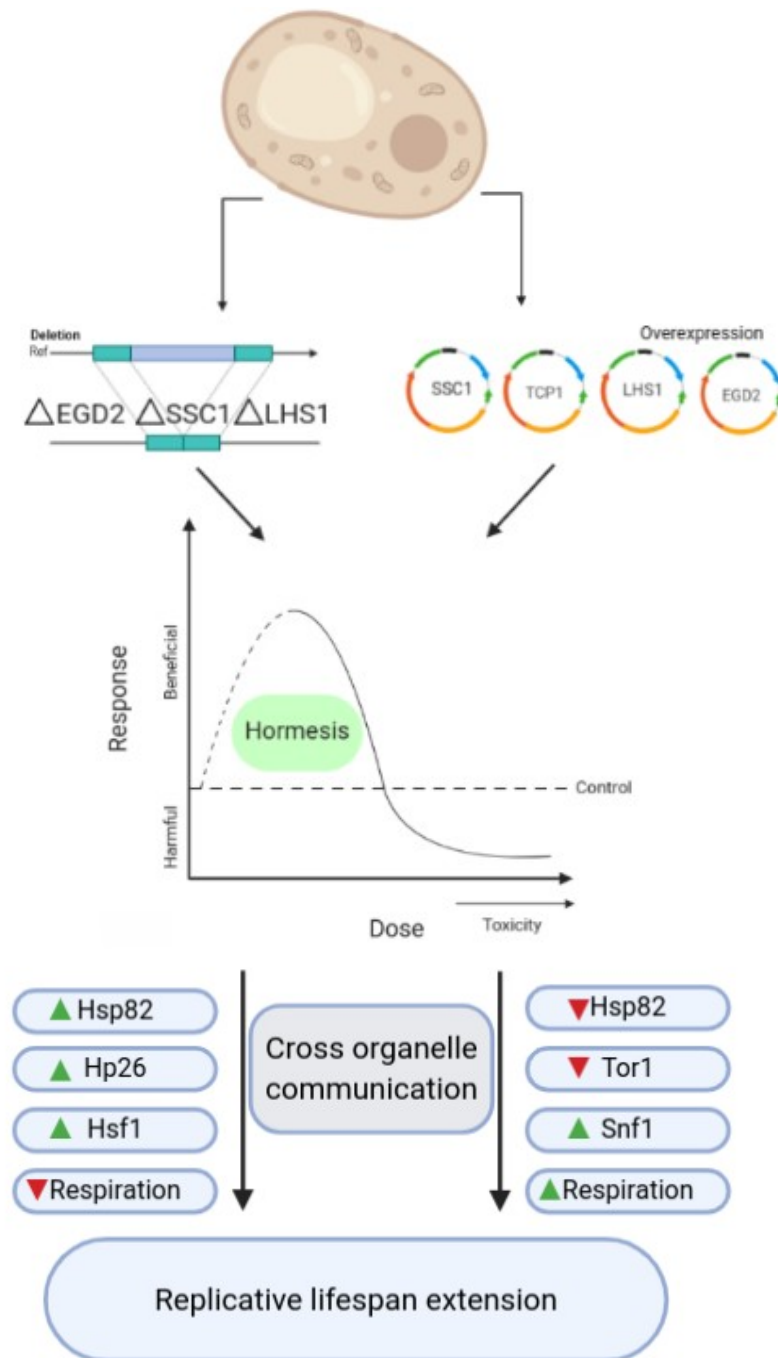


Figure 68| **Schematic representation of compendium from both studies.** Improvement of proteostasis, as well as a mild deterioration, leads up to extension of lifespan, irrespective of the origin of alteration (created with “BioRender.com”).

## 6. BIBLIOGRAPHY

- Alderson, T. R., Kim, J. H., & Markley, J. L. (2016). Dynamical Structures of Hsp70 and Hsp70-Hsp40 Complexes. *Structure*, 24(7), 1014–1030. <https://doi.org/10.1016/j.str.2016.05.011>
- Anders, S., Pyl, P. T., & Huber, W. (2015). Genome analysis HTSeq—A Python framework to work with high-throughput sequencing data. *Bioinformatics*, 31(2), 166–169. <https://doi.org/10.1093/bioinformatics/btu638>
- Anoop, V. M., Basu, U., Mccammon, M. T., Mcalister-henn, L., Taylor, G. J., Sciences, B., & A, C. T. G. V. M. (2003). Modulation of Citrate Metabolism Alters Aluminum Tolerance in Yeast and Transgenic Canola Overexpressing a Mitochondrial Citrate Synthase 1. *Plant Physiology*, 132(August), 2205–2217. <https://doi.org/10.1104/pp.103.023903.gest>
- Bader, V., Tomppo, L., Trossbach, S. V., Bradshaw, N. J., Prikulis, I., Leliveld, S. R., Lin, C. Y., Ishizuka, K., Sawa, A., & Ramos, A. (2012). Proteomic, genomic and translational approaches to identify CRMP1 for a role in schizophrenia and its underlying traits. *Human Molecular Genetics*, 21, 2206–4418.
- Barton, A. A. (1949). Some Aspects of Cell Division in *Saccharomyces cerevisiae*. *Journal of General Microbiology*, 4(1), 4.
- Bitterman, K. J., Medvedik, O., & Sinclair, D. A. (2003). Longevity Regulation in *Saccharomyces cerevisiae*: Linking Metabolism, Genome Stability, and Heterochromatin. *Microbiology and Molecular Biology Reviews*, 67(3), 376–399. <https://doi.org/10.1128/MMBR.67.3.376-399.2003>
- Blamowska, M., Sichting, M., Mapa, K., Mokranjac, D., Neupert, W., & Hell, K. (2010). ATPase Domain and Interdomain Linker Play a Key Role in Aggregation of Mitochondrial Hsp70 Chaperone Ssc1. *Journal of Biological Chemistry*, 285(7), 4423–4431. <https://doi.org/10.1074/jbc.M109.061697>
- Bonawitz, N. D., Chatenay-Lapointe, M., Pan, Y., & Shadel, G. S. (2007). Reduced TOR Signaling Extends Chronological Life Span via Increased Respiration and Upregulation of Mitochondrial Gene Expression. *Cell Metabolism*, 5(4), 265–277. <https://doi.org/10.1016/j.cmet.2007.02.009>
- Boratyn, G. M., Schäffer, A. A., Agarwala, R., Altschul, S. F., Lipman, D. J., & Madden, T. L. (2012). Domain enhanced lookup time accelerated BLAST. *Biology Direct*, 7(1), 12. <https://doi.org/10.1186/1745-6150-7-12>
- Borkovich, K. A., Farrelly, F. W., Finkelstein, D. B., Taulien, J., & Lindquist, S. (1989). Hsp82 is an essential protein that is required in higher concentrations for growth of cells at higher temperatures. *Molecular and Cellular Biology*, 9(9), 3919–3930. <https://doi.org/10.1128/MCB.9.9.3919>
- Botstein, D., & Fink, G. R. (2011). Yeast: An Experimental Organism for 21st Century Biology. *Genetics*, 189(3), 695–704. <https://doi.org/10.1534/genetics.111.130765>

- Brackley, K. I., & Grantham, J. (2009). Activities of the chaperonin containing TCP-1 (CCT): Implications for cell cycle progression and cytoskeletal organisation. *Cell Stress and Chaperones*, 14(1), 23–31. <https://doi.org/10.1007/s12192-008-0057-x>
- Bradford, M. M. (1976). A Rapid and Sensitive Method for the Quantitation Microgram Quantities of Protein Utilizing the Principle of Protein-Dye Binding. *Analytical Biochemistry*, 254, 248–254.
- Brauer, M. J., Saldanha, A. J., Dolinski, K., & Botstein, D. (2005a). Homeostatic Adjustment and Metabolic Remodeling in Glucose-limited Yeast Cultures. *Molecular Biology of the Cell*, 16, 15.
- Brejning, J., Jespersen, L., & Arneborg, N. (2003b). Genome-wide transcriptional changes during the lag phase of *Saccharomyces cerevisiae*. *Archives of Microbiology*, 179(4), 278–294. <https://doi.org/10.1007/s00203-003-0527-6>
- Broach, J. R. (2012b). Nutritional Control of Growth and Development in Yeast. *Genetics*, 192(1), 73–105. <https://doi.org/10.1534/genetics.111.135731>
- Brodsky, J. L., Werner, E. D., Dubas, M. E., Goekeler, J. L., Kruse, K. B., & McCracken, A. A. (1999). The Requirement for Molecular Chaperones during Endoplasmic Reticulum-associated Protein Degradation Demonstrates That Protein Export and Import Are Mechanistically Distinct. *Journal of Biological Chemistry*, 274(6), 3453–3460. <https://doi.org/10.1074/jbc.274.6.3453>
- Buchberger, A., Bukau, B., & Sommer, T. (2010). Protein Quality Control in the Cytosol and the Endoplasmic Reticulum: Brothers in Arms. *Molecular Cell*, 40(2), 238–252. <https://doi.org/10.1016/j.molcel.2010.10.001>
- Bukau, B., Deuerling, E., Pfund, C., & Craig, E. A. (2000). Getting Newly Synthesized Proteins into Shape. *Cell*, 101(2), 119–122. [https://doi.org/10.1016/S0092-8674\(00\)80806-5](https://doi.org/10.1016/S0092-8674(00)80806-5)
- Busti, S., Coccetti, P., Alberghina, L., & Vanoni, M. (2010). Glucose Signaling-Mediated Coordination of Cell Growth and Cell Cycle in *Saccharomyces Cerevisiae*. *Sensors*, 10(6), 6195–6240. <https://doi.org/10.3390/s100606195>
- Calabrese, E. J., & Baldwin, L. A. (2002b). Defining hormesis. *Human & Experimental Toxicology*, 21(2), 91–97. <https://doi.org/10.1191/0960327102ht217oa>
- Catalina-Rodriguez, O., Kolukula, V. K., Tomita, Y., Preet, A., Palmieri, F., Wellstein, A., Byers, S., Giaccia, A. J., Glasgow, E., Albanese, C., & Avantaggiati, M. L. (2012). The mitochondrial citrate transporter, CIC, is essential for mitochondrial homeostasis. *Oncotarget*, 3(10). <https://doi.org/10.18632/oncotarget.714>
- Chacinska, A., Koehler, C. M., Milenkovic, D., Lithgow, T., & Pfanner, N. (2009). Importing Mitochondrial Proteins: Machineries and Mechanisms. *Cell*, 138(4), 628–644. <https://doi.org/10.1016/j.cell.2009.08.005>
- Chen, B., Retzlaff, M., Roos, T., & Frydman, J. (2011). Cellular Strategies of Protein Quality Control. *Cold Spring Harbor Perspectives in Biology*, 3(8), a004374–a004374. <https://doi.org/10.1101/cshperspect.a004374>

- Chen, I., Dellisanti, C., & Moorefield, B. (2015). An unexpected role for mitochondrial ClpX. *Nature Publishing Group*, 22(6), 441. <https://doi.org/10.1038/nsmb.3046>
- Chiti, F., & Dobson, C. M. (2006b). Protein Misfolding, Functional Amyloid, and Human Disease. *Annual Review of Biochemistry*, 75(1), 333–366. <https://doi.org/10.1146/annurev.biochem.75.101304.123901>
- Choi, K.-M., Hong, S.-J., van Deursen, J. M., Kim, S., Kim, K. H., & Lee, C.-K. (2018). Caloric Restriction and Rapamycin Differentially Alter Energy Metabolism in Yeast. *The Journals of Gerontology: Series A*, 73(1), 29–38. <https://doi.org/10.1093/gerona/glx024>
- Ciechanover, A., & Kwon, Y. T. (2017b). Protein Quality Control by Molecular Chaperones in Neurodegeneration. *Frontiers in Neuroscience*, 11. <https://doi.org/10.3389/fnins.2017.00185>
- Dalle-Donne, I., Aldini, G., Carini, M., Colombo, R., Rossi, R., & Milzani, A. (2006). Protein carbonylation, cellular dysfunction, and disease progression. *Journal of Cellular and Molecular Medicine*, 10(2), 389–406. <https://doi.org/10.1111/j.1582-4934.2006.tb00407.x>
- de Alteriis, E., Carteni, F., Parascandola, P., Serpa, J., & Mazzoleni, S. (2018). Revisiting the Crabtree/Warburg effect in a dynamic perspective: A fitness advantage against sugar-induced cell death. *Cell Cycle*, 17(6), 688–701. <https://doi.org/10.1080/15384101.2018.1442622>
- de Keyzer, J., Steel, G. J., Hale, S. J., Humphries, D., & Stirling, C. J. (2009). Nucleotide Binding by Lhs1p Is Essential for Its Nucleotide Exchange Activity and for Function *in Vivo*. *Journal of Biological Chemistry*, 284(46), 31564–31571. <https://doi.org/10.1074/jbc.M109.055160>
- De Virgilio, C. (2012). The essence of yeast quiescence. *FEMS Microbiology Reviews*, 36(2), 306–339. <https://doi.org/10.1111/j.1574-6976.2011.00287.x>
- DeRisi, J. L., Iyer, V. R., & Brown, P. O. (1997). Exploring the Metabolic and Genetic Control of Gene Expression on a Genomic Scale. *Science, New Series*, 278(5338), 680–686.
- Deuerling, E., & Bukau, B. (2004). Chaperone-assisted folding of newly synthesized proteins in the cytosol. *Critical Reviews in Biochemistry and Molecular Biology*, 39(5–6), 261–277. <https://doi.org/10.1080/10409230490892496>
- Dobson, C. M. (2003). Protein Folding and Misfolding.Pdf. *Nature*, 426(6968), 884–90. <https://doi.org/10.1007/978-3-642-22230-6>
- Dobson, C. M. (2004). Principles of protein folding, misfolding and aggregation. *Seminars in Cell and Developmental Biology*, 15(1), 3–16. <https://doi.org/10.1016/j.semcdb.2003.12.008>
- Dobson, C. M., Šali, A., & Karplus, M. (1998). Protein folding: A perspective from theory and experiment. *Angewandte Chemie - International Edition*, 37(7), 868–893. [https://doi.org/10.1002/\(SICI\)1521-3773\(19980420\)37:7<868::AID-ANIE868>3.0.CO;2-H](https://doi.org/10.1002/(SICI)1521-3773(19980420)37:7<868::AID-ANIE868>3.0.CO;2-H)

- Doyle, S. M., Genest, O., & Wickner, S. (2013). Protein rescue from aggregates by powerful molecular chaperone machines. *Nature Publishing Group*, 14(10), 617–629.  
<https://doi.org/10.1038/nrm3660>
- Dukan, S., Farewell, A., Ballesteros, M., Taddei, F., Radman, M., & Nystrom, T. (2000). Protein oxidation in response to increased transcriptional or translational errors. *Proceedings of the National Academy of Sciences*, 97(11), 5746–5749.  
<https://doi.org/10.1073/pnas.100422497>
- Egner, A., Jakobs, S., & Hell, S. W. (2002). Fast 100-nm resolution three-dimensional microscope reveals structural plasticity of mitochondria in live yeast. *Proceedings of the National Academy of Sciences*, 99(6), 3370–3375.  
<https://doi.org/10.1073/pnas.052545099>
- Fabrizio, P., & Longo, V. D. (2007). The Chronological Life Span of *Saccharomyces cerevisiae*. In T. O. Tollefsbol (Ed.), *Biological Aging* (Vol. 371, pp. 89–95). Humana Press.  
[https://doi.org/10.1007/978-1-59745-361-5\\_8](https://doi.org/10.1007/978-1-59745-361-5_8)
- Fernández-Fernández, M. R., & Valpuesta, J. M. (2018). Hsp70 chaperone: A master player in protein homeostasis. *F1000Research*, 7(0), 1497.  
<https://doi.org/10.12688/f1000research.15528.1>
- Fuge, E K, Braun, E. L., & Werner-Washburne, M. (1994). Protein synthesis in long-term stationary-phase cultures of *Saccharomyces cerevisiae*. *Journal of Bacteriology*, 176(18), 5802–5813. <https://doi.org/10.1128/jb.176.18.5802-5813.1994>
- Fumagalli, F., Noack, J., Bergmann, T. J., Cebollero, E., Pisoni, G. B., Fasana, E., Fregno, I., Galli, C., Loi, M., Soldà, T., D’Antuono, R., Raimondi, A., Jung, M., Melnyk, A., Schorr, S., Schreiber, A., Simonelli, L., Varani, L., Wilson-Zbinden, C., ... Molinari, M. (2016). Translocon component Sec62 acts in endoplasmic reticulum turnover during stress recovery. *Nature Cell Biology*, 18(11), 1173–1184. <https://doi.org/10.1038/ncb3423>
- Gancedo, J. M. (1998a). Yeast Carbon Catabolite Repression. *MICROBIOL. MOL. BIOL. REV.*, 62, 28.
- Gardner, J. M., & Jaspersen, S. L. (2014). Manipulating the Yeast Genome: Deletion, Mutation, and Tagging by PCR. In J. S. Smith & D. J. Burke (Eds.), *Yeast Genetics* (Vol. 1205, pp. 45–78). Springer New York. [https://doi.org/10.1007/978-1-4939-1363-3\\_5](https://doi.org/10.1007/978-1-4939-1363-3_5)
- Gershon, H., & Gershon, D. (2000b). The budding yeast, *Saccharomyces cerevisiae*, as a model for aging research: A critical review. *Mechanisms of Ageing and Development*, 120, 22.
- Gething, M.-J., & Sambrook, J. (1992). Protein folding in the cell. *Nature*, 355(6355), 33–45.  
<https://doi.org/10.1038/355033a0>
- Gidalevitz, T., Prahlad, V., & Morimoto, R. I. (2011). The Stress of Protein Misfolding: From Single Cells to Multicellular Organisms. *Cold Spring Harbor Perspectives in Biology*, 3(6), a009704–a009704. <https://doi.org/10.1101/cshperspect.a009704>
- Gietz, R. D., & Schiestl, R. H. (2008). High-efficiency yeast transformation using the LiAc / SS carrier DNA / PEG method. *Nature Protocols*, 2(1), 31–35.  
<https://doi.org/10.1038/nprot.2007.13>



- Girstmair, H., Tippel, F., Lopez, A., Tych, K., Stein, F., Haberkant, P., Schmid, P. W. N., Helm, D., Rief, M., Sattler, M., & Buchner, J. (2019). The Hsp90 isoforms from *S. cerevisiae* differ in structure, function and client range. *Nature Communications*, 10(1). <https://doi.org/10.1038/s41467-019-11518-w>
- Gnoni, G. V., Priore, P., Geelen, M. J. H., & Siculella, L. (2009b). The mitochondrial citrate carrier: Metabolic role and regulation of its activity and expression. *IUBMB Life*, 61(10), 987–994. <https://doi.org/10.1002/iub.249>
- Goldring, E. S., Grossman, L. I., & Julius, M. (1971). Petite Mutation in Yeast. *Journal of Bacteriology*, 107(1), 377–381.
- Goldstein, A. L., & Cusker, J. H. M. (1999). Three New Dominant Drug Resistance Cassettes for Gene Disruption in *Saccharomyces cerevisiae*. *Yeast*, 1553(November 1998), 1541–1553.
- Gong, Y., Kakihara, Y., Krogan, N., Greenblatt, J., Emili, A., Zhang, Z., & Houry, W. A. (2009). An atlas of chaperone-protein interactions in *Saccharomyces cerevisiae*: Implications to protein folding pathways in the cell. *Molecular Systems Biology*, 5(275), 1–14. <https://doi.org/10.1038/msb.2009.26>
- Hahn, J.-S., & Thiele, D. J. (2004). Activation of the *Saccharomyces cerevisiae* Heat Shock Transcription Factor Under Glucose Starvation Conditions by Snf1 Protein Kinase. *Journal of Biological Chemistry*, 279(7), 5169–5176. <https://doi.org/10.1074/jbc.M311005200>
- Hardt, M., Chantaravisoot, N., & Tamanoi, F. (2011). Activating mutations of TOR (target of rapamycin): TOR activating mutations. *Genes to Cells*, 16(2), 141–151. <https://doi.org/10.1111/j.1365-2443.2010.01482.x>
- Harman, D. (1956). Aging: A theory based on free radical and radiation chemistry. *Journal of Gerontology*, 11, 298–300.
- Hartl, F. U., Bracher, A., & Hayer-Hartl, M. (2011). Molecular chaperones in protein folding and proteostasis. *Nature*, 475(7356), 324–332. <https://doi.org/10.1038/nature10317>
- Hartl, F. U., & Hayer-Hartl, M. (2002). Molecular Chaperones in the cytosol nascent chain to folded protein. *Science's Compass*, 295(March), 1852–1858.
- Haslbeck, M. (1999). Hsp26: A temperature-regulated chaperone. *The EMBO Journal*, 18(23), 6744–6751. <https://doi.org/10.1093/emboj/18.23.6744>
- Haynes, C. M., & Ron, D. (2010). The mitochondrial UPR - protecting organelle protein homeostasis. *Journal of Cell Science*, 123(22), 3849–3855. <https://doi.org/10.1242/jcs.075119>
- Hedbacker, K. (2008). SNF1/AMPK pathways in yeast. *Frontiers in Bioscience*, 13(13), 2408. <https://doi.org/10.2741/2854>
- Higgins, R., Kabbaj, M.-H., Hatcher, A., & Wang, Y. (2018). The absence of specific yeast heat-shock proteins leads to abnormal aggregation and compromised autophagic clearance of mutant Huntingtin proteins. *PLOS ONE*, 13(1), e0191490. <https://doi.org/10.1371/journal.pone.0191490>

- Higuchi-Sanabria, R., Pernice, W. M. A., Vevea, J. D., Alessi Wolken, D. M., Boldogh, I. R., & Pon, L. A. (2014). Role of asymmetric cell division in lifespan control in *Saccharomyces cerevisiae*. *FEMS Yeast Research*, 14(8), 1133–1146. <https://doi.org/10.1111/1567-1364.12216>
- Hill, S. M., Hanzén, S., & Nyström, T. (2017b). Restricted access: Spatial sequestration of damaged proteins during stress and aging. *EMBO Reports*, 18(3), 377–391. <https://doi.org/10.15252/embr.201643458>
- Hipp, M. S., Park, S., & Hartl, F. U. (2014). Proteostasis impairment in protein- misfolding and - aggregation diseases. *Trends in Cell Biology, Figure 2*, 1–9. <https://doi.org/10.1016/j.tcb.2014.05.003>
- Huang, H., Chen, J., Lu, H., Zhou, M., Chai, Z., & Hu, Y. (2017). Two mTOR inhibitors, rapamycin and Torin 1, differentially regulate iron-induced generation of mitochondrial ROS. *BioMetals*, 30(6), 975–980. <https://doi.org/10.1007/s10534-017-0059-1>
- Huber, W., Carey, V. J., Gentleman, R., Anders, S., Carlson, M., Carvalho, B. S., Bravo, H. C., Davis, S., & Gatto, L. (2015). Orchestrating high-throughput genomic analysis with Bioconductor. *Nature Methods*, 12(2), 115–121. <https://doi.org/10.1038/nmeth.3252>. Orchestrating
- Ikai, N., Nakazawa, N., Hayashi, T., & Yanagida, M. (2011b). The reverse, but coordinated, roles of Tor2 (TORC1) and Tor1 (TORC2) kinases for growth, cell cycle and separase-mediated mitosis in *Schizosaccharomyces pombe*. *Open Biology*, 1(3), 110007. <https://doi.org/10.1098/rsob.110007>
- Inoue, Y., & Nomura, W. (2018). TOR Signaling in Budding Yeast. *IntechOpen*, 55–77.
- Jacobson, J., Duchen, M. R., & Heales, S. J. R. (2002). Intracellular distribution of the fluorescent dye nonyl acridine orange responds to the mitochondrial membrane potential: Implications for assays of cardiolipin and mitochondrial mass: Intracellular distribution of the fluorescent dye nonyl acridine orange. *Journal of Neurochemistry*, 82(2), 224–233. <https://doi.org/10.1046/j.1471-4159.2002.00945.x>
- Janssens, G. E., & Veenhoff, L. M. (2016b). The Natural Variation in Lifespans of Single Yeast Cells Is Related to Variation in Cell Size, Ribosomal Protein, and Division Time. *PLOS ONE*, 11(12), e0167394. <https://doi.org/10.1371/journal.pone.0167394>
- Jazwinski, S. M. (2013b). The retrograde response: When mitochondrial quality control is not enough. *Biochimica et Biophysica Acta (BBA) - Molecular Cell Research*, 1833(2), 400–409. <https://doi.org/10.1016/j.bbamcr.2012.02.010>
- Jiang, J. C., Stumpferl, S. W., Tiwari, A., Qin, Q., Rodriguez-Quinones, J. F., & Jazwinski, S. M. (2016). Identification of the Target of the Retrograde Response that Mediates Replicative Lifespan Extension in *Saccharomyces cerevisiae*. *Genetics*, 204(2), 659–673. <https://doi.org/10.1534/genetics.116.188086>
- Johnson, S. C., Rabinovitch, P. S., & Kaeberlein, M. (2013). MTOR is a key modulator of ageing and age-related disease. *Nature*, 493(7432), 338–345. <https://doi.org/10.1038/nature11861>

- Johnston, M. (1999b). Feasting, fasting and fermenting: Glucose sensing in yeast and other cells. *Trends in Genetics*, 15(1), 29–33. [https://doi.org/10.1016/S0168-9525\(98\)01637-0](https://doi.org/10.1016/S0168-9525(98)01637-0)
- Joshi, D. C., & Bakowska, J. C. (2011b). Determination of Mitochondrial Membrane Potential and Reactive Oxygen Species in Live Rat Cortical Neurons. *Journal of Visualized Experiments*, 51. <https://doi.org/10.3791/2704>
- Jovaisaite, V., Mouchiroud, L., & Auwerx, J. (2014). The mitochondrial unfolded protein response, a conserved stress response pathway with implications in health and disease. *Journal of Experimental Biology*, 217(1), 137–143. <https://doi.org/10.1242/jeb.090738>
- Kaeberlein, M. (2010b). Lessons on longevity from budding yeast. *Nature*, 464(7288), 513–519. <https://doi.org/10.1038/nature08981>
- Kaeberlein, M., Burtner, C. R., & Kennedy, B. K. (2007b). Recent Developments in Yeast Aging. *PLoS Genetics*, 3(5), e84. <https://doi.org/10.1371/journal.pgen.0030084>
- Kaganovich, D., Kopito, R., & Frydman, J. (2008b). Misfolded proteins partition between two distinct quality control compartments. *Nature*, 454(7208), 1088–1095. <https://doi.org/10.1038/nature07195>
- Kanehara, K., Xie, W., & Ng, D. T. W. (2010). Modularity of the Hrd1 ERAD complex underlies its diverse client range. *The Journal of Cell Biology*, 188(5), 707–716. <https://doi.org/10.1083/jcb.200907055>
- Kasianowicz, J., Benz, R., & McLaughlin, S. (1984). The kinetic mechanism by which CCCP (carbonyl cyanidem-Chlorophenylhydrazine) transports protons across membranes. *The Journal of Membrane Biology*, 82(2), 179–190. <https://doi.org/10.1007/BF01868942>
- Kayikci, Ö., & Nielsen, J. (2015). Glucose repression in *Saccharomyces cerevisiae*. *FEMS Yeast Research*, 15(6), fov068. <https://doi.org/10.1093/femsyr/fov068>
- Kim, J.-H., Roy, A., Jouandot, D., & Cho, K. H. (2013). The glucose signaling network in yeast. *Biochimica et Biophysica Acta (BBA) - General Subjects*, 1830(11), 5204–5210. <https://doi.org/10.1016/j.bbagen.2013.07.025>
- Kimata, Y., Kimata, Y. I., Shimizu, Y., Abe, H., Farcasanu, I. C., Takeuchi, M., Rose, M. D., & Kohno, K. (2003b). Genetic Evidence for a Role of BiP/Kar2 That Regulates Ire1 in Response to Accumulation of Unfolded Proteins. *Molecular Biology of the Cell*, 14(6), 2559–2569. <https://doi.org/10.1091/mbc.e02-11-0708>
- Klaips, C. L., Jayaraj, G. G., & Hartl, F. U. (2018). Pathways of cellular proteostasis in aging and disease. *Journal of Cell Biology*, 217(1), 51–63. <https://doi.org/10.1083/jcb.201709072>
- Koga, H., Kaushik, S., & Cuervo, A. M. (2011). Protein Homeostasis and Aging: The importance of exquisite quality control. *Ageing Res Rev*, 10(2), 205–215. <https://doi.org/10.1016/j.arr.2010.02.001>
- Korovila, I., Hugo, M., Castro, J. P., Weber, D., & Höhn, A. (2017). Redox Biology Proteostasis , oxidative stress and aging. *Redox Biology*, 13(December 2016), 550–567. <https://doi.org/10.1016/j.redox.2017.07.008>
- Krisko, A., & Radman, M. (2019). Protein damage, ageing and age-related diseases. *Open Biology*, 9(3), 180249. <https://doi.org/10.1098/rsob.180249>

## BIBLIOGRAPHY

---

- Kumar, C. M. S., Mande, S. C., & Mahajan, G. (2015). Multiple chaperonins in bacteria—Novel functions and non-canonical behaviors. *Cell Stress and Chaperones*, 20(4), 555–574. <https://doi.org/10.1007/s12192-015-0598-8>
- Kyriakakis, E., Princz, A., & Tavernarakis, N. (2015b). Stress Responses During Ageing: Molecular Pathways Regulating Protein Homeostasis. In C. M. Osowski (Ed.), *Stress Responses* (Vol. 1292, pp. 215–234). Springer New York. [https://doi.org/10.1007/978-1-4939-2522-3\\_16](https://doi.org/10.1007/978-1-4939-2522-3_16)
- Le Pape, S. (2013). *EasyqpcR for low-throughput real-time quantitative PCR data analysis*. <http://www.bioconductor.org/packages/release/bioc/html/EasyqpcR.html>
- Lee, Y. J., Hoe, K. L., & Maeng, P. J. (2007b). Yeast Cells Lacking the *CIT1* -encoded Mitochondrial Citrate Synthase Are Hypersusceptible to Heat- or Aging-induced Apoptosis. *Molecular Biology of the Cell*, 18(9), 3556–3567. <https://doi.org/10.1091/mbc.e07-02-0118>
- Leliveld, S. R., Bader, V., Hendriks, P., Prikulis, I., Sajani, G., Requena, J. R., & Korth, C. (2008). Insolubility of Disrupted-in-Schizophrenia 1 Disrupts Oligomer-Dependent Interactions with Nuclear Distribution Element 1 and Is Associated with Sporadic Mental Disease. *Journal of Neuroscience*, 28(15), 3839–3845. <https://doi.org/10.1523/JNEUROSCI.5389-07.2008>
- Lesage, G., & Bussey, H. (2006). Cell Wall Assembly in *Saccharomyces cerevisiae*. *Microbiology and Molecular Biology Reviews*, 70(2), 317–343. <https://doi.org/10.1128/MMBR.00038-05>
- Levin, D. E. (2005). Cell Wall Integrity Signaling in *Saccharomyces cerevisiae*. *Microbiology and Molecular Biology Reviews*, 69(2), 262–291. <https://doi.org/10.1128/MMBR.69.2.262-291.2005>
- Lin, S.-J., Kaeberlein, M., Andalis, A. A., Sturtz, L. A., Defossez, P.-A., Culotta, V. C., Fink, G. R., & Guarente, L. (2002). Lifespan by increasing respiration. *Letters to Nature*, 418, 5.
- Linxweiler, M., Schick, B., & Zimmermann, R. (2017b). Let's talk about Secs: Sec61, Sec62 and Sec63 in signal transduction, oncology and personalized medicine. *Signal Transduction and Targeted Therapy*, 2(1). <https://doi.org/10.1038/sigtrans.2017.2>
- Liu, Y., & Chang, A. (2008b). Heat shock response relieves ER stress. *The EMBO Journal*, 27(7), 1049–1059. <https://doi.org/10.1038/emboj.2008.42>
- Liu, Y., Zhang, X., Chen, W., Tan, Y. L., & Kelly, J. W. (2015). Fluorescence Turn-On Folding Sensor To Monitor Proteome Stress in Live Cells. *Journal of the American Chemical Society*, 137(35), 11303–11311. <https://doi.org/10.1021/jacs.5b04366>
- Lloyd, D., Kristensen, B., & Degn, H. (1983). Glycolysis and respiration in yeasts. The Pasteur effect studied by mass spectrometry. *Biochemical Journal*, 212(3), 749–754. <https://doi.org/10.1042/bj2120749>
- Loewith, R., & Hall, M. N. (2011b). Target of Rapamycin (TOR) in Nutrient Signaling and Growth Control. *Genetics*, 189(4), 1177–1201. <https://doi.org/10.1534/genetics.111.133363>

- Longo, V D, & Fabrizio, P. (2002). *Cellular and Molecular Life Sciences Visions & Reflections Regulation of longevity and stress resistance: A molecular strategy conserved from yeast to humans ?* <https://doi.org/10.1007/s00018-002-8477-8>
- Longo, Valter D., Shadel, G. S., Kaeblerlein, M., & Kennedy, B. (2012). Replicative and Chronological Aging in *Saccharomyces cerevisiae*. *Cell Metabolism*, 16(1), 18–31. <https://doi.org/10.1016/j.cmet.2012.06.002>
- López-Otín, C., Blasco, M. A., Partridge, L., Serrano, M., & Kroemer, G. (2013b). The Hallmarks of Aging. *Cell*, 153(6), 1194–1217. <https://doi.org/10.1016/j.cell.2013.05.039>
- Love, M. I., Huber, W., & Anders, S. (2014). Moderated estimation of fold change and dispersion for RNA-seq data with DESeq2. *Genome Biology*, 550, 1–21. <https://doi.org/10.1186/s13059-014-0550-8>
- Lu, J., & Deutsch, C. (2005b). Folding zones inside the ribosomal exit tunnel. *Nature Structural & Molecular Biology*, 12(12), 1123–1129. <https://doi.org/10.1038/nsmb1021>
- Maftah, A., Petit, J. M., Ratinaud, M.-H., & Julien, R. (1989). 10-N Nonyl-acridine orange: A fluorescent probe which stains mitochondria independently of their energetic state. *Biochemical and Biophysical Research Communications*, 164(16), 185–190.
- Marchi, S., Giorgi, C., Suski, J. M., Agnoletto, C., Bononi, A., Bonora, M., De Marchi, E., Missiroli, S., Patergnani, S., Poletti, F., Rimessi, A., Duszynski, J., Wieckowski, M. R., & Pinton, P. (2012). Mitochondria-Ros Crosstalk in the Control of Cell Death and Aging. *Journal of Signal Transduction*, 2012, 1–17. <https://doi.org/10.1155/2012/329635>
- Marco Sandri, J. R. (2014). Proteotoxicity: An Underappreciated Pathology in Cardiac Disease. *J Mol Cell Cardiol*, 0, 3–10. <https://doi.org/10.1158/0008-5472.CAN-10-4002.BONE>
- Martin, J., Mahlke, K., & Pfanner, N. (1991). Role of an Energized Inner Membrane in Mitochondrial Protein Import. Delta psi drives the movement of presequences. *The Journal of Biological Chemistry*, 266(27), 18051–18057.
- Masoro, E. J. (2006). The Role of Hormesis in Life Extension by Dietary Restriction. In C. V. Mobbs, K. Yen, & P. R. Hof (Eds.), *Interdisciplinary Topics in Gerontology* (pp. 1–17). KARGER. <https://doi.org/10.1159/000096552>
- Mauricio Valerio-Santiago, F. M.-C. (2011). *CIL\_13897, Saccharomyces cerevisiae* [Data set]. CIL. <https://doi.org/10.7295/W9CIL13897>
- Mei, S.-C., & Brenner, C. (2015). Calorie Restriction-Mediated Replicative Lifespan Extension in Yeast Is Non-Cell Autonomous. *PLOS Biology*, 13(1), e1002048. <https://doi.org/10.1371/journal.pbio.1002048>
- Merkwirth, C., Jovaisaite, V., Durieux, J., Shaw, R. J., Auwerx, J., Dillin, A., Merkwirth, C., Jovaisaite, V., Durieux, J., Matilainen, O., Jordan, S. D., & Quiros, P. M. (2016). Two Conserved Histone Demethylases Regulate Article Two Conserved Histone Demethylases Regulate Mitochondrial Stress-Induced Longevity. *Cell*, 165(5), 1209–1223. <https://doi.org/10.1016/j.cell.2016.04.012>
- Miceli, M. V., Jiang, J. C., Tiwari, A., Rodriguez-Quinones, J. F., & Jazwinski, S. M. (2012). Loss of Mitochondrial Membrane Potential Triggers the Retrograde Response Extending

- Yeast Replicative Lifespan. *Frontiers in Genetics*, 2.  
<https://doi.org/10.3389/fgene.2011.00102>
- Mick, D. U., Vukotic, M., Piechura, H., Meyer, H. E., Warscheid, B., Deckers, M., & Rehling, P. (2010b). Coa3 and Cox14 are essential for negative feedback regulation of COX1 translation in mitochondria. *The Journal of Cell Biology*, 191(1), 141–154.  
<https://doi.org/10.1083/jcb.201007026>
- Milardi, D., & Rizzarelli, E. (2011). *Neurodegeneration: Metallostasis and Proteostasis*. Royal Society of Chemistry.
- Minois, N., Frajnt, M., Wilson, C., & Vaupel, J. W. (2004). Advances in measuring lifespan in the yeast *Saccharomyces cerevisiae*. *PNAS*, 102(2).  
<https://doi.org/10.1073/pnas.0408332102>
- Mogk, A., Bukau, B., & Kampinga, H. H. (2018). Cellular Handling of Protein Aggregates by Disaggregation Machines. *Molecular Cell*, 69(2), 214–226.  
<https://doi.org/10.1016/j.molcel.2018.01.004>
- Mortimer, R. K., & Johnston, J. R. (1959). Life Span of Individual Yeast Cells. *Nature*, 183(4677), 1751–1752. <https://doi.org/10.1038/1831751a0>
- Nayak, V., Zhao, K., Wyce, A., Schwartz, M. F., Lo, W.-S., Berger, S. L., & Marmorstein, R. (2006). Structure and Dimerization of the Kinase Domain from Yeast Snf1, a Member of the Snf1/AMPK Protein Family. *Structure*, 14(3), 477–485.  
<https://doi.org/10.1016/j.str.2005.12.008>
- Nedeva, T. S., Petrova, V. Y., Zamfirova, D. R., Stephanova, E. V., & Kujumdzieva, A. V. (2004). Cu/Zn superoxide dismutase in yeast mitochondria – a general phenomenon. *FEMS Microbiology Letters*, 230(1), 19–25. [https://doi.org/10.1016/S0378-1097\(03\)00855-3](https://doi.org/10.1016/S0378-1097(03)00855-3)
- Nicastro, R., Tripodi, F., Guzzi, C., Reghellin, V., Khoomrung, S., Capusoni, C., Compagno, C., Airoidi, C., Nielsen, J., Alberghina, L., & Coccetti, P. (2015). Enhanced amino acid utilization sustains growth of cells lacking Snf1/AMPK. *Biochimica et Biophysica Acta (BBA) - Molecular Cell Research*, 1853(7), 1615–1625.  
<https://doi.org/10.1016/j.bbamcr.2015.03.014>
- Nystrom, T. (2005). Role of oxidative carbonylation in protein quality control and senescence. *The EMBO Journal*, 24(7), 1311–1317. <https://doi.org/10.1038/sj.emboj.7600599>
- O. Tiroli-Cepeda, A., & H.I. Ramos, C. (2011). An Overview of the Role of Molecular Chaperones in Protein Homeostasis. *Protein & Peptide Letters*, 18(2), 101–109.  
<https://doi.org/10.2174/092986611794475093>
- Ocampo, A., Liu, J., Schroeder, E. A., Shadel, G. S., & Barrientos, A. (2012). Mitochondrial Respiratory Thresholds Regulate Yeast Chronological Life Span and its Extension by Caloric Restriction. *Cell Metabolism*, 16(1), 55–67.  
<https://doi.org/10.1016/j.cmet.2012.05.013>
- Oliveira, A. V., Vilaça, R., Santos, C. N., Costa, V., & Menezes, R. (2017). Exploring the power of yeast to model aging and age-related neurodegenerative disorders. *Biogerontology*, 18(1), 3–34. <https://doi.org/10.1007/s10522-016-9666-4>

- Onuchic, J. N., Socci, N. D., Luthey-Schulten, Z., & Wolynes, P. G. (1996). Protein folding funnels: The nature of the transition state ensemble. *Library Services to Latinos: An Anthology*, 1, 441–450. [https://doi.org/10.1016/S1359-0278\(96\)00060-0](https://doi.org/10.1016/S1359-0278(96)00060-0)
- Orlova, M., Kanter, E., Krakovich, D., & Kuchin, S. (2006). Nitrogen Availability and TOR Regulate the Snf1 Protein Kinase in *Saccharomyces cerevisiae*. *Eukaryotic Cell*, 5(11), 1831–1837. <https://doi.org/10.1128/EC.00110-06>
- Ott, A.-K., Locher, L., Koch, M., & Deuerling, E. (2015). Functional Dissection of the Nascent Polypeptide-Associated Complex in *Saccharomyces cerevisiae*. *PLOS ONE*, 10(11), e0143457. <https://doi.org/10.1371/journal.pone.0143457>
- Ozcan, S., & Johnston, M. (1999). Function and Regulation of Yeast Hexose Transporters. *MICROBIOL. MOL. BIOL. REV.*, 63, 16.
- Palmieri, F., Agrimi, G., Blanco, E., Castegna, A., Di Noia, M. A., Iacobazzi, V., Lasorsa, F. M., Marobbio, C. M. T., Palmieri, L., Scarcia, P., Todisco, S., Vozza, A., & Walker, J. (2006). Identification of mitochondrial carriers in *Saccharomyces cerevisiae* by transport assay of reconstituted recombinant proteins. *Biochimica et Biophysica Acta (BBA) - Bioenergetics*, 1757(9–10), 1249–1262. <https://doi.org/10.1016/j.bbabo.2006.05.023>
- Pan, Y., & Shadel, G. S. (2009). Extension of chronological life span by reduced TOR signaling requires down-regulation of Sch9p and involves increased mitochondrial OXPHOS complex density. *Aging*, 1(1), 131–145. <https://doi.org/10.18632/aging.100016>
- Perić, M., Lovrić, A., Musa, M., Dib, P. B., Rudan, M., Nikolić, A., Sobočanec, S., Mikecin, A., Dennerlein, S., Vlahoviček, K., Raimundo, N., & Kriško, A. (2017). TORC1-mediated sensing of chaperone activity alters glucose metabolism and extends lifespan. *Aging Cell*, 994–1005. <https://doi.org/10.1111/ace.12623>
- Polacek, N., & Mankin, A. S. (2005). The Ribosomal Peptidyl Transferase Center: Structure, Function, Evolution, Inhibition. *Critical Reviews in Biochemistry and Molecular Biology*, 40(5), 285–311. <https://doi.org/10.1080/10409230500326334>
- Postnikoff, S. D. L., & Harkness, T. A. A. (2014). *Replicative and Chronological Life-Span Assays* (Vol. 1163). Humana Press.
- Postnikoff, S. D. L., Johnson, J. E., & Tyler, J. K. (2017). The integrated stress response in budding yeast lifespan extension. *Microbial Cell*, 4(11), 368–375. <https://doi.org/10.15698/mic2017.11.597>
- Preissler, S., & Deuerling, E. (2012). Ribosome-associated chaperones as key players in proteostasis. *Trends in Biochemical Sciences*, 37(7), 274–283. <https://doi.org/10.1016/j.tibs.2012.03.002>
- Qian, S.-B., Zhang, X., Sun, J., Bennink, J. R., Yewdell, J. W., & Patterson, C. (2010). MTORC1 Links Protein Quality and Quantity Control by Sensing Chaperone Availability. *Journal of Biological Chemistry*, 285(35), 27385–27395. <https://doi.org/10.1074/jbc.M110.120295>
- Radwan, M., Wood, R. J., & Hatters, D. M. (2017). When Proteostasis Goes Bad: Protein Aggregation in the Cell Nuts and Bolts of Proteostasis Failure of Proteostasis and

- Protein. *International Union of Biochemistry and Molecular Biology*, 69(15), 49–54.  
<https://doi.org/10.1002/iub.1597>
- Ramachandran, V., & Herman, P. K. (2011). Antagonistic Interactions Between the cAMP-Dependent Protein Kinase and Tor Signaling Pathways Modulate Cell Growth in *Saccharomyces cerevisiae*. *Genetics*, 187(2), 441–454.  
<https://doi.org/10.1534/genetics.110.123372>
- Ramu, H., Vázquez-Laslop, N., Klepacki, D., Dai, Q., Piccirilli, J., Micura, R., & Mankin, A. S. (2011). Nascent Peptide in the Ribosome Exit Tunnel Affects Functional Properties of the A-Site of the Peptidyl Transferase Center. *Molecular Cell*, 41(3), 321–330.  
<https://doi.org/10.1016/j.molcel.2010.12.031>
- Reggiori, F., & Klionsky, D. J. (2013b). Autophagic Processes in Yeast: Mechanism, Machinery and Regulation. *Genetics*, 194(2), 341–361. <https://doi.org/10.1534/genetics.112.149013>
- Richard I. Morimoto. (2008). Proteotoxic stress and inducible chaperone networks in neurodegenerative disease and aging. *Genes and Development*, 22(11), 1427–1438.  
<https://doi.org/10.1101/gad.1657108>
- Rødkaer, S. V., & Faergeman, N. J. (2014). Glucose- and nitrogen sensing and regulatory mechanisms in *Saccharomyces cerevisiae*. *FEMS Yeast Research*, 14(5), 683–696. <https://doi.org/10.1111/1567-1364.12157>
- Rolland, F., Winderickx, J., & Thevelein, J. M. (2002b). Glucose-sensing and -signalling mechanisms in yeast. *FEMS Yeast Research*, 2(2), 183–201.  
<https://doi.org/10.1111/j.1567-1364.2002.tb00084.x>
- Rothe, S., Prakash, A., & Tyedmers, J. (2018b). The Insoluble Protein Deposit (IPOD) in Yeast. *Frontiers in Molecular Neuroscience*, 11. <https://doi.org/10.3389/fnmol.2018.00237>
- Saarikangas, J., & Barral, Y. (2015). Protein aggregates are associated with replicative aging without compromising protein quality control. *ELife*, 4.  
<https://doi.org/10.7554/eLife.06197>
- Sakamuru, S., Attene-Ramos, M. S., & Xia, M. (2016). Mitochondrial Membrane Potential Assay. *Methods Mol Biol*, 6(5), 17–22. <https://doi.org/10.1007/978-1-4939-6346-1>
- Sala, A. J., Bott, L. C., & Morimoto, R. I. (2017b). Shaping proteostasis at the cellular, tissue, and organismal level. *The Journal of Cell Biology*, 216(5), 1231–1241.  
<https://doi.org/10.1083/jcb.201612111>
- Salari, R., & Salari, R. (2017). Investigation of the Best *Saccharomyces cerevisiae* Growth Condition. *Electronic Physician*, 9(1), 3592–3597. <https://doi.org/10.19082/3592>
- Samanfar, B., Shostak, K., Moteshareie, H., Hajikarimlou, M., Shaikho, S., Omid, K., Hooshyar, M., Burnside, D., Márquez, I. G., Kazmirchuk, T., Naing, T., Ludovico, P., York-Lyon, A., Szereszewski, K., Leung, C., Jin, J. Y., Megarbane, R., Smith, M. L., Babu, M., ... Golshani, A. (2017). The sensitivity of the yeast, *Saccharomyces cerevisiae*, to acetic acid is influenced by *DOM34* and *RPL36A*. *PeerJ*, 5, e4037.  
<https://doi.org/10.7717/peerj.4037>



- Sampaio-Marques, B., & Ludovico, P. (2018). Linking cellular proteostasis to yeast longevity. *FEMS Yeast Research*, 18(5). <https://doi.org/10.1093/femsyr/foy043>
- Schopf, F. H., Biebl, M. M., & Buchner, J. (2017). The HSP90 chaperone machinery. *Nature Reviews Molecular Cell Biology*, 18(6), 345–360. <https://doi.org/10.1038/nrm.2017.20>
- Sherman, F. (1998). An Introduction to the Genetics and Molecular Biology of the Yeast *Saccharomyces cerevisiae*. *The Encyclopedia of Molecular Biology and Molecular Medicine*, 6, 302–325.
- Simons, J. F., Ferro-Novick, S., Rose, M. D., & Helenius, A. (1995). BiP/Kar2p serves as a molecular chaperone during carboxypeptidase Y folding in yeast. *The Journal of Cell Biology*, 130(1), 41–49. <https://doi.org/10.1083/jcb.130.1.41>
- Singh, A., Chowdhury, D., Gupta, A., Meena, R. C., & Chakrabarti, A. (2018). TORC1-signalling is down-regulated in *Saccharomyces cerevisiae* *hsp30*  $\Delta$  cells by *SNF1* - dependent mechanisms. *Yeast*, 35(12), 653–667. <https://doi.org/10.1002/yea.3360>
- Singh, M. V., & Weil, P. A. (2002). A method for plasmid purification directly from yeast. *Analytical Biochemistry*, 307, 13–14.
- Smets, B., Ghillebert, R., De Snijder, P., Binda, M., Swinnen, E., De Virgilio, C., & Winderickx, J. (2010). Life in the midst of scarcity: Adaptations to nutrient availability in *Saccharomyces cerevisiae*. *Current Genetics*, 56(1), 1–32. <https://doi.org/10.1007/s00294-009-0287-1>
- Soulard, A., Cremonesi, A., Moes, S., Schütz, F., Jenö, P., & Hall, M. N. (2010). The Rapamycin-sensitive Phosphoproteome Reveals That TOR Controls Protein Kinase A Toward Some But Not All Substrates. *Molecular Biology of the Cell*, 21(19), 3475–3486. <https://doi.org/10.1091/mbc.e10-03-0182>
- Specht, S., Miller, S. B. M., Mogk, A., & Bukau, B. (2011). Hsp42 is required for sequestration of protein aggregates into deposition sites in *Saccharomyces cerevisiae*. *The Journal of Cell Biology*, 195(4), 617–629. <https://doi.org/10.1083/jcb.201106037>
- Stahl, G., Salem, S. N. B., Chen, L., Zhao, B., & Farabaugh, P. J. (2004b). Translational Accuracy during Exponential, Postdiauxic, and Stationary Growth Phases in *Saccharomyces cerevisiae*. *Eukaryotic Cell*, 3(2), 331–338. <https://doi.org/10.1128/EC.3.2.331-338.2004>
- Su, K.-H., Cao, J., Tang, Z., Dai, S., He, Y., Sampson, S. B., Benjamin, I. J., & Dai, C. (2016). HSF1 critically attunes proteotoxic stress sensing by mTORC1 to combat stress and promote growth. *Nature Cell Biology*, 18(5), 527–539. <https://doi.org/10.1038/ncb3335>
- Surguchev, A., & Surguchov, A. (2010b). Conformational diseases: Looking into the eyes. *Brain Research Bulletin*, 81(1), 12–24. <https://doi.org/10.1016/j.brainresbull.2009.09.015>
- Svetlov, M. S. (2005). Effective cotranslational folding of firefly luciferase without chaperones of the Hsp70 family. *Protein Science*, 15(2), 242–247. <https://doi.org/10.1110/ps.051752506>
- Synoradzki, K., & Bieganski, P. (2015). Middle domain of human Hsp90 isoforms differentially binds Aha1 in human cells and alters Hsp90 activity in yeast. *Biochimica et*

- Biophysica Acta (BBA) - Molecular Cell Research*, 1853(2), 445–452.  
<https://doi.org/10.1016/j.bbamcr.2014.11.026>
- Tirolì-Cepeda, A. O., & Ramos, C. H. I. (2011). An Overview of the Role of Molecular Chaperones in Protein Homeostasis. *Protein & Peptide Letters*, 18(2), 101–109.  
<https://doi.org/10.2174/092986611794475093>
- Trendeleva, T. A., & Zvyagil'skaya, R. A. (2018b). Retrograde Signaling as a Mechanism of Yeast Adaptation to Unfavorable Factors. *Biochemistry (Moscow)*, 83(2), 98–106. <https://doi.org/10.1134/S0006297918020025>
- Ungelenk, S., Moayed, F., Ho, C.-T., Grousl, T., Scharf, A., Mashaghi, A., Tans, S., Mayer, M. P., Mogk, A., & Bukau, B. (2016). Small heat shock proteins sequester misfolding proteins in near-native conformation for cellular protection and efficient refolding. *Nature Communications*, 7(1). <https://doi.org/10.1038/ncomms13673>
- Urban, J., Soulard, A., Huber, A., Lippman, S., Mukhopadhyay, D., Deloche, O., Wanke, V., Anrather, D., Ammerer, G., Riezman, H., Broach, J. R., De Virgilio, C., Hall, M. N., & Loewith, R. (2007). Sch9 Is a Major Target of TORC1 in *Saccharomyces cerevisiae*. *Molecular Cell*, 26(5), 663–674. <https://doi.org/10.1016/j.molcel.2007.04.020>
- Ursic, D., & Culbertson, M. R. (1991). The Yeast Homolog to Mouse Tcp-1 Affects Microtubule-Mediated Processes. *MOL. CELL. BIOL.*, 11(5), 12.
- van Dyck, L., Dembowski, M., Neupert, W., & Langer, T. (1998). Mcx1p, a ClpX homologue in mitochondria of *Saccharomyces cerevisiae*. *FEBS Letters*, 438(3), 250–254.  
[https://doi.org/10.1016/S0014-5793\(98\)01310-6](https://doi.org/10.1016/S0014-5793(98)01310-6)
- Vashist, S., Cushman, M., & Shorter, J. (2010). Applying Hsp104 to protein-misfolding disorders. This paper is one of a selection of papers published in this special issue entitled 8th International Conference on AAA Proteins and has undergone the Journal's usual peer review process. *Biochemistry and Cell Biology*, 88(1), 1–13. <https://doi.org/10.1139/O09-121>
- Vendruscolo, M., Knowles, T. P. J., & Dobson, C. M. (2011). Protein solubility and protein homeostasis: A generic view of protein misfolding disorders. *Cold Spring Harbor Perspectives in Biology*, 3(12). <https://doi.org/10.1101/cshperspect.a010454>
- Verghese, J., Abrams, J., Wang, Y., & Morano, K. A. (2012). Biology of the Heat Shock Response and Protein Chaperones: Budding Yeast (*Saccharomyces cerevisiae*) as a Model System. *Microbiology and Molecular Biology Reviews*, 76(2), 115–158.  
<https://doi.org/10.1128/MMBR.05018-11>
- Voisine, C., Pedersen, J. S., & Morimoto, R. I. (2010). Chaperone networks: Tipping the balance in protein folding diseases. *Neurobiology of Disease*, 40(1), 12–20.  
<https://doi.org/10.1016/j.nbd.2010.05.007>
- Vowinckel, J., Hartl, J., Butler, R., & Ralser, M. (2015). Mitochondrion MitoLoc: A method for the simultaneous quantification of mitochondrial network morphology and membrane potential in single cells. *MITOCH*, 24, 77–86. <https://doi.org/10.1016/j.mito.2015.07.001>

- Wang, M., & Kaufman, R. J. (2016b). Protein misfolding in the endoplasmic reticulum as a conduit to human disease. *Nature*, 529(7586), 326–335.  
<https://doi.org/10.1038/nature17041>
- Wang, X., & Chen, X. J. (2015b). A cytosolic network suppressing mitochondria-mediated proteostatic stress and cell death. *Nature*, 524(7566), 481–484.  
<https://doi.org/10.1038/nature14859>
- Wilkinson, B., & Gilbert, H. F. (2004b). Protein disulfide isomerase. *Biochimica et Biophysica Acta (BBA) - Proteins and Proteomics*, 1699(1–2), 35–44.  
<https://doi.org/10.1016/j.bbapap.2004.02.017>
- Wittig, I., Karas, M., & Scha, H. (2007). High Resolution Clear Native Electrophoresis for In-gel Functional Assays and Fluorescence Studies of Membrane Protein Complexes \*. *Molecular and Cellular Proteomics*, 1215–1225. <https://doi.org/10.1074/mcp.M700076-MCP200>
- Yaffe, M. P., & Schatz, G. (1984). Two nuclear mutations that block mitochondrial protein import in yeast. *Proceedings of the National Academy of Sciences*, 81(15), 4819–4823.  
<https://doi.org/10.1073/pnas.81.15.4819>
- Yerbury, J. J., Ooi, L., Dillin, A., Saunders, D. N., Hatters, D. M., Beart, P. M., Cashman, N. R., Wilson, M. R., & Ecroyd, H. (2016). Walking the tightrope: Proteostasis and neurodegenerative disease. *Journal of Neurochemistry*, 137, 489–505.  
<https://doi.org/10.1111/jnc.13575>
- Yun, J., & Finkel, T. (2014b). Mitohormesis. *Cell Metabolism*, 19(5), 757–766.  
<https://doi.org/10.1016/j.cmet.2014.01.011>
- Yusupova, G., & Yusupov, M. (2017b). Crystal structure of eukaryotic ribosome and its complexes with inhibitors. *Philosophical Transactions of the Royal Society B: Biological Sciences*, 372(1716), 20160184. <https://doi.org/10.1098/rstb.2016.0184>
- Zaman, S., Lippman, S. I., Zhao, X., & Broach, J. R. (2008b). How *Saccharomyces* Responds to Nutrients. *Annual Review of Genetics*, 42(1), 27–81.  
<https://doi.org/10.1146/annurev.genet.41.110306.130206>
- Zhang, Y., Wölfe, T., & Rospert, S. (2013). Interaction of Nascent Chains with the Ribosomal Tunnel Proteins Rpl4, Rpl17, and Rpl39 of *Saccharomyces cerevisiae*. *Journal of Biological Chemistry*, 288(47), 33697–33707. <https://doi.org/10.1074/jbc.M113.508283>
- Zimmermann, A., Hofer, S., Pendl, T., Kainz, K., Madeo, F., & Carmona-Gutierrez, D. (2018). Yeast as a tool to identify anti-aging compounds. *FEMS Yeast Research*, 18(6).  
<https://doi.org/10.1093/femsyr/foy020>
- Zorova, L. D., Popkov, V. A., Plotnikov, E. Y., Silachev, D. N., Pevzner, I. B., Jankauskas, S. S., Babenko, V. A., Zorov, S. D., Balakireva, A. V., Juhaszova, M., Sollott, S. J., & Zorov, D. B. (2018). Mitochondrial membrane potential. *Analytical Biochemistry*, 552, 50–59.  
<https://doi.org/10.1016/j.ab.2017.07.009>

## CURRICULUM VITAE

---

Matea Kanunnikau

Date of birth: 12<sup>th</sup> August 1989

Place of birth: Mostar, Bosnia and Herzegovina

### EMPLOYMENT:

**July 2014 – September 2018:** PhD student, Macromolecular homeostasis in aging, Mediterranean Institute for Life Sciences, Split, Croatia

**July 2012 – July 2014:** Volunteer, Macromolecular homeostasis in aging, Mediterranean Institute for Life Sciences, Split, Croatia

**September 2010 – May, 2012:** Microbiology laboratory assistant, Anatomy and Embriology laboratory assistant, and Insect biology laboratory assistant, Methodist University, Fayetteville, NC, USA

### EDUCATION:

**2013- present:** *PhD student* at the Doctoral school of Biophysics, Faculty of Science, University of Split, Split, Croatia

Thesis: "Modifying the proteostasis status: the role of cross-organelle communication"

**2008 – 2012:** *Bachelor of Science*, Major in Biology with double concentration in Microbiology and Cellular physiology, and Health occupation science, Minor in Chemistry, Methodist University, Fayetteville, NC, USA

Thesis: "Induced Pluripotency of Stem Cells by Nuclear Reprogramming by Transduction of Defined Transcription Factors"

**2006 – 2008:** *International Baccalaureate*, United World College (UWC), Mostar, Bosnia and Herzegovina

### HONOR ACHIEVEMENTS AND AWARDS

Member of Beta Beta Beta, Biology honor society (2011)

Member of Gamma Sigma Epsilon, Chemistry honor society (2012)

Clark Memorial Science Award for outstanding achievements in science (2012)

Graduated with Honors- *Magna Cum Laude* (2012)

## LIST OF PUBLICATIONS

---

1. Musa, M.\*, **Perić, M.\***, Bou Dib, P., Sobočanec, S., Šarić, A., Nikolić, A., Milošević, I., Vlahoviček, K., Raimundo, N., Kriško, A. (2018). Heat-induced longevity in budding yeast requires respiratory metabolism and glutathione recycling. *Aging*, 10;9, 2407-2427. \*equal contribution
2. Rudan M, Bou Dip P, Musa M, **Kanunnikau M**, Sobočanec S, Rueda D, Warnecke T & Kriško A (2018) Normal mitochondrial function in *Saccharomyces cerevisiae* has become dependent on inefficient splicing. *eLIFE* 7:e35330
3. **Perić M\***, Lovrić A\*, Musa M, Bou Dib P, Rudan M, Nikolić A, Sobočanec S, Mikecin A, Dennerlein S, Milošević I, Vlahoviček K, Raimundo N & Kriško A (2017) TORC1-mediated sensing of chaperone activity alters glucose metabolism and extends lifespan. *Aging Cell* 16, 994-1005. \*equal contribution
4. **Perić M**, Bou Dib P, Dennerlein S, Musa M, Rudan M, Lovrić A, Nikolić A, Šarić A, Sobočanec S, Mačak Ž, Raimundo N & Kriško A (2016) Crosstalk between cellular compartments protects against proteotoxicity and extends lifespan. *Sci Rep* 6, 28751.
5. Nikolić A, **Perić M**, Ladouce R, Mikecin AM, Martin FA, et al. (2016) Death by UVC Light Correlates with Protein Damage in Isogenic Human Tumor Cells: Primary Tumor SW480 versus its Metastasis SW620. *J Proteomics Computational Biol* 2(1): 12